

## LSST: FROM SCIENCE DRIVERS TO REFERENCE DESIGN AND ANTICIPATED DATA PRODUCTS

Ž. IVEZIĆ<sup>1</sup>, J.A. TYSON<sup>2</sup>, B. ABEL<sup>3</sup>, E. ACOSTA<sup>4</sup>, R. ALLSMAN<sup>4</sup>, Y. ALSAYYAD<sup>1</sup>, S.F. ANDERSON<sup>1</sup>, J. ANDREW<sup>5</sup>, R. ANGEL<sup>6</sup>, G. ANGELI<sup>4</sup>, R. ANSARI<sup>7</sup>, P. ANTILOGUS<sup>8</sup>, K.T. ARNDT<sup>9</sup>, P. ASTIER<sup>8</sup>, É. AUBOURG<sup>10</sup>, T. AXELROD<sup>4</sup>, D.J. BARD<sup>11</sup>, J.D. BARR<sup>5</sup>, A. BARRAU<sup>12</sup>, J.G. BARTLETT<sup>13</sup>, B.J. BAUMAN<sup>14</sup>, S. BAUMONT<sup>15,16</sup>, A.C. BECKER<sup>1</sup>, J. BECLA<sup>11</sup>, C. BELDICA<sup>17</sup>, S. BELLAVIA<sup>18</sup>, G. BLANC<sup>19,20</sup>, R.D. BLANDFORD<sup>21</sup>, J.S. BLOOM<sup>22</sup>, J. BOGART<sup>21</sup>, K. BORNE<sup>23</sup>, J.F. BOSCH<sup>24</sup>, D. BOUTIGNY<sup>25,26</sup>, W.N. BRANDT<sup>27</sup>, M.E. BROWN<sup>28</sup>, J.S. BULLOCK<sup>29</sup>, P. BURCHAT<sup>21</sup>, D.L. BURKE<sup>21</sup>, G. CAGNOLI<sup>30</sup>, D. CALABRESE<sup>4</sup>, S. CHANDRASEKHARAN<sup>5</sup>, S. CHESLEY<sup>31</sup>, E.C. CHEU<sup>32</sup>, J. CHIANG<sup>21</sup>, C.F. CLAVER<sup>4</sup>, A.J. CONNOLLY<sup>1</sup>, K.H. COOK<sup>4</sup>, A. COORAY<sup>29</sup>, K.R. COVEY<sup>33</sup>, C. CRIBBS<sup>17</sup>, W. CUI<sup>9</sup>, R. CUTRI<sup>34</sup>, G. DAUBARD<sup>8</sup>, G. DAUES<sup>17</sup>, F. DELGADO<sup>35</sup>, S. DIGEL<sup>11</sup>, P. DOHERTY<sup>36</sup>, R. DUBOIS<sup>11</sup>, G.P. DUBOIS-FELSMANN<sup>11</sup>, J. DURECH<sup>37</sup>, M. ERACLEOUS<sup>27</sup>, H. FERGUSON<sup>38</sup>, J. FRANK<sup>18</sup>, M. FREEMON<sup>17</sup>, E. GANGLER<sup>39</sup>, E. GAWISER<sup>40</sup>, J.C. GEARY<sup>41</sup>, P. GEE<sup>2</sup>, M. GEHA<sup>42</sup>, R.R. GIBSON<sup>1</sup>, D.K. GILMORE<sup>21</sup>, T. GLANZMAN<sup>11</sup>, I. GOODENOW<sup>4</sup>, W.J. GRESSLER<sup>5</sup>, P. GRIS<sup>43</sup>, A. GUYONNET<sup>8</sup>, P.A. HASCALL<sup>11</sup>, J. HAUPT<sup>18</sup>, F. HERNANDEZ<sup>44</sup>, C. HOGAN<sup>45</sup>, D. HUANG<sup>18</sup>, M.E. HUFFER<sup>21</sup>, W.R. INNES<sup>21</sup>, S.H. JACOBY<sup>4</sup>, B. JAIN<sup>46</sup>, J. JEE<sup>2</sup>, J.G. JERNIGAN<sup>47</sup>, D. JEVREMOVIC<sup>48</sup>, K. JOHNS<sup>32</sup>, R.L. JONES<sup>1</sup>, C. JURAMY-GILLES<sup>8</sup>, M. JURIĆ<sup>1</sup>, S.M. KAHN<sup>4,21</sup>, J.S. KALIRAI<sup>38</sup>, N. KALLIVAYALIL<sup>49</sup>, B. KALMBACH<sup>1</sup>, J.P. KANTOR<sup>4</sup>, M.M. KASLIWAL<sup>50</sup>, R. KESSLER<sup>45</sup>, D. KIRKBY<sup>51</sup>, L. KNOX<sup>2</sup>, I. KOTOV<sup>18</sup>, V.L. KRABBENDAM<sup>4</sup>, S. KRUGHOFF<sup>1</sup>, P. KUBÁNEK<sup>52</sup>, J. KUCZEWSKI<sup>18</sup>, S. KULKARNI<sup>53</sup>, R. LAMBERT<sup>35</sup>, L. LE GUILLOU<sup>15,16</sup>, D. LEVINE<sup>34</sup>, M. LIANG<sup>5</sup>, K-T. LIM<sup>11</sup>, C. LINTOTT<sup>54</sup>, R.H. LUPTON<sup>24</sup>, A. MAHABAL<sup>53</sup>, P. MARSHALL<sup>21</sup>, S. MARSHALL<sup>21</sup>, M. MAY<sup>18</sup>, R. MCKERCHER<sup>4</sup>, M. MIGLIORE<sup>12</sup>, M. MILLER<sup>5</sup>, D.J. MILLS<sup>5</sup>, D.G. MONET<sup>55</sup>, M. MONIEZ<sup>7</sup>, D.R. NEILL<sup>5</sup>, J-Y. NIEF<sup>26</sup>, A. NOMEROVTSKI<sup>18</sup>, M. NORDBY<sup>11</sup>, P. O'CONNOR<sup>18</sup>, J. OLIVER<sup>36,56</sup>, S.S. OLIVIER<sup>14</sup>, K. OLSEN<sup>5</sup>, S. ORTIZ<sup>4</sup>, R.E. OWEN<sup>1</sup>, R. PAIN<sup>8</sup>, J.R. PETERSON<sup>9</sup>, C.E. PETRY<sup>4</sup>, F. PIERFEDERICI<sup>38</sup>, S. PIETROWICZ<sup>17</sup>, R. PIKE<sup>57</sup>, P.A. PINTO<sup>6</sup>, R. PLANTE<sup>17</sup>, S. PLATE<sup>18</sup>, P.A. PRICE<sup>24</sup>, M. PROUZA<sup>52</sup>, V. RADEKA<sup>18</sup>, J. RAJAGOPAL<sup>5</sup>, A. RASMUSSEN<sup>9</sup>, N. REGNAULT<sup>8</sup>, S.T. RIDGWAY<sup>5</sup>, S. RITZ<sup>58</sup>, W. ROSING<sup>59</sup>, C. ROUCELLE<sup>13</sup>, M.R. RUMORE<sup>18</sup>, S. RUSSO<sup>8</sup>, A. SAHA<sup>5</sup>, B. SASSOLAS<sup>30</sup>, T.L. SCHALK<sup>58</sup>, R.H. SCHINDLER<sup>21</sup>, D.P. SCHNEIDER<sup>27</sup>, G. SCHUMACHER<sup>35</sup>, J. SEBAG<sup>5</sup>, G.H. SEMBROSKI<sup>9</sup>, L.G. SEPPALA<sup>14</sup>, I. SHIPSEY<sup>9,54</sup>, N. SILVESTRI<sup>1</sup>, J.A. SMITH<sup>60</sup>, R.C. SMITH<sup>35</sup>, M.A. STRAUSS<sup>22</sup>, C.W. STUBBS<sup>36,56</sup>, D. SWEENEY<sup>4</sup>, A. SZALAY<sup>61</sup>, P. TAKACS<sup>18</sup>, J.J. THALER<sup>62</sup>, R. VAN BERG<sup>11,46</sup>, D. VANDEN BERK<sup>63</sup>, K. VETTER<sup>18</sup>, F. VIRIEUX<sup>10</sup>, B. XIN<sup>4</sup>, L. WALKOWICZ<sup>24</sup>, C.W. WALTER<sup>64</sup>, D.L. WANG<sup>11</sup>, M. WARNER<sup>35</sup>, B. WILLMAN<sup>65</sup>, D. WITTMAN<sup>2</sup>, S.C. WOLFF<sup>4</sup>, W.M. WOOD-VASEY<sup>66</sup>, P. YOACHIM<sup>1</sup>, AND H. ZHAN<sup>67</sup>,

FOR THE LSST COLLABORATION

*A living LSST document (arXiv:0805.2366); version 3.1 of Aug 29, 2014*

## ABSTRACT

Major advances in our understanding of the Universe frequently arise from dramatic improvements in our ability to accurately measure astronomical quantities. Aided by rapid progress in information technology, current sky surveys are changing the way we view and study the Universe. Next-generation surveys will maintain this revolutionary progress. We describe here the most ambitious survey currently planned in the optical, the Large Synoptic Survey Telescope (LSST). A vast array of science will be enabled by a single wide-deep-fast sky survey, and LSST will have unique survey capability in the faint time domain. The LSST design is driven by four main science themes: probing dark energy and dark matter, taking an inventory of the Solar System, exploring the transient optical sky, and mapping the Milky Way. LSST will be a large, wide-field ground-based system designed to obtain multiple images covering the sky visible from Cerro Pachón in northern Chile. The telescope will have an 8.4 m (6.5 m effective) primary mirror, a 9.6 deg<sup>2</sup> field of view, and a 3.2 Gigapixel camera. This system can image about 10,000 square degrees of sky in three clear nights using pairs of 15-second exposures twice per night, with typical 5 $\sigma$  depth for point sources of  $r \sim 24.5$  (AB). The system is designed to yield high image quality as well as superb astrometric and photometric accuracy. The project is in the construction phase and will begin regular survey operations by 2022. The survey area will be contained within 30,000 deg<sup>2</sup> with  $\delta < +34.5^\circ$ , and will be imaged multiple times in six bands, *ugrizy*, covering the wavelength range 320–1050 nm. About 90% of the observing time will be devoted to a deep-wide-fast survey mode which will uniformly observe a 18,000 deg<sup>2</sup> region about 800 times (summed over all six bands) during the anticipated 10 years of operations, and yield a coadded map to  $r \sim 27.5$ . These data will result in databases including 20 billion galaxies and a similar number of stars, and will serve the majority of the primary science programs. The remaining 10% of the observing time will be allocated to special projects such as a Very Deep and Fast time domain survey. We illustrate how the LSST science drivers led to these choices of system parameters, and describe the expected data products and their characteristics. The goal is to make LSST data products including a relational database of about 32 trillion observations of 40 billion objects available to the public and scientists around the world – everyone will be able to view and study a high-definition color movie of the deep Universe.

*Subject headings:* astronomical data bases: atlases, catalogs, surveys — Solar System — stars — the Galaxy — galaxies — cosmology

## 1. INTRODUCTION

Major advances in our understanding of the Universe have historically arisen from dramatic improvements in our ability to “see”. We have developed progressively larger telescopes over the past century, allowing us to peer further into space, and further back in time. With the development of advanced instrumentation – imag-

ing, spectroscopic, and polarimetric – we have been able to parse radiation detected from distant sources over the full electromagnetic spectrum in increasingly subtle ways. These data have provided the detailed information needed to construct physical models of planets, stars, galaxies, quasars, and larger structures.

Until recently, most astronomical investigations have focused on small samples of cosmic sources or individual objects. This is because our largest telescope facilities

<sup>2</sup> Physics Department, University of California, One Shields Avenue, Davis, CA 95616

<sup>3</sup> Olympic College, 1600 Chester Ave., Bremerton, WA 98337-1699

<sup>4</sup> LSST Project Office, 933 N. Cherry Avenue, Tucson, AZ 85721

<sup>5</sup> National Optical Astronomy Observatory, 950 N. Cherry Ave, Tucson, AZ 85719

<sup>6</sup> Steward Observatory, The University of Arizona, 933 N Cherry Ave., Tucson, AZ 85721

<sup>7</sup> Laboratoire de l'Accélérateur Linéaire, IN2P3-CNRS, Université de Paris-Sud, B.P. 34, 91898 Orsay Cedex, France

<sup>8</sup> Laboratoire de Physique Nucléaire et des Hautes Energies, Université Pierre et Marie Curie, Université Paris Diderot, CNRS/IN2P3, 4 place Jussieu, 75005 Paris, France

<sup>9</sup> Department of Physics and Astronomy, Purdue University, 525 Northwestern Ave., West Lafayette, IN 47907

<sup>10</sup> AstroParticule et Cosmologie, Université Paris Diderot, CNRS/IN2P3, CEA/Irfu, Observatoire de Paris, Sorbonne Paris Cité, 10, rue Alice Domon et Léonie Duquet, Paris Cedex 13, France

<sup>11</sup> SLAC National Accelerator Laboratory, 2575 Sand Hill Rd, Menlo Park CA 94025

<sup>12</sup> Laboratoire de Physique Subatomique et de Cosmologie, Université Grenoble-Alpes, CNRS/IN2P3, 53 av. des Martyrs, 38026 Grenoble cedex, France

<sup>13</sup> APC, AstroParticule et Cosmologie, Université Paris Diderot, CNRS/IN2P3, CEA/Irfu, Observatoire de Paris, Sorbonne Paris Cité, 10, rue Alice Domon et Léonie Duquet, Paris Cedex 13, France

<sup>14</sup> Lawrence Livermore National Laboratory, 7000 East Avenue, Livermore, CA 94550

<sup>15</sup> Sorbonne Universités, UPMC Univ Paris 06, UMR 7585, LPNHE, F-75005, Paris, France

<sup>16</sup> CNRS, UMR 7585, Laboratoire de Physique Nucléaire et des Hautes Energies, 4 place Jussieu, 75005 Paris, France

<sup>17</sup> NCSA, University of Illinois at Urbana-Champaign, 1205 W. Clark St., Urbana, IL 61801

<sup>18</sup> Brookhaven National Laboratory, Upton, NY 11973

<sup>19</sup> Laboratoire de l'Accélérateur Linéaire, Univ. Paris Sud/CNRS/IN2P3, Bat. 200, 91898 Orsay Cedex, France

<sup>20</sup> Université Paris Diderot, Sorbonne Paris Cité, F-75013 Paris, France

<sup>21</sup> Kavli Institute for Particle Astrophysics and Cosmology, SLAC National Accelerator Laboratory, Stanford University, Stanford, CA 94025

<sup>22</sup> Astronomy Department, University of California, 601 Campbell Hall, Berkeley, CA 94720

<sup>23</sup> School of Physics, Astronomy and Computational Sciences, George Mason University, 4400 University Drive, Fairfax, VA 22030

<sup>24</sup> Department of Astrophysical Sciences, Princeton University, Princeton, NJ 08544

<sup>25</sup> SLAC National Accelerator Laboratory, Stanford University, Stanford, CA 94025

<sup>26</sup> Centre de Calcul de l'IN2P3, USR 6402 du CNRS-IN2P3, 43 Bd. du 11 Novembre 1918, 69622 Villeurbanne Cedex, France

<sup>27</sup> Department of Astronomy and Astrophysics, The Pennsylvania State University, 525 Davey Lab, University Park, PA 16802

<sup>28</sup> Division of Geological and Planetary Sciences, California Institute of Technology, Pasadena, CA 91125

<sup>29</sup> Center for Cosmology, University of California, Irvine, CA 92697

<sup>30</sup> Laboratoire des Materiaux Avances (LMA), IN2P3/CNRS, Université de Lyon, F-69622 Villeurbanne, Lyon, France

<sup>31</sup> Jet Propulsion Laboratory, California Institute of Technology, Pasadena, CA 91109

<sup>32</sup> Department of Physics, University of Arizona, 1118 E. Fourth Street, Tucson, AZ 85721

<sup>33</sup> 1400 W. Mars Hill Rd., Lowell Observatory, Flagstaff, AZ 86001

<sup>34</sup> IPAC, California Institute of Technology, MS 100-22, Pasadena, CA 91125

<sup>35</sup> Cerro Tololo InterAmerican Observatory, La Serena, Chile

<sup>36</sup> Departments of Physics, Center for Astrophysics, Harvard University, 60 Garden St., Cambridge, MA 02138

<sup>37</sup> Astronomical Institute, Charles University, Praha, Czech Republic

<sup>38</sup> Space Telescope Science Institute, 3700 San Martin Drive, Baltimore, MD 21218

<sup>39</sup> Clermont Université, Université Blaise Pascal, CNRS/IN2P3, Laboratoire de Physique Corpusculaire, BP 10448, F-63000 Clermont-Ferrand, France

<sup>40</sup> Department of Physics and Astronomy, Rutgers University, 136 Frelinghuysen Rd, Piscataway, NJ 08854

<sup>41</sup> Smithsonian Astrophysical Observatory, 60 Garden St., Cambridge MA 02138

<sup>42</sup> Astronomy Department, Yale University, New Haven, CT 06520

<sup>43</sup> Laboratoire de Physique Corpusculaire de Clermont-Ferrand, Université Blaise Pascal, IN2P3/CNRS, 24 avenue des Landais, 63171 Aubière Cedex, France

<sup>44</sup> IN2P3 Computing Center, CNRS/IN2P3, Lyon-Villeurbanne, France

<sup>45</sup> Department of Astronomy and Astrophysics, University of Chicago, 5640 South Ellis Avenue, Chicago, IL 60637

<sup>46</sup> Department of Physics & Astronomy, University of Pennsylvania, 209 South 33rd Street, Philadelphia, PA 19104-6396

<sup>47</sup> Space Sciences Lab, University of California, 7 Gauss Way, Berkeley, CA 94720-7450

<sup>48</sup> Astronomical Observatory, Volgina 7, P.O.Box 74, 11060 Belgrade, Serbia

<sup>49</sup> Department of Astronomy, University of Virginia, Charlottesville, VA 22904

<sup>50</sup> The Observatories, Carnegie Institution for Science, Pasadena CA 91101, Hubble Fellow and Carnegie-Princeton Fellow, Visiting Associate, California Institute of Technology, Pasadena CA 91125

<sup>51</sup> Department of Physics and Astronomy, University of California, 4129 Frederick Reines Hall, Irvine, CA 92697

<sup>52</sup> Institute of Physics, Academy of Sciences of the Czech Republic, Na Slovance 2, 182 21 Praha 8, Czech Republic

<sup>53</sup> Astronomy Department, California Institute of Technology, 1200 East California Blvd., Pasadena CA 91125

<sup>54</sup> Department of Physics, University of Oxford, Denys Wilkinson Building, Keble Road, Oxford, OX1 3RH, UK

<sup>55</sup> U.S. Naval Observatory Flagstaff Station, 10391 Naval Observatory Road, Flagstaff, AZ 86001

<sup>56</sup> Department of Astronomy, Center for Astrophysics, Harvard University, 60 Garden St., Cambridge, MA 02138

<sup>57</sup> Google Inc., 1600 Amphitheatre Parkway Mountain View, CA 94043

<sup>58</sup> Santa Cruz Institute for Particle Physics and Physics Department, University of California-Santa Cruz, 1156 High St., Santa Cruz, CA 95064

<sup>59</sup> Las Cumbres Observatory, 6740 Cortona Dr. Suite 102, Santa Barbara, CA 93117

<sup>60</sup> Austin Peay State University, Clarksville, TN 37044

<sup>61</sup> Department of Physics and Astronomy, The John Hopkins University, 3701 San Martin Drive, Baltimore, MD 21218

<sup>62</sup> University of Illinois, Physics and Astronomy Departments, 1110 W. Green St., Urbana, IL 61801

<sup>63</sup> Saint Vincent College, Department of Physics, 300 Fraser Purchase Road, Latrobe, PA 15650

<sup>64</sup> Department of Physics, Duke University, Durham, NC 27708

typically had rather small fields of view, and those with large fields of view could not detect very faint sources. With all of our existing telescope facilities, we have still surveyed only a small fraction of the observable Universe (except when considering the most luminous quasars).

Over the past two decades, however, advances in technology have made it possible to move beyond the traditional observational paradigm and to undertake large-scale sky surveys. As vividly demonstrated by surveys such as the Sloan Digital Sky Survey (SDSS; York et al. 2000), the Two Micron All Sky Survey (2MASS; Skrutskie et al. 2006), and the Galaxy Evolution Explorer (GALEX; Martin et al. 2006), to name but a few, sensitive and accurate multi-color surveys over a large fraction of the sky enable an extremely broad range of new scientific investigations. These projects, based on a synergy of advances in telescope construction, detectors, and above all, information technology, have dramatically impacted nearly all fields of astronomy – and many areas of fundamental physics. In addition, the world-wide attention received by Sky in Google Earth<sup>68</sup> (Scranton et al. 2007) and the hundreds of thousands of volunteers classifying galaxies in the Galaxy Zoo project (Lintott et al. 2011) and its extensions demonstrate that the impact of sky surveys extends far beyond fundamental science progress and reaches all of society.

Motivated by the evident scientific progress enabled by large sky surveys, three nationally-endorsed reports by the U.S. National Academy of Sciences<sup>69</sup> concluded that a dedicated ground-based wide-field imaging telescope with an effective aperture of 6–8 meters is a high priority for planetary science, astronomy, and physics over the next decade. The Large Synoptic Survey Telescope (LSST) described here is such a system. The LSST will be a large, wide-field ground-based telescope designed to obtain multi-band images over a substantial fraction of the sky every few nights. The survey will yield contiguous overlapping imaging of over half the sky in six optical bands, with each sky location visited close to 1000 times over 10 years. The recent 2010 report “New Worlds, New Horizons in Astronomy and Astrophysics” by the Committee for a Decadal Survey of Astronomy and Astrophysics<sup>70</sup> ranked LSST as its top priority for large ground-based projects, and in May 2014 the National Science Board approved the project for construction.

The purpose of this paper is to provide an overall summary of the main LSST science drivers and how they led to the current system design parameters (§ 2), to describe anticipated data products (§ 3), and to provide a few examples of the science programs that LSST will enable (§ 4). The community involvement is discussed in § 5, and broad educational and societal impacts in § 6. Con-

<sup>65</sup> Department of Astronomy, Haverford College, 370 Lancaster Avenue, Haverford, PA 19041

<sup>66</sup> Department of Physics and Astronomy, University of Pittsburgh, 3941 O’Hara Street, Pittsburgh PA 15260

<sup>67</sup> National Astronomical Observatories, Chinese Academy of Sciences, A20 Datun Rd, Chaoyang District, Beijing 100012, China

<sup>68</sup> <http://earth.google.com/sky/>

<sup>69</sup> Astronomy and Astrophysics in the New Millennium, NAS 2001; Connecting Quarks with the Cosmos: Eleven Science Questions for the New Century, NAS 2003; New Frontiers in the Solar System: An Integrated Exploration Strategy, NAS 2003.

<sup>70</sup> [http://www.nap.edu/catalog.php?record\\_id=12951](http://www.nap.edu/catalog.php?record_id=12951)

cluding remarks are presented in § 7. This publication will be maintained at the arXiv.org site<sup>71</sup>, and will also be available from the LSST website ([www.lsst.org](http://www.lsst.org)). The latest arXiv version of this paper should be consulted and referenced for the most up-to-date information about the LSST system.

## 2. FROM SCIENCE DRIVERS TO REFERENCE DESIGN

The most important characteristic that determines the speed at which a system can survey a given sky area to a given flux limit (i.e., its étendue (or grasp), the product of its primary mirror area and the angular area of its field of view (for a given set of observing conditions, such as seeing and sky brightness). The effective étendue for LSST will be greater than  $300 \text{ m}^2 \text{ deg}^2$ , which is more than an order of magnitude larger than that of any existing facility. For example, the SDSS, with its 2.5-m telescope (Gunn et al. 2006) and a camera with 30 imaging CCDs (Gunn et al. 1998), has an effective étendue of only  $5.9 \text{ m}^2 \text{ deg}^2$ .

The range of scientific investigations which will be enabled by such a dramatic improvement in survey capability is extremely broad. Guided by the community-wide input assembled in the report of the Science Working Group of the LSST in 2004<sup>72</sup>, the LSST is designed to achieve goals set by four main science themes:

1. Probing Dark Energy and Dark Matter;
2. Taking an Inventory of the Solar System;
3. Exploring the Transient Optical Sky;
4. Mapping the Milky Way.

Each of these four themes itself encompasses a variety of analyses, with varying sensitivity to instrumental and system parameters. These themes fully exercise the technical capabilities of the system, such as photometric and astrometric accuracy and image quality. About 90% of the observing time will be devoted to a deep-wide-fast (main) survey mode. The working paradigm is that all scientific investigations will utilize a common database constructed from an optimized observing program (the main survey mode), such as that discussed in § 3.1. Here we briefly describe these science goals and the most challenging requirements for the telescope and instrument that are derived from those goals, which will inform the overall system design decisions discussed below. For a more detailed discussion, we refer the reader to the LSST Science Requirements Document<sup>73</sup>, the LSST Science Book (2009; hereafter SciBook), as well as to numerous LSST poster presentations at recent meetings of the AAS<sup>74</sup>.

### 2.1. The Main Science Drivers

The main science drivers are used to optimize various system parameters. Ultimately, in this high-dimensional parameter space, there is a manifold defined by the total

<sup>71</sup> <http://arxiv.org/abs/0805.2366>

<sup>72</sup> Available as <http://www.lsst.org/files/docs/DRM2.pdf>

<sup>73</sup> Available at <http://www.lsst.org/files/docs/SRD.pdf>

<sup>74</sup> See <http://www.lsst.org/lsst/content/aas2013> and further links at <http://www.lsst.org/lsst/news>.

project cost. The science drivers must both justify this cost, as well as provide guidance on how to optimize various parameters while staying within the cost envelope.

Here we summarize the dozen or so most important interlocking constraints on data and system properties placed by the four main science themes:

1. The depth of a single visit;
2. Image quality;
3. Photometric accuracy;
4. Astrometric accuracy;
5. Optimal exposure time;
6. The filter complement;
7. The distribution of revisit times (i.e., the cadence of observations), including the survey lifetime;
8. The total number of visits to a given area of sky;
9. The coadded survey depth;
10. The distribution of visits on the sky, and the total sky coverage;
11. The distribution of visits per filter; and
12. Data processing and data access (e.g., time delay for reporting transient sources and the software contribution to measurement errors).

We present a detailed discussion of how these science-driven data properties are transformed to system parameters below.

### 2.1.1. Probing Dark Energy and Dark Matter

Current models of cosmology require the existence of both dark matter and dark energy to match observational constraints (Riess et al. 2007; Komatsu et al. 2009; Percival et al. 2010; LSST Dark Energy Science Collaboration 2012, and references therein). Dark energy affects the cosmic history of both the Hubble expansion and mass clustering. Distinguishing competing models for the physical nature of dark energy, or alternative explanations involving modifications of the General Theory of Relativity, will require percent level measurements of both the cosmic expansion and the growth of dark matter structure as a function of redshift. Any given cosmological probe is sensitive to, and thus constrains degenerate combinations of, several cosmological parameters. Therefore the most robust cosmological constraints are the result of using interlocking combinations of probes. The most powerful probes include weak gravitational lens cosmic shear (WL), baryon acoustic oscillations (BAO), and photometry of type Ia supernovae (SN) – all as functions of redshift. Using the cosmic microwave background fluctuations as the normalization, the combination of these probes can yield the needed precision to distinguish among models of dark energy (Zhan 2006, and references therein). In addition, strong galaxy and cluster lensing as a function of cosmic time probes the physics of dark matter, because the positions and shapes of multiple images of a source galaxy depend sensitively

on the total mass distribution, including the dark matter, in the lensing object.

The three major programs from this science theme, WL, BAO and SN, provide unique and independent constraints on the system design (SciBook Ch. 11–15).

Weak lensing (WL) techniques can be used to map the distribution of mass as a function of redshift and thereby trace the history of both the expansion of the Universe and the growth of structure (e.g., Hu & Tegmark 1999; for reviews see Bartelmann & Schneider 2001 and Weinberg et al. 2013). Measurements of cosmic shear as a function of redshift allow determination of angular distances versus cosmic time, providing multiple independent constraints on the nature of dark energy. These investigations require deep wide-area multi-color imaging with stringent requirements on shear systematics in at least two bands, and excellent photometry in at least five bands to measure photometric redshifts (a requirement shared with BAO, and indeed all extragalactic science drivers). The strongest constraints on the LSST image quality arise from this science program. In order to control systematic errors in shear measurement, the desired depth must be achieved with many short exposures (allowing for systematics in the measurement of galaxy shapes related to the PSF and telescope pointing to be diagnosed and removed). Detailed simulations of weak lensing techniques show that imaging over  $\sim 20,000 \text{ deg}^2$  to a  $5\sigma$  point-source depth of  $r_{AB} \sim 27.5$  gives adequate signal to measure shapes for of order 4 billion galaxies for weak lensing. These numbers are adequate to reach Stage IV goals for dark energy, as defined by the Dark Energy Task Force (Albrecht et al. 2006). This depth, and the corresponding deep surface brightness limit, optimize the number of galaxies with measured shapes in ground-based seeing, and allow their detection in significant numbers to beyond a redshift of two. Analyzing these data will require sophisticated data processing techniques. For example, rather than simply coadding all images in a given region of sky, the individual exposures, each with their own PSF and noise characteristics, should be analyzed simultaneously to optimally measure the shapes of galaxies (Tyson et al. 2008a; Jee and Tyson, 2011).

Type Ia supernovae provided the first robust evidence that the expansion of the Universe is accelerating (Riess et al. 1998; Perlmutter et al. 1999). To fully exploit the supernova science potential, light curves sampled in multiple bands every few days over the course of a few months are required. This is essential to search for systematic differences in supernova populations (e.g., due to differing progenitor channels) which may masquerade as cosmological effects, as well as to determine photometric redshifts from the supernovae themselves. Unlike other cosmological probes, even a single object gives information on the relationship between redshift and distance. Thus a large number of SN across the sky allows one to search for any dependence of dark energy properties on direction, which would be an indicator of new physics. The results from this method can be compared with similar measures of anisotropy from the combination of WL and BAO (Zhan et al. 2009). Given the expected SN flux distribution at the redshifts where dark energy is important, the single visit depth should be at least  $r \sim 24$ . Good image quality is required to separate

SN photometrically from their host galaxies. Observations in at least five photometric bands will allow proper K-corrected light curves to be measured over a range of redshift. Carrying out these K-corrections requires that the calibration of the relative offsets in photometric zero points between filters and the system response functions, especially near the edges of bandpasses, must be accurate to about 1% (Wood-Vasey et al. 2007), similar to the requirements from photometric redshifts of galaxies. Deeper data ( $r > 26$ ) for small areas of the sky can extend the discovery of SN to a mean redshift of 0.7 (from  $\sim 0.5$  for the main survey), with some objects beyond  $z \sim 1$  (Garnavich et al. 2005; Pinto et al. 2005; SciBook Ch. 11). The added statistical leverage on the “pre-acceleration” era ( $z \gtrsim 1$ ) would improve constraints on the properties of dark energy as a function of redshift.

Finally, there will be powerful cross checks and complementarities with other planned or proposed surveys, such as Euclid (Laureijs et al. 2011) and WFIRST-AFTA (Spergel et al. 2013) (wide-field optical-IR imaging from space), DESI (Levi et al. 2013) and PFS (Takada et al. 2014) (spectroscopic BAO with several millions of galaxies), and SKA<sup>75</sup> (radio). Large survey volumes are key to probing dynamical dark energy models (with sub-horizon dark energy clustering or anisotropic stresses). The cross-correlation of the three-dimensional mass distribution (as probed by HI in SKA, or galaxies in DESI and PFS) with the gravitational growth probed by tomographic shear in LSST will be complementary way to constrain dark energy properties beyond simply characterizing its equation of state.

### 2.1.2. Taking an Inventory of the Solar System

The small-body populations in the Solar System, such as asteroids, trans-Neptunian objects (TNOs) and comets, are remnants of its early assembly. The history of accretion, collisional grinding, and perturbation by existing and vanished giant planets is preserved in the orbital elements and size distributions of those objects. Cataloging the orbital parameters, size distributions, colors and light curves of these small-body populations requires a large number of observations in multiple filters, and will lead to insights into planetary formation and evolution by providing the basis and constraints for new theoretical models. In addition, collisions in the main asteroid belt between Mars and Jupiter still occur, and occasionally eject objects on orbits that may place them on a collision course with Earth. Studying the properties of main belt asteroids at sub-kilometer sizes is important for linking the near-Earth Object (NEO) population with its source in the main belt. About 20% of NEOs, the potentially hazardous asteroids (PHAs), are in orbits that pass sufficiently close to Earth’s orbit, to within 0.05 AU, that perturbations with time scales of a century can lead to intersections and the possibility of collision. In December 2005, the U.S. Congress directed<sup>76</sup> NASA to implement a NEO survey that would catalog 90% of NEOs with diameters larger than 140 meters by 2020.

Discovering and linking objects in the Solar System moving with a wide range of apparent velocities (from several degrees per day for NEOs to a few arc seconds

per day for the most distant TNOs) places strong constraints on the cadence of observations, requiring closely spaced pairs of observations (two or preferably three times per lunation) in order to link detections unambiguously and derive orbits (SciBook Ch. 5). Individual exposures should be shorter than about 30 seconds each to minimize the effects of trailing for the majority of moving objects. The images must be well sampled to enable accurate astrometry, with absolute accuracy of at least 0.1 arcsec in order to measure orbital parameters of TNOs with enough precision to constrain theoretical models and enable prediction of occultations. The photometry should be better than 1-2% to measure asteroids’ colors and thus determine their types. The different filters should be observed over a short time span to reduce apparent variations in color due to changes in observing geometry, but should be repeated over many lunations in order to determine phase curves and allow shape modeling.

The Congressional mandate can be fulfilled with a 10-meter-class telescope equipped with a multi-gigapixel camera, and a sophisticated and robust data processing system (Ivezić et al. 2007a). The images should reach a depth of at least 24.5 ( $5\sigma$  for point sources) in the  $r$  band to reach high completeness down to the 140 m mandate for NEOs. Such an instrument would probe the  $\sim 100$  m size range at main-belt distances, and discover rare distant TNOs such as Sedna (Brown, Trujillo & Rabinowitz 2004) and 2012 VP113 (Trujillo & Sheppard 2014).

### 2.1.3. Exploring the Transient Optical Sky

Recent surveys have shown the power of measuring variability for studying gravitational lensing, searching for supernovae, determining the physical properties of gamma-ray burst sources, probing the structure of active galactic nuclei, studying variable star populations, discovering exoplanets and many other subjects at the forefront of astrophysics (SciBook Ch. 8; Law et al. 2009; Djorgovski et al. 2012; Rowe et al. 2014). Wide area, dense temporal coverage to deep limiting magnitudes would enable the discovery and analysis of rare and exotic objects such as neutron stars and black hole binaries, novae and stellar flares, gamma-ray bursts and X-ray flashes, active galactic nuclei, stellar disruptions by black holes (Bloom et al. 2011; Gezari et al. 2012), and possibly new classes of transients, such as binary mergers of black holes (Shields & Bonning 2008; Thornton et al. 2013). Such a survey would likely detect numerous microlensing events in the Local Group and perhaps beyond, and open the possibility of discovering populations of binaries and planets via transits (e.g., Beaulieu et al. 2006; Drake et al. 2010; Choi et al. 2013; Batista et al. 2014), as well as obtaining spectra of lensed stars in distant galaxies.

Time-domain science requires large area coverage to enhance the probability of detecting rare events; good time sampling, because light curves are necessary to distinguish certain types of variables and in some cases to infer their properties (e.g. determining the intrinsic luminosity of Type Ia supernovae depends on measurements of their rate of decline); accurate color information to assist with the classification of variable objects; good image quality to enable differencing of images, especially in crowded fields; and rapid data reduction, classification

<sup>75</sup> <https://www.skatelescope.org>

<sup>76</sup> For details see <http://neo.jpl.nasa.gov/neo/report2007.html>

and reporting to the community in order to flag interesting objects for spectroscopic observations and follow-up in other wavebands.

Time series ranging between one minute and ten years cadence should be probed over a significant fraction of the sky. Rapid cadence makes it possible to serendipitously catch very short-lived events, such as eclipses in ultra-compact double degenerate binary systems (Anderson et al. 2005), to constrain the properties of fast faint transients (such as optical flashes associated with gamma-ray bursts; Bloom et al. 2008), to detect electromagnetic counterparts to gravitational waves (Nissanke, Kasliwal & Georgieva 2013) and to further constrain the properties of new classes of transients discovered by programs such as the Deep Lens Survey (Becker et al. 2004), the Catalina Real-time Transient Survey (Drake et al. 2009) and the Palomar Transient Factory (Law et al. 2009). Observations over a decade would enable the study of long period variables and quasars (Kaspi et al. 2007; MacLeod et al. 2010; Graham et al. 2014). The next frontier in this field will require measuring the colors of fast transients, and to probe variability at faint magnitudes. Classification of transients in close to real time will require access to the full photometric history of the objects, both before and after the transient event (e.g., Mahabal et al. 2011).

#### 2.1.4. Mapping the Milky Way

A major challenge in extragalactic cosmology today concerns the formation of structure on sub-galactic scales, where baryon physics becomes important, and the nature of dark matter may manifest itself in observable ways (e.g., Weinberg et al. 2013). The Milky Way and its environment provide a unique dataset for understanding the detailed processes that shape galaxy formation and for testing the small-scale predictions of our standard cosmological model. However, we still lack answers to two basic questions about our Galaxy:

- What is the detailed structure and accretion history of the Milky Way?
- What are the fundamental properties of all the stars within 300 pc of the Sun?

Mapping the Galaxy requires large area coverage, excellent image quality to maximize photometric and astrometric accuracy, especially in crowded fields, photometric precision of at least 1% to separate main sequence and giant stars (e.g., Helmi et al. 2003) as well as to identify variable stars such as RR Lyrae (Sesar et al. 2010, Sharma et al. 2011), and astrometric precision of about 10 mas per observation to enable parallax and proper motion measurements (SciBook Ch. 6,7). In order to probe the halo out to its presumed edge at  $\sim 100$  kpc (Ivezić et al. 2003) using main-sequence stars, the total coadded depth must reach  $r > 27$ , with a similar depth in the  $g$  band. The metallicity distribution of stars can be studied photometrically in the Sgr tidal stream (e.g., see Majewski et al. 2003, Chou et al. 2007) and other halo substructures ( $\sim 30$  kpc, Carollo et al. 2007), yielding new insights into how they formed. These metallicities are limited by the coadded depth in the  $u$  band. To reach the limit of the stellar halo, this must reach  $u \sim 24.5$ . To

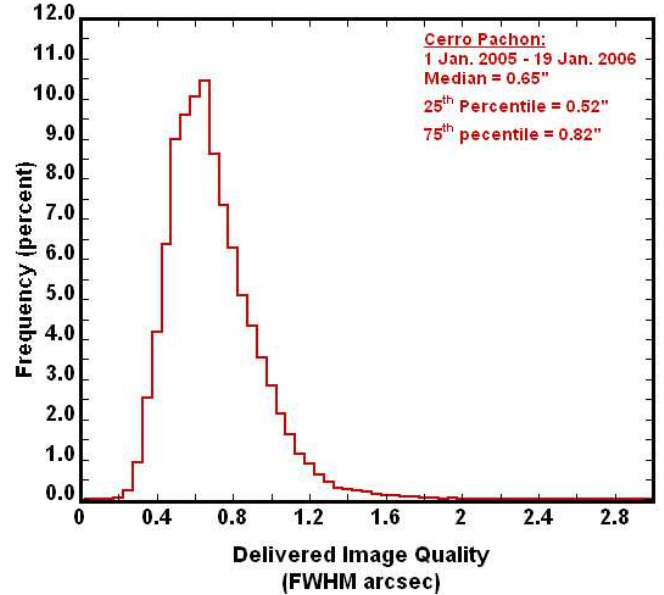


Fig. 1.— The image quality distribution measured at the Cerro Pachón site using a differential image motion monitor (DIMM) at  $\lambda = 500$  nm, and corrected using an outer scale parameter of 30 m over an 8.4 m aperture. For details about the outer scale correction see Tokovinin (2002). The observed distribution is well described by a log-normal distribution, with the parameters shown in the figure.

detect RR Lyrae stars beyond the Galaxy's tidal radius at  $\sim 300$  kpc, the single-visit depth must be  $r \sim 24.5$ .

In order to measure the tangential velocity of stars at a distance of 10 kpc, where the halo dominates over the disk, to within 10 km s $^{-1}$  (comparable with the accuracy of large-scale radial velocity surveys), the proper motion accuracy should be 0.2 mas yr $^{-1}$  or better. This is the same accuracy as will be delivered by the recently launched Gaia mission<sup>77</sup> (Perryman et al. 2001; de Bruijne 2012) at its faint limit ( $r \sim 20$ ). In order to measure distances to solar neighborhood stars out to a distance of 300 pc (the thin disk scale height), with geometric distance accuracy of at least 30%, trigonometric parallax measurements accurate to 1 mas ( $1\sigma$ ) are required over 10 years. To achieve the required proper motion and parallax accuracy with an assumed astrometric accuracy of 10 mas per observation per coordinate, approximately 1,000 separate observations are required. This requirement for a large number of observations is in good agreement with that from minimizing systematics in weak lensing observations (§ 2.1.1).

#### 2.1.5. A Summary and Synthesis of Science-driven Constraints on Data Properties

The goals of all the science programs discussed above (and many more, of course) can be accomplished by satisfying the minimal constraints listed below. For a more elaborate listing of various constraints, including detailed specification of various probability density distribution functions, please see the LSST Science Requirements Document<sup>78</sup> and the LSST Science Book.

1. The single visit depth should reach  $r \sim 24.5$ . This limit is primarily driven by the search for NEOs,

<sup>77</sup> <http://sci.esa.int/gaia/>

<sup>78</sup> <http://www.lsst.org/files/docs/SRD.pdf>

variable sources (e.g., SN, RR Lyrae stars), and by proper motion and trigonometric parallax measurements for stars. Indirectly, it is also driven by the requirements on the coadded survey depth and the minimum number of exposures required by WL science. We will split a single visit into two exposures of equal length to identify and remove cosmic rays.

2. *Image quality* should maintain the limit set by the atmosphere (the median free-air seeing is 0.65 arcsec in the  $r$  band at the chosen site, see Fig. 1), and not be degraded appreciably by the hardware. In addition to stringent constraints from weak lensing, good image quality is driven by the required survey depth for point sources and by image differencing techniques.
3. *Photometric repeatability* should achieve 5 mmag precision at the bright end, with zeropoint stability across the sky of 10 mmag and band-to-band calibration errors not larger than 5 mmag. These requirements are driven by the need for high photometric redshift accuracy, the separation of stellar populations, detection of low-amplitude variable objects (such as eclipsing planetary systems), and the search for systematic effects in type Ia supernova light curves.
4. *Astrometric precision* should maintain the limit set by the atmosphere, of about 10 mas per visit at the bright end (on scales below 20 arcmin). This precision is driven by the desire to achieve a proper motion accuracy of  $0.2 \text{ mas yr}^{-1}$  and parallax accuracy of 1.0 mas over the course of a 10-year survey (see §3.2.3).
5. *The single visit exposure time* (including both exposures in a visit, which are required for cosmic ray rejection) should be less than about a minute to prevent trailing of fast moving objects and to aid control of various systematic effects induced by the atmosphere. It should be longer than  $\sim 20$  seconds to avoid significant efficiency losses due to finite readout, slew time, and read noise.
6. *The filter complement* should include at least six filters in the wavelength range limited by atmospheric absorption and silicon detection efficiency (320–1050 nm), with roughly rectangular filters and no large gaps in the coverage, in order to enable robust and accurate photometric redshifts and stellar typing. An SDSS-like  $u$  band (Fukugita et al. 1996) is extremely important for separating low-redshift quasars from hot stars, and for estimating the metallicities of F/G main sequence stars. A bandpass with an effective wavelength of about 1 micron would enable studies of sub-stellar objects, high-redshift quasars (to redshifts of  $\sim 7.5$ ), and regions of the Galaxy that are obscured by interstellar dust.
7. *The revisit time distribution* should enable determination of orbits of Solar System objects and sample

SN light curves every few days, while accommodating constraints set by proper motion and trigonometric parallax measurements.

8. *The total number of visits* of any given area of sky, when accounting for all filters, should be of the order of 1,000, as mandated by WL science, the search for NEOs, and proper motion and trigonometric parallax measurements. Studies of transient sources also benefit from a large number of visits.
9. *The coadded survey depth* should reach  $r \sim 27.5$ , with sufficient signal-to-noise ratio in other bands to address both extragalactic and Galactic science drivers.
10. *The distribution of visits per filter* should enable accurate photometric redshifts, separation of stellar populations, and sufficient depth to enable detection of faint extremely red sources (e.g., brown dwarfs and high-redshift quasars). Detailed simulations of photometric redshift estimates suggest an approximately flat distribution of visits among bandpasses (because the system throughput and atmospheric properties are wavelength dependent, the achieved depths are different in different bands). The adopted time allocation (see Table 1) includes a slight preference to the  $r$  and  $i$  bands because of their dominant role in star/galaxy separation and weak lensing measurements.
11. *The distribution of visits on the sky* should extend over at least  $\sim 20,000 \text{ deg}^2$  to obtain the required number of galaxies for WL studies, with attention paid to include “special” regions such as the Ecliptic and Galactic planes, and the Large and Small Magellanic Clouds (if in the Southern Hemisphere). Note that  $20,000 \text{ deg}^2$  is comparable to the full area observable from any given ground-based site at reasonably low airmass (the LSST survey area will be contained within  $30,000 \text{ deg}^2$  with  $\delta < +34.5^\circ$ ).
12. *Data processing, data products and data access* should result in data products that approach the statistical uncertainties in the raw data; i.e., the processing must be close to optimal. To enable fast and efficient response to transient sources, the processing latency for variable sources should be less than a minute, with a robust and accurate preliminary characterization of all reported variables.

Remarkably, even with these joint requirements, none of the individual science programs is severely overdesigned, i.e., despite their significant scientific diversity, these programs are highly compatible in terms of desired data characteristics. Indeed, any one of the four main science drivers could be removed, and the remaining three would still yield very similar requirements for most system parameters. As a result, the LSST system can adopt a highly efficient survey strategy where *a single dataset serves most science programs* (instead of science-specific surveys executed in series). One can view this project as *massively parallel astrophysics*. The vast majority (about 90%) of the observing time will be devoted to a deep-wide-fast survey mode, with the remaining 10% allocated

TABLE 1  
THE LSST BASELINE DESIGN AND SURVEY PARAMETERS

Quantity	Baseline Design Specification
Optical Config.	3-mirror modified Paul-Baker
Mount Config.	Alt-azimuth
Final f-ratio, aperture	f/1.234, 8.4 m
Field of view, étendue	9.6 deg <sup>2</sup> , 319 m <sup>2</sup> deg <sup>2</sup>
Plate Scale	50.9 μm/arcsec (0.2" pix)
Pixel count	3.2 Gigapix
Wavelength Coverage	320 – 1050 nm, <i>ugrizy</i>
Single visit depths, design <sup>a</sup>	23.9, 25.0, 24.7, 24.0, 23.3, 22.1
Single visit depths, min. <sup>b</sup>	23.4, 24.6, 24.3, 23.6, 22.9, 21.7
Mean number of visits <sup>c</sup>	56, 80, 184, 184, 160, 160
Final (coadded) depths <sup>d</sup>	26.1, 27.4, 27.5, 26.8, 26.1, 24.9

<sup>a</sup> Design specification from the Science Requirements Document (SRD) for 5σ depths for point sources in the *ugrizy* bands, respectively. The listed values are expressed on AB magnitude scale, and correspond to point sources and fiducial zenith observations (about 0.2 mag loss of depth is expected for realistic airmass distributions, see Table 2 for more details). <sup>b</sup> Minimum specification from the Science Requirements Document for 5σ depths. <sup>c</sup> An illustration of the distribution of the number of visits as a function of bandpass, taken from Table 24 in the SRD. <sup>d</sup> Idealized depth of coadded images, based on design specification for 5σ depth and the number of visits in the penultimate row (taken from Table 24 in the SRD).

to special programs which will also address multiple science goals. Before describing these surveys in detail, we discuss the main system parameters.

## 2.2. The Main System Design Parameters

Given the minimum science-driven constraints on the data properties listed in the previous section, we now discuss how they are translated into constraints on the main system design parameters: the aperture size, the survey lifetime, the optimal exposure time, and the filter complement.

### 2.2.1. The Aperture Size

The product of the system's étendue and the survey lifetime, for given observing conditions, determines the sky area that can be surveyed to a given depth. The LSST field-of-view area is maximized to its practical limit, ~10 deg<sup>2</sup>, determined by the requirement that the delivered image quality be dominated by atmospheric seeing at the chosen site (Cerro Pachón in Northern Chile). A larger field-of-view would lead to unacceptable deterioration of the image quality. This constraint leaves the primary mirror diameter and survey lifetime as free parameters. The adopted survey lifetime of 10 years is a compromise between a shorter time that leads to an excessively large and expensive mirror (15 m for a 3 year survey and 12 m for a 5 year survey) and not as effective proper motion measurements, and a smaller telescope that would require more time to complete the survey, with the associated increase in operations cost.

The primary mirror size is a function of the required survey depth and the desired sky coverage. By and large, the anticipated science outcome scales with the number of detected sources. For practically all astronomical source populations, in order to maximize the number of detected sources, it is more advantageous to maximize the area first, and then the detection depth<sup>79</sup>. For this

<sup>79</sup> If the total exposure time is doubled and used to double the

reason, the sky area for the main survey is maximized to its practical limit, 18,000 deg<sup>2</sup>, determined by the requirement to avoid airmasses less than 1.5, which would substantially deteriorate the image quality and the survey depth (see eq. 6).

With the adopted field-of-view area, the sky coverage and the survey lifetime fixed, the primary mirror diameter is fully driven by the required survey depth. There are two depth requirements: the final (coadded) survey depth,  $r \sim 27.5$ , and the depth of a single visit,  $r \sim 24.5$ . The two requirements are compatible if the number of visits is several hundred per band, which is in good agreement with independent science-driven requirements on the latter.

The required coadded survey depth provides a direct constraint, independent of the details of survey execution such as the exposure time per visit, on the minimum effective primary mirror diameter of 6.5 m, as illustrated in Fig. 2.

### 2.2.2. The Optimal Exposure Time

The single visit depth depends on both the primary mirror diameter and the chosen exposure time,  $t_{\text{vis}}$ . In turn, the exposure time determines the time interval to revisit a given sky position and the total number of visits, and each of these quantities has its own science drivers. We summarize these simultaneous constraints in terms of the single-visit exposure time:

- The single-visit exposure time should not be longer than about a minute to prevent trailing of fast Solar System moving objects, and to enable efficient control of atmospheric systematics.
- The mean revisit time (assuming uniform cadence) for a given position on the sky,  $n$ , scales as

$$n = \left( \frac{t_{\text{vis}}}{10 \text{ sec}} \right) \left( \frac{A_{\text{sky}}}{10,000 \text{ deg}^2} \right) \left( \frac{10 \text{ deg}^2}{A_{\text{FOV}}} \right) \text{ days}, \quad (1)$$

where two visits per night are assumed (required for efficient detection of Solar System objects, see below), and the losses for realistic observing conditions have been taken into account (with the aid of the Operations Simulator described below). Science drivers such as supernova light curves and moving objects in the Solar System require that  $n < 4$  days, or equivalently  $t_{\text{vis}} < 40$  seconds for the nominal values of  $A_{\text{sky}}$  and  $A_{\text{FOV}}$ .

- The number of visits to a given position on the sky,  $N_{\text{visit}}$ , with losses for realistic observing conditions taken into account, is given by

$$N_{\text{visit}} = \left( \frac{3000}{n} \right) \left( \frac{T}{10 \text{ yr}} \right). \quad (2)$$

The requirement  $N_{\text{visit}} > 800$  again implies that  $n < 4$  and  $t_{\text{vis}} < 40$  seconds if the survey lifetime,  $T \sim 10$  years.

survey area, the number of sources increases by a factor of two. If the survey area is kept fixed, the increased exposure time will result in ~0.4 mag deeper data (see eq. 6). For cumulative source counts described by  $\log(N) = C + k * m$ , the number of sources will increase by more than a factor of two only if  $k > 0.75$ . Apart from  $z < 2$  quasars, practically all populations have  $k$  at most 0.6 (the Euclidean value), and faint stars and galaxies have  $k < 0.5$ . For more details, please see Nemiroff (2003).

- These three requirements place a firm upper limit on the optimal visit exposure time of  $t_{vis} < 40$  seconds. Surveying efficiency (the ratio of open-shutter time to the total time spent per visit) considerations place a lower limit on  $t_{vis}$  due to finite detector read-out and telescope slew time (the longest acceptable read-out time is set to 2 seconds, the shutter open-and-close time is 2 seconds, and the slew and settle time is set to 5 seconds, including the read-out time for the second exposure in a visit):

$$\epsilon = \left( \frac{t_{vis}}{t_{vis} + 9 \text{ sec}} \right). \quad (3)$$

To maintain efficiency losses below  $\sim 30\%$  (i.e., at least below the limit set by the weather patterns), and to minimize the read noise impact,  $t_{vis} > 20$  seconds is required.

Taking these constraints simultaneously into account, as summarized in Fig. 3, yielded the following reference design:

1. A primary mirror effective diameter of  $\sim 6.5$  m. With the adopted optical design, described below, this effective diameter corresponds to a geometrical diameter of  $\sim 8$  m. Motivated by characteristics of the existing equipment at the Steward Mirror Laboratory, which is fabricating the primary mirror, the adopted geometrical diameter is set to 8.4 m.
2. A visit exposure time of 30 seconds (using two 15 second exposures to efficiently reject cosmic rays), yielding  $\epsilon = 77\%$ .
3. A revisit time of 3 days on average for 10,000 deg $^2$  of sky, with two visits per night.

To summarize, the chosen primary mirror diameter is the *minimum* diameter that simultaneously satisfies the depth ( $r \sim 24.5$  for single visit and  $r \sim 27.5$  for coadded depth) and cadence (revisit time of 3-4 days, with 30 seconds per visit) constraints described above.

### 2.3. System Design Trade-offs

We note that the Pan-STARRS project (Kaiser et al. 2002), with similar science goals as LSST, has adopted a distributed aperture design, where the total system étendue is a sum of étendue values for an array of small telescopes (the prototype PS1 telescope has an étendue 1/24<sup>th</sup> that of LSST). Similarly, the LSST system could perhaps be made as two smaller copies with 6m mirrors, or 4 copies with 4m mirrors, or 16 copies with 2m mirrors. Each of these clones would have to have its own 3 Gigapixel camera (see below), and given the added risk and complexity (e.g., maintenance, data processing), the monolithic design seems advantageous for a system with such a large étendue as LSST.

It is informative to consider the tradeoffs that would be required for a system with a smaller aperture, if the science requirements were to be maintained. For this comparison, we consider a four-telescope version of the Pan-STARRS survey (PS4). With an étendue about 6 times smaller than that of LSST (effective diameters of 6.5 m and 3.0 m, and a field-of-view area of 9.6 deg $^2$  vs.

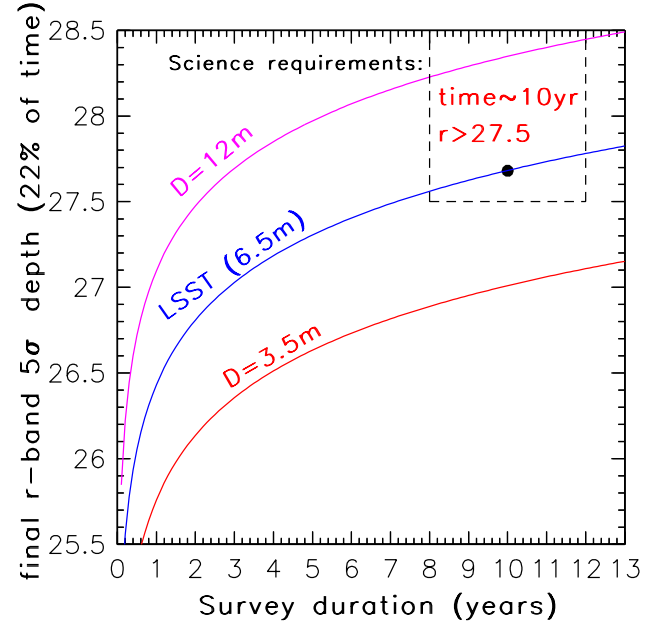


FIG. 2.— The coadded depth in the  $r$  band (AB magnitudes) vs. the effective aperture and the survey lifetime. It is assumed that 22% of the total observing time (corrected for weather and other losses) is allocated for the  $r$  band, and that the ratio of the surveyed sky area to the field-of-view area is 2,000.

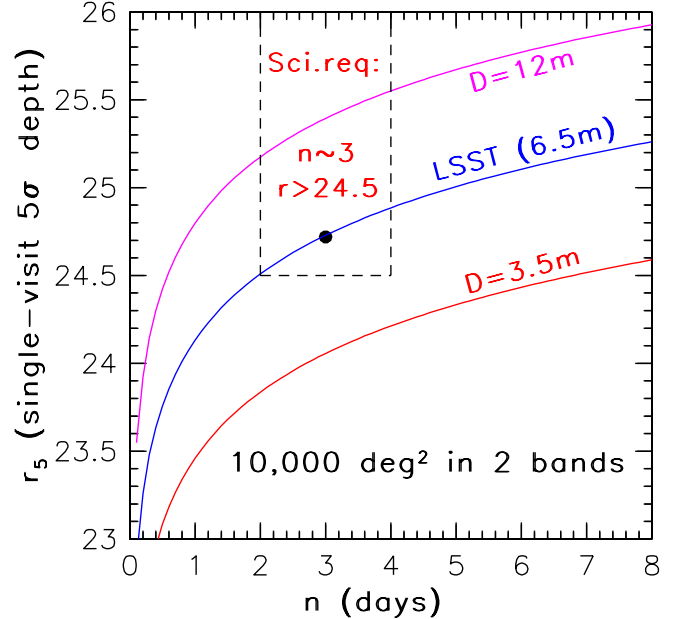


FIG. 3.— The single-visit depth in the  $r$  band ( $5\sigma$  detection for point sources, AB magnitudes) vs. revisit time,  $n$  (days), as a function of the effective aperture size. With a coverage of 10,000 deg $^2$  in two bands, the revisit time directly constrains the visit exposure time,  $t_{vis} = 10n$  seconds. In addition to direct constraints on optimal exposure time,  $t_{vis}$  is also driven by requirements on the revisit time,  $n$ , the total number of visits per sky position over the survey lifetime,  $N_{visit}$ , and the survey efficiency,  $\epsilon$  (see eqs. 1-3). Note that these constraints result in a fairly narrow range of allowed  $t_{vis}$  for the main deep-wide-fast survey.

7.2 deg $^2$ ), and all observing conditions being equal, the PS4 system could in principle use an identical cadence as that of LSST. The main difference in the datasets would

be a faint limit shallower by about 1 mag in a given survey lifetime. As a result, for Euclidean populations the sample sizes would go down by a factor of 4, while for shallower populations (e.g., galaxies around redshift of 1) the samples would be smaller by a factor 2-3. The distance limits for nearby sources, such as Milky Way stars, would drop to 60% of their corresponding LSST values, and the NEO completeness level mandated by the U.S. Congress would not be reached.

If instead the survey coadded depth were to be maintained, then the survey sky area would have to be 6 times smaller ( $\sim 3,500 \text{ deg}^2$ ). If the survey single-visit depth were to be maintained, then the exposure time would have to be about 6 times longer (ignoring the slight difference in the field-of-view area and simply scaling by the étendue ratio), resulting in non-negligible trailing losses for Solar System objects, and either i) a factor of six smaller sky area observed within  $n = 3$  days, or ii) the same sky area revisited every  $n = 18$  days. Given these conflicts, one solution would be to split the observing time and allocate it to individual specialized programs (e.g., large sky area vs. deep coadded data vs. deep single-visit data vs. small  $n$  data, etc.), as is being done by the PS1 Consortium<sup>80</sup>.

In summary, *given the science requirements as stated here, there is a minimum étendue of  $\sim 300 \text{ deg}^2 \text{ m}^2$  which enables our seemingly disparate science goals to be addressed with a single data set.* A system with a smaller étendue would require separate specialized surveys to address the science goals, which results in a loss of surveying efficiency<sup>81</sup>. The LSST is designed to reach this minimum étendue for the science goals stated in its Science Requirements Document.

#### 2.4. The Filter Complement

The LSST filter complement (*ugrizy*, see Fig. 4) is modeled after the Sloan Digital Sky Survey (SDSS) system (Fukugita et al. 1996) because of its demonstrated success in a wide variety of applications, including photometric redshifts of galaxies (Budavári et al. 2003), separation of stellar populations (Lenz et al. 1998; Helmi et al. 2003), and photometric selection of quasars (Richards et al. 2002; Ross et al. 2012). The extension of the SDSS system to longer wavelengths (the *y* band at  $\sim 1$  micron) is driven by the increased effective redshift range achievable with the LSST due to deeper imaging, the desire to study sub-stellar objects, high-redshift quasars, and regions of the Galaxy that are obscured by interstellar dust, and the scientific opportunity enabled by modern CCDs with high quantum efficiency in the near infrared.

The chosen filter complement corresponds to a design “sweet spot”. We have investigated the possibility of replacing the *ugrizy* system with a filter complement that includes only five filters. For example, each filter width could be increased by 20% over the same wavelength range (neither a shorter wavelength range, nor gaps in the wavelength coverage are desirable options), but this option is not satisfactory. Placing the red edge of the *u* band blueward of the Balmer break allows optimal

<sup>80</sup> More information about Pan-STARRS is available from <http://pan-starrs.ifa.hawaii.edu>.

<sup>81</sup> The converse is also true: for every étendue there is a set of optimal science goals that such a system can address with a high efficiency.

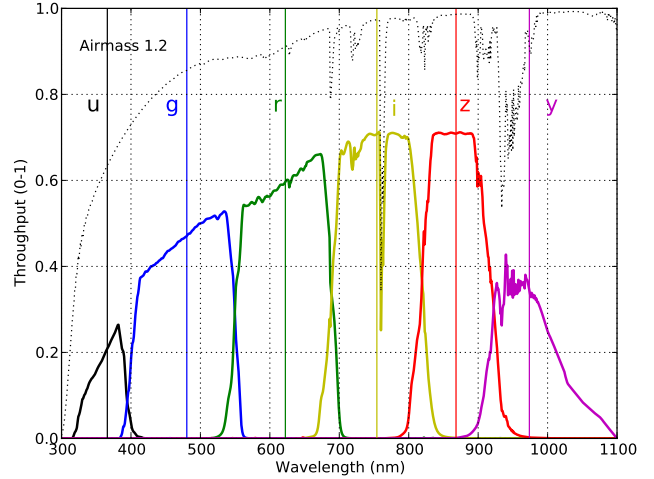


FIG. 4.— The LSST bandpasses. The vertical axis shows the total throughput. The computation includes the atmospheric transmission (assuming an airmass of 1.2, dotted line), optics, and the detector sensitivity.

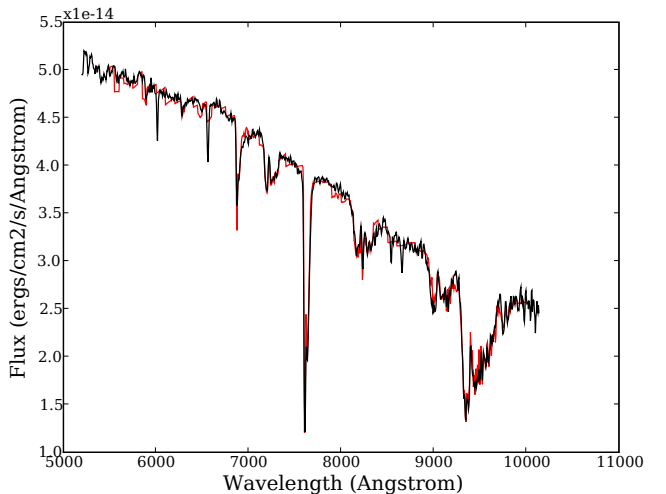


FIG. 5.— An example of determination of the atmospheric opacity by simultaneously fitting a three-parameter stellar model SED (Kurucz 1979) and six physical parameters of a sophisticated atmospheric model (MODTRAN, Anderson et al. 1999) to an observed F-type stellar spectrum ( $F_\lambda$ ). The black line is the observed spectrum and the red line is the best fit. Note that the atmospheric water feature around  $0.9\text{--}1.0 \mu\text{m}$  is exquisitely well fit. The components of the best-fit atmospheric opacity are shown in Fig. 6. Adapted from Burke et al. (2007).

separation of stars and quasars, and the telluric water absorption feature at  $9500\text{\AA}$  effectively defines the blue edge of the *y* band. Of the remaining four filters (*griz*), the *g* band is already quite wide. As a last option, the *riz* bands could be redesigned as two wider bands. However, this option is also undesirable because the *r* and *i* bands are the primary bands for weak lensing studies and for star/galaxy separation, and chromatic atmospheric refraction would worsen the point spread function for a wider bandpass.

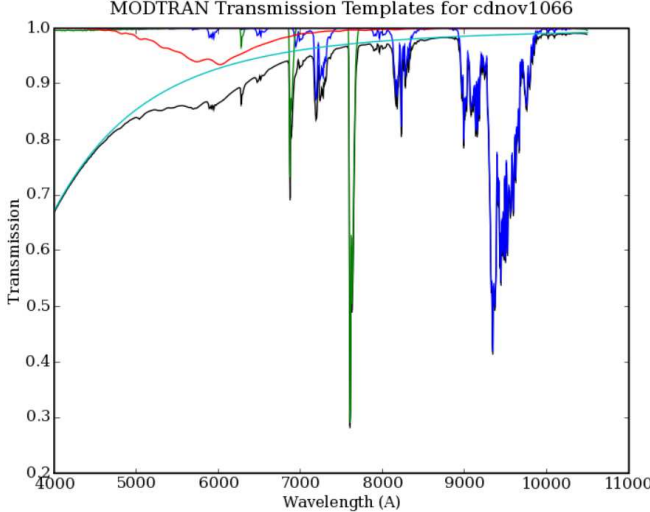


FIG. 6.— The components of the best-fit atmospheric opacity used to model the observed stellar spectrum shown in Fig. 5. The atmosphere model (MODTRAN, Anderson et al. 1999) includes six components: water vapor (blue), oxygen and other trace molecules (green), ozone (red), Rayleigh scattering (cyan), a gray term with a transmission of 0.989 (not shown) and an aerosol contribution proportional to  $\lambda^{-1}$  and extinction of 1.3% at  $\lambda=0.675\text{ }\mu\text{m}$  (not shown). The black line shows all six components combined. Adapted from Burke et al. (2007).

### 2.5. The Calibration Methods

Precise determination of the point spread function across each image, accurate photometric and astrometric calibration, and continuous monitoring of system performance and observing conditions will be needed to reach the full potential of the LSST mission. Extensive precursor data including the massive SDSS dataset and our own data obtained using telescopes close to the LSST site of Cerro Pachón (e.g., the SOAR and Gemini South telescopes), as well as telescopes of similar aperture (e.g., Subaru), indicate that the photometric and astrometric accuracy will be limited not by our instrumentation or software, but rather by atmospheric effects.

SDSS data and PS1 data taken in good photometric conditions have approached the LSST requirement of 1% photometric calibration (Padmanabhan et al. 2008; Schlafly et al. 2012), although measurements with ground-based telescopes typically produce data with errors a factor of two or so larger. Analysis of repeated SDSS scans obtained in varying observing conditions demonstrates that data obtained in non-photometric conditions can also be calibrated with sufficient accuracy (Ivezić et al. 2007b), as long as high-quality photometric data also exist in the region.

The LSST calibration plan builds on experience gained from the SDSS survey. The planned calibration process decouples the establishment of a stable and uniform internal relative calibration from the task of assigning absolute optical flux to celestial objects. Celestial sources will be used to define the internal photometric system and to monitor stability and uniformity of photometric data. There will be  $>100$  main-sequence stars with  $17 < r < 20$  per detector ( $14 \times 14\text{ arcmin}^2$ ) even at high Galactic latitudes. Standardization of photometric scales will be achieved through direct observation of stars with well-understood spectral energy distributions (SEDs).

While the primary source of data used for photometric

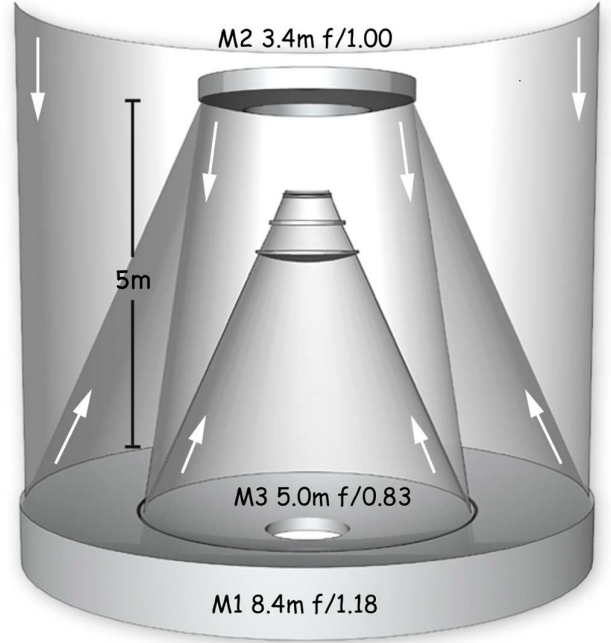


FIG. 7.— The LSST baseline optical design (modified three-mirror Paul-Baker) with its unique monolithic mirror: the primary and tertiary mirrors are positioned such that they form a continuous compound surface, allowing them to be polished from a single substrate.

calibration will be science images taken with the main telescope, these images alone will be insufficient to fully characterize instrumental and atmospheric temporal and spatial variations that can affect photometric measurements. A separate 1.5-meter calibration telescope will obtain spectra of standard stars in LSST fields, calibrating the atmospheric throughput as a function of wavelength (Stubbs et al. 2007; see Figs. 5 and 6). A tunable monochromatic light source, calibrated with a photodiode, will measure the relative throughput of the telescope plus camera system as a function of wavelength (Stubbs & Tonry 2006).

### 2.6. The LSST Reference Design

We briefly describe the reference design for the main LSST system components. Detailed discussion of the flow-down from science requirements to system design parameters, and extensive system engineering analysis can be found in the LSST Science Book (Ch. 2–3).

#### 2.6.1. Telescope and Site

The large LSST étendue is achieved in a novel three-mirror design (modified Paul-Baker Mersenne-Schmidt system; Angel, Lesser & Sarlot 2000) with a very fast  $f/1.234$  beam. The optical design has been optimized to yield a large field of view ( $9.6\text{ deg}^2$ ), with seeing-limited image quality, across a wide wavelength band (320–1050 nm). Incident light is collected by an annular primary mirror, having an outer diameter of 8.4 m and inner diameter of 5.0 m, creating an effective filled aperture of  $\sim 6.5\text{ m}$  in diameter. The collected light is reflected to a 3.4 m convex secondary, then onto a 5 m concave tertiary, and finally into the three refractive lenses of the camera (see Fig. 7). In broad terms, the primary-secondary mirror pair acts as a beam condenser, while the aspheric portion of the secondary and tertiary mirror acts as a

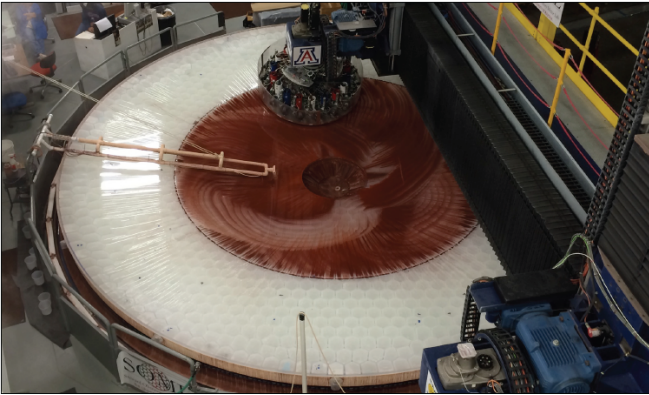


FIG. 8.— The polishing of the primary-tertiary mirror pair at the Steward Observatory Mirror Lab.

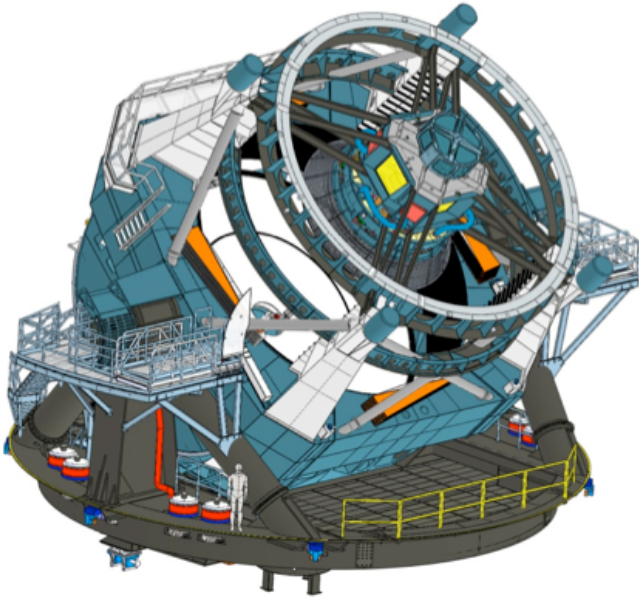


FIG. 9.— The baseline design for the LSST telescope. The small focal ratio allows for a very squat telescope, and thus a very stiff structure. Note the figure of a person for scale.

Schmidt camera. The 3-element refractive optics of the camera correct for the chromatic aberrations induced by the necessity of a thick dewar window and flatten the focal surface. During design optimization, the primary and tertiary mirror surfaces were placed such that the primary's inner diameter coincides with the tertiary's outer diameter, thus making it possible to fabricate the mirror pair from a single monolithic blank using spin-cast borosilicate technology. The secondary mirror is fabricated from a thin 100 mm thick meniscus substrate, made from Corning's ultra-low expansion material. All three mirrors will be actively supported to control wave-front distortions introduced by gravity and environmental stresses on the telescope. The primary-tertiary mirror and the secondary mirror were cast<sup>82</sup> in 2008 and 2009. The primary-tertiary mirror pair is currently being polished at the Steward Observatory Mirror Lab (see Fig. 8) and is expected to be completed in the second half of 2014. The polishing of the secondary should start around that time.

<sup>82</sup> <http://www.lsst.org/News/enews/m1m3-1004.html>

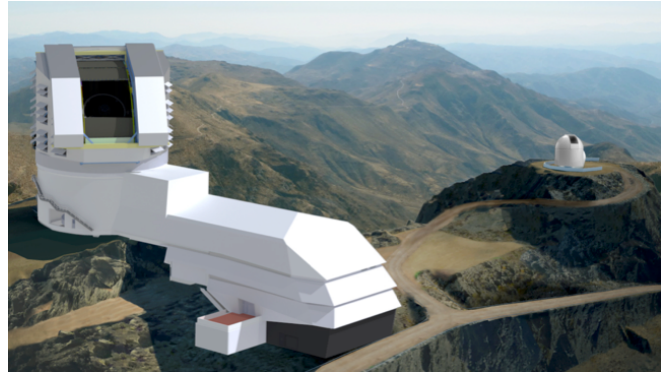


FIG. 10.— The LSST Observatory: artist's rendering of the dome enclosure with the attached summit support building on Cerro Pachón. The LSST calibration telescope is shown on an adjacent rise to the right.

The LSST Observing Facility (Fig. 10), consisting of the telescope enclosure and summit support building, will be constructed atop Cerro Pachón in northern Chile, sharing the ridge with the Gemini South and SOAR telescopes<sup>83</sup> (latitude: S  $30^{\circ} 14' 40.68''$ ; longitude: W  $70^{\circ} 44' 57.90''$ ; elevation: 2652 m; Mamajek 2012). The telescope enclosure houses a compact, stiff telescope structure (see Fig. 9) atop a 15 m high concrete pier with a fundamental frequency of 8 Hz, that is crucial for achieving the required fast slew-and-settle times. The height of the pier was set to place the telescope above the degrading effects of the turbulent ground layer. Capping the telescope enclosure is a 30 m diameter dome with extensive ventilation to reduce dome seeing and to maintain a uniform thermal environment over the course of the night. Furthermore, the summit support building has been oriented with respect to the prevailing winds to shed its turbulence away from the telescope enclosure. The summit support building includes a coating chamber for recoating the three LSST mirrors and clean room facilities for maintaining and servicing the camera.

### 2.6.2. Camera

The LSST camera provides a 3.2 Gigapixel flat focal plane array, tiled by 189  $4\text{K}\times 4\text{K}$  CCD science sensors with  $10\ \mu\text{m}$  pixels (see Figs. 11 and 12). This pixel count is a direct consequence of sampling the  $9.6\ \text{deg}^2$  field-of-view (0.64m diameter) with  $0.2\times 0.2\ \text{arcsec}^2$  pixels (Nyquist sampling in the best expected seeing of  $\sim 0.4\ \text{arcsec}$ ). The sensors are deep depleted high resistivity silicon back-illuminated devices with a highly segmented architecture that enables the entire array to be read in 2 seconds. The detectors are grouped into  $3\times 3$  rafts (see Fig. 13); each contains its own dedicated electronics. The rafts are mounted on a silicon carbide grid inside a vacuum cryostat, with an intricate thermal control system that maintains the CCDs at an operating temperature of 173 K. The entrance window to the cryostat is the third (L3) of the three refractive lenses in the camera. The other two lenses (L1 and L2) are mounted in an optics structure at the front of the camera body, which also contains a mechanical shutter, and a carousel assembly that holds five large optical filters. The sixth optical filter

<sup>83</sup> Coordinates listed in older versions of this paper were incorrect. We thank E. Mamajek for pointing this error to us.

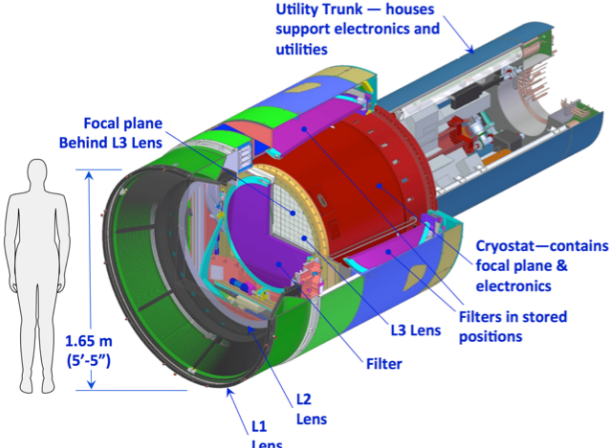


FIG. 11.— A cutaway view of LSST camera. The camera is positioned in the middle of the telescope. The shutter (not shown) is positioned between the filter and lens L3.

can replace any of the five via a procedure accomplished during daylight hours.

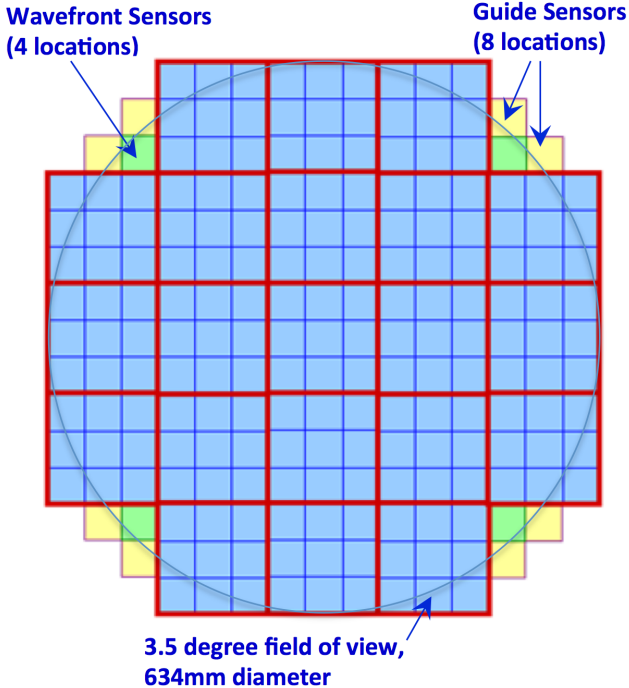


FIG. 12.— The LSST focal plane. Each cyan square represents one  $4096 \times 4096$  pixel sensor. Nine sensors are assembled into a raft; the 21 rafts are outlined in red. There are 189 science sensors, each with 16.8 megapixels, for a total of 3.2 gigapixels.

### 2.6.3. Data Management

The rapid cadence and scale of the LSST observing program will produce approximately 15 TB per night of raw imaging data<sup>84</sup>. The large data volume, the real-time aspects, and the complexity of processing involved makes it impractical to defer the data reduction to the LSST end-users. Instead, the data collected

<sup>84</sup> For comparison, the volume of all imaging data collected over a decade and published in SDSS Data Release 7 (Abazajian et al. 2009) is approximately 16 TB.

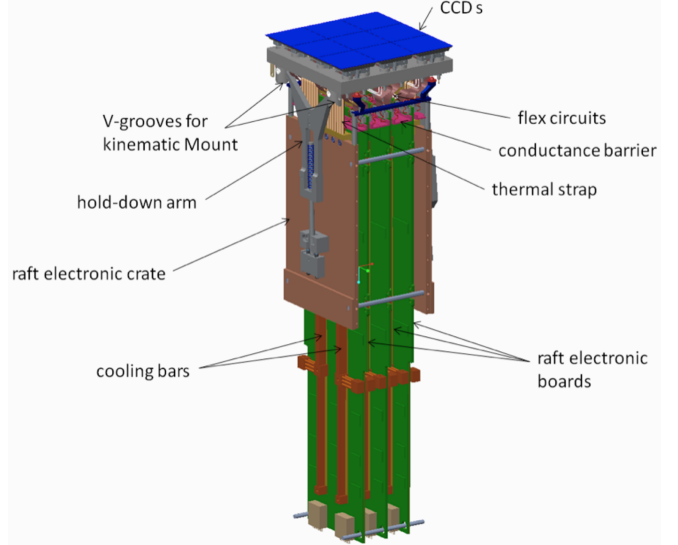


FIG. 13.— The LSST raft module with integrated front-end electronics and thermal connections. Each raft (corresponding to the red squares in Fig. 12) includes 9 sensors, and can be replaced.

by the LSST system will be automatically reduced to scientifically useful catalogs and images by the LSST Data Management (DM) system.

The principal functions of the LSST Data Management system are to:

- Process, in real time, the incoming stream of images generated by the camera system during observing by archiving raw images, generating alerts to new sources or sources whose properties have changed, and updating the relevant catalogs (“Level 1” data products; § 3.3).
- Periodically process the accumulated survey data to provide a uniform photometric and astrometric calibration, measure the properties of all detected objects, and characterize objects based on their time-dependent behavior. The results of such a processing run form a *Data Release* (DR), which is a static, self-consistent data set suitable for use in performing scientific analyses of LSST data and publication of the results (the “Level 2” data products; § 3.3). All data releases will be archived for the entire operational life of the LSST archive.
- Facilitate the creation of added-value (“Level 3”; § 3.3) data products, by providing suitable software, application programming interfaces (APIs), and computing infrastructure at the LSST data access centers.
- Make all LSST data available through an interface that utilizes community-based standards to the maximum possible extent. Provide enough processing, storage, and network bandwidth to enable user analyses of the data without the need for petabyte-scale data transfers.

Over the ten years of LSST operations and 11 data releases, this processing will result in a cumulative *processed* data size approaching 500 petabytes (PB) for imaging, and over 50 PB for the catalog databases. The

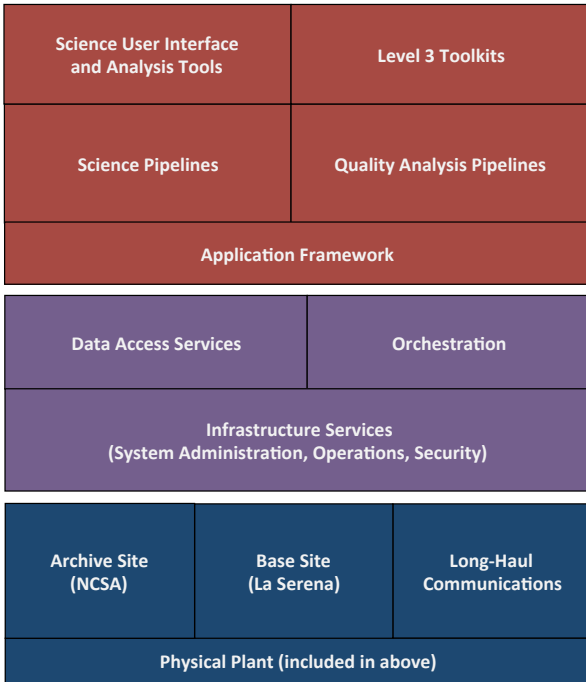


FIG. 14.— The three-layered architecture of the data management system (application [red, top], middleware [purple, middle], and infrastructure [blue, bottom] layers) enables scalability, reliability, and evolutionary capability.

final data release catalog database alone is expected to be approximately 15 PB in size.

The data management system is conceptually divided into three layers: an infrastructure layer consisting of the computing, storage, and networking hardware and system software; a middleware layer, which handles distributed processing, data access, user interface, and system operations services; and an applications layer, which includes the data pipelines and products and the science data archives (see Fig. 14).

Physically, the DM system components will span three key facilities on two continents: the Summit Facility at Cerro Pachón (where the initial detector cross-talk correction will be performed), the Base Facility in La Serena (which will serve as a retransmission hub for data uploads to North America, as well as the data access center for the Chilean community), and the central Archive Facility at the National Center for Supercomputing Applications (NCSA) in Champaign, Illinois All Level 1 (nightly) and Level 2 (data release) processing will take place at the Archive Facility, which will also serve as a data access center for the US community.

The data will be transported between the centers over existing high-speed optical fiber links from South America to the U.S. (see Fig. 15). Although the data processing center will have substantial computing power (e.g., the central facility will peak at  $\sim 1.6$  petaflops of compute power), the continuation of current trends suggests that the center will not qualify for the top 500 list by the time of first light. Hence, while LSST is making a novel use of advances in information technology, it is not taking the risk of pushing the expected technology to the limit, reducing the overall risk to the project.

A novel aspect of the LSST DM system will be its “Level 3” capabilities, allowing the end-users to create, store, and share custom data products not created by standard LSST processing. These could be new catalogs created by simple post-processing of the LSST data release catalogs, or entirely new data products generated by running custom code on raw LSST data. The LSST software stack (described below) will be made available to LSST end-users, as a basis on which to quickly build such code. Approximately 10% of the total budget for the LSST Archive Center compute and storage capacity has been reserved for end-user, Level 3, processing support infrastructure<sup>85</sup>.

#### 2.6.4. *The LSST software stack*

The *LSST Software Stack* is a well documented, state-of-the-art, high-performance, scalable, multi-camera, open source, O/IR survey data processing and analysis system, built to enable LSST survey data reduction and the writing of custom, user-driven, code for Level 3 processing. It comprises all science pipelines needed to accomplish LSST data processing tasks (e.g., calibration, single frame processing, coaddition, image differencing, multi-epoch measurement, asteroid orbit determination, etc.), the necessary data access and orchestration middleware, as well as the database and user interface components.

Algorithm development for the LSST software builds on the expertise and experience of prior large astronomical surveys (including SDSS, Pan-STARRS, DES, SuperMACHO, ESSENCE, DLS, CFHTLS, and UKIDSS). The pipelines written for these surveys have demonstrated that it is possible to carry out largely autonomous data reduction of large data sets, automated detection of sources and objects, and the extraction of scientifically useful characteristics of those objects. While firmly rooted in this prior history, the LSST software stack has largely been written anew, for reasons of performance, extendability, and maintainability. All LSST codes have been designed and implemented following software engineering best practices, including modularity, clear definition of interfaces, continuous integration, utilization of unit testing, a single set of documentation and coding standards, and others. The primary implementation language is Python and, where necessary for performance reasons, C++<sup>86</sup>.

The LSST data management software has been prototyped for over eight years. It has been exercised in eight data challenges, with increasing degrees of complexity. Besides processing simulated LSST data (§ 2.7.3), it has been used to process images from CFHTLS and SDSS (Abazajian et al. 2009). As an example, Figure 16 shows a small region in the vicinity of M2 taken from a large coaddition of SDSS Stripe 82 data, generated with LSST software stack prototypes.

The LSST software stack is free software, licensed un-

<sup>85</sup> Furthermore, the data management system architecture will enable Level 3 tasks to “piggyback” onto annual Level 2 reprocessings, leveraging considerable I/O and computing resources employed in the production of a data release.

<sup>86</sup> All components implemented in C++ have been wrapped and exposed as Python modules to the rest of the system. Python truly is the “native language of LSST”.

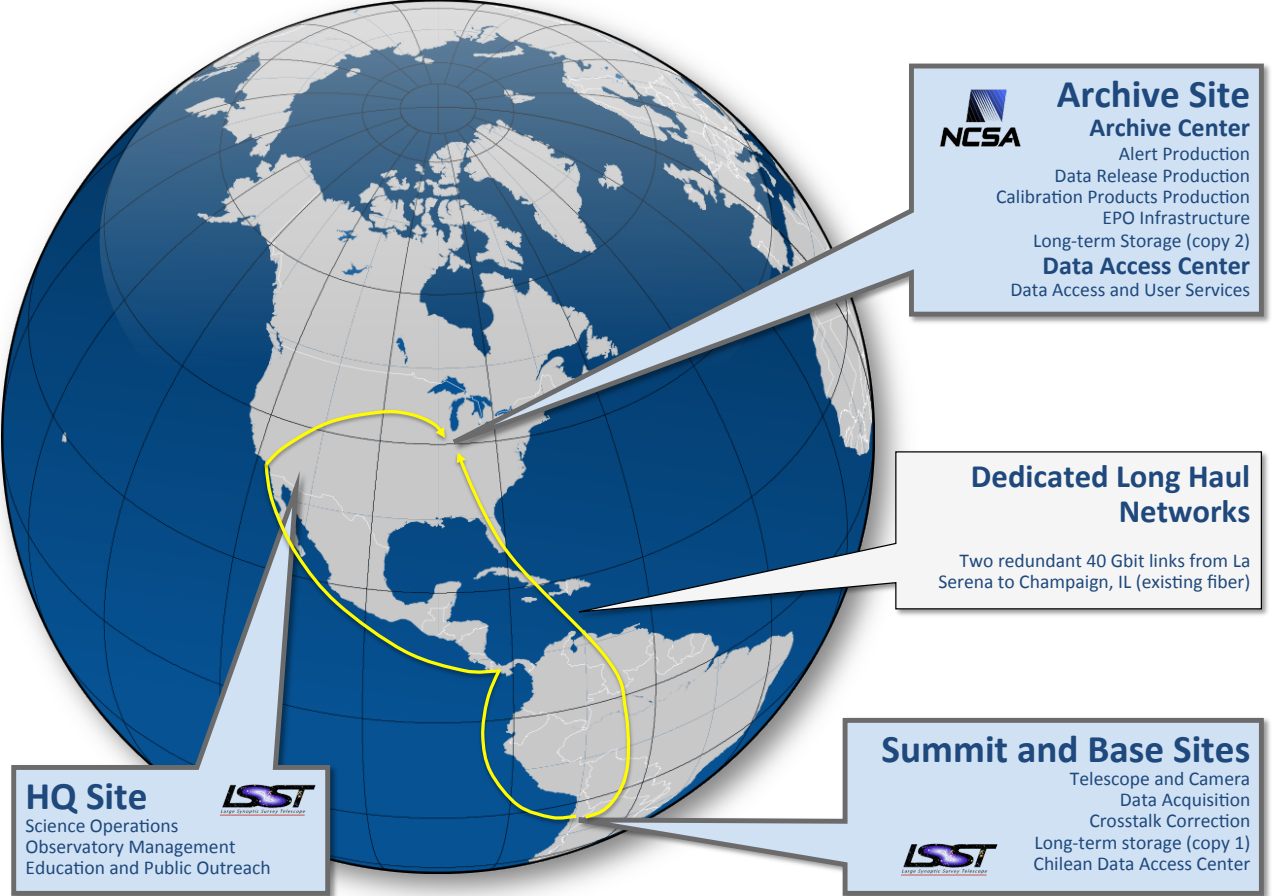


FIG. 15.— The LSST data flow from the mountain summit/base facility in Chile to the data access center and archive centers in the U.S.

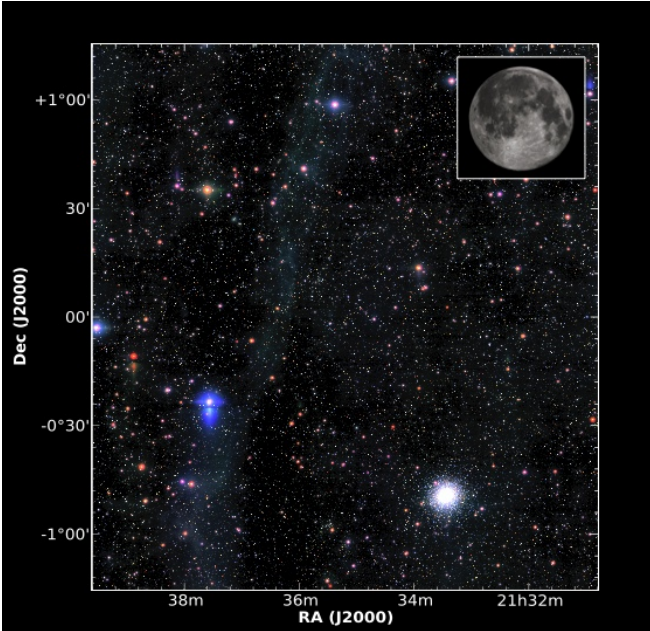


FIG. 16.— A small region in the vicinity of globular cluster M2, taken from a coadd of SDSS Stripe 82 data produced with LSST software stack prototypes. The coaddition employs a novel “background matching” technique that improves background estimation and preserves the diffuse structures in the resulting coadd. The full coadd can be browsed at <http://moe.astro.washington.edu/sdss>.

der the terms of the GNU General Public License, Version 3. The stack prototype code and documentation are available via <http://ls.st/ug>. Its open source nature, an open development process, attention to software engineering, a long-term project commitment and a modular design that can be modified for use with other cameras may make it useful for the processing of imaging data beyond LSST.

### 2.7. Simulating the LSST System

Throughout its design, construction and commissioning, the LSST needs to be able demonstrate that it can achieve the requirements laid out in the Science Requirements Documents (SRD) given its design and as-delivered components, that the system can be calibrated to the required level of fidelity, that the data management software can extract the appropriate astrophysical signals, and that this can be achieved with sufficient efficiency such that the telescope can complete its primary objectives within the ten years of its duration (including surveying 18,000 sq degrees of the sky, and completing the Deep Drilling Fields, see §3.1.2).

Realizing these objectives requires that the project can characterize the performance of the LSST including the performance of the opto-mechanical systems, the response of the detectors and their electronics, and the

capabilities of the analysis software. A simulation framework provides such a capability; delivering a virtual prototype LSST against which design decisions, optimizations (including descoping), and trade studies can be evaluated (Connolly et al. 2010).

The framework underlying the LSST simulations is designed to be extensible and scalable (i.e. capable of being run on a single processor or across many-thousand core compute clusters). It comprises four primary components: a simulation of the survey scheduler (§ 2.7.1), databases of simulated astrophysical catalogs of stars, galaxies, quasars and Solar System objects (§ 2.7.2), a system for generating observations based on the pointing of the telescope, and a system for generating realistic LSST images of a given area of sky (§ 2.7.3). Computationally intensive routines are written in *C/C++* with the overall framework and database interactions using *Python*. The purpose of this design is to enable the generation of a wide range of data products for use by the collaboration; from all-sky catalogs used in simulations of the LSST calibration pipeline, to studies of the impact of survey cadence on recovering variability, to simulated images of a single LSST focal plane.

### 2.7.1. The LSST Operations Simulator

The LSST Operations Simulator was developed to enable a detailed quantitative analysis of the various science tradeoffs described in this paper. It contains detailed models of site conditions, hardware and software performance, and an algorithm for scheduling observations which will, eventually, drive the largely robotic observatory. Observing conditions include a model for seeing derived from an extensive body of on-site MASS/DIMM (Multi-Aperture Scintillation Sensor and Differential Image Motion Monitor) measurements obtained during site selection and characterization (see Fig. 1). It not only reproduces the observed seeing distribution, but includes the auto-correlation spectrum of seeing with time over intervals from minutes to seasons. Weather data are taken from ten years of hourly measurements at nearby Cerro Tololo. The time history of site conditions is important if the simulation is to faithfully reproduce a sequence of observations. Thus, for example, the simulator correctly represents the variation of limiting magnitude between pairs of observations used to detect NEOs and the correlation between, for example, seasonal weather patterns and observing conditions at any given point on the sky. In addition, down time for observatory maintenance is also included.

The signal-to-noise ratio of each observation is determined using a sky background model which includes the dark sky brightness in each filter, the effects of seeing and atmospheric transparency, and a detailed model for scattered light from the moon and/or twilight at each observation. The time taken to move from one observation to the next is given by a detailed model of the camera, telescope, and dome. It includes such effects as the acceleration/deceleration profiles employed in moving the telescope, the dome, and the wind screen, the time needed to damp vibrations excited by each slew, cable wrap, the time taken for active optics lock and correction as a function of slew distance, and the time for filter changes and focal plane readout.

Observations are scheduled by a ranking algorithm.

After a given exposure, all possible next observations are assigned a score which depends upon their locations, times, and filters according to a set of scientific requirements which can vary with time and location. For example, if an ecliptic field has been observed in the  $r$  band, the score for another  $r$ -band observation of the same field will initially be quite low, but it will rise in time to peak about an hour after the first observation, and decline thereafter. This algorithm results in observations being acquired as pairs roughly an hour apart, which enables efficient association of NEO detections. To ensure uniform sky coverage, fields with fewer previous observations will be scored more highly than those which have already been observed more frequently.

Once all possible next observations have been scored for scientific priority, their scores are modified according to observing conditions (e.g., seeing, airmass, and sky brightness) and to criteria such as low slew time to move from the current position, time required to change filters, etc. The highest-ranked observation is then performed, and the cycle repeats. The result of a simulator run is a detailed history of which locations on the sky were observed when, in what filter, and with what sky background, seeing and other observing conditions. It takes a few days to produce a decade-long simulation using an average PC.

### 2.7.2. Catalog Generation

The simulated astronomical catalogs are stored in an SQL database. This base catalog is queried using sequences of observations derived from the Operations Simulator. Each simulated pointing provides a position and time of the observation together with the appropriate sky conditions (e.g. seeing, moon phase and angle, sky brightness and sky transparency). Positions of sources are propagated to the time of observation (including proper motions for stars and orbits for Solar System sources). Magnitudes and source counts are derived using the atmospheric and filter response functions appropriate for the airmass of the observation and after applying corrections for source variability. The resulting catalogs are then formatted for either output to users, or fed into an image simulator. Images are generated by ray-tracing individual photons through the atmosphere, telescope and camera systems. Photons are drawn from the spectral energy distributions that define the simulated sources and ray-traced through the atmosphere and optical system before conversion to electrons by simulating the camera physics. Images are read out using a simulation of the camera electronics and amplifier layout and formatted for ingestion into the LSST data management system. All observing conditions, defined by the Operations Simulator, are propagated through the catalog and image generation to preserve fidelity and consistency between the derived catalogs and images.

The current version of the LSST simulation framework incorporates galaxies derived from an N-body simulation of a  $\Lambda$ CDM cosmology, quasars/AGNs, stars that match the observed stellar distributions within our Galaxy, asteroids generated from simulations of our Solar System, and a 3-D model for Galactic extinction. Stellar sources are based on the Galactic structure models of Jurić et al. (2008) and include thin-disk, thick-disk, and halo star components. The distribution and colors of the stars

match those observed by SDSS. Each star in the simulation is matched to a template spectral energy distribution (SED). Kurucz (1993) model spectra are used to represent main-sequence F, G, and K stars as well as RGB stars, blue horizontal branch stars, and RR Lyrae variables. SEDs for white dwarf stars are taken from Bergeron et al. (1995). SEDs for M, L, and T dwarfs are generated from a combination of spectral models and by stacking spectra from the SDSS (e.g., Cushing et al. 2005, Bochanski et al. 2007, Burrows et al. 2006, Petterson & Hawley 1989, Kowalski et al. 2010). The adopted metallicity for each star is based on a model from Ivezić et al. (2008a), and proper motions are based on the kinematic model of Bond et al. (2010). Light curve templates are randomly assigned to a subset of the stellar population so that variability may also be simulated. For Galactic reddening, a value of  $E(B-V)$  is assigned to each star using the three-dimensional Galactic model of Amores & Lepine (2005). To provide consistency with the modeling of extragalactic fluxes in the simulations, the dust model in the Milky Way integrated to 100 kpc is re-normalized to match the Schlegel et al. (1998) dust maps.

Galaxy catalogs are derived from the Millennium simulations of de Lucia et al. (2006). These models extend pure dark matter N-body simulations to include gas cooling, star formation, supernovae and AGN, and are designed to reproduce the observed colors, luminosities, and clustering of galaxies as a function of redshift. To generate the LSST simulated catalogs, a light cone, covering redshifts  $0 < z < 6$ , was constructed from 58 simulation snapshots  $500\text{h}^{-1}\text{Mpc}$  on a side. This light cone extends to a depth of approximately  $r = 28$  and covers a  $4.5^\circ \times 4.5^\circ$  footprint on the sky. Replicating this catalog across the sky simulates the full LSST footprint. As with the stellar catalog, an SED is fit to the colors of each source using Bruzual & Charlot (2003) spectral synthesis models. These fits are undertaken separately for the bulge and disk components and, for the disk, include inclination-dependent reddening. Morphologies are modeled using two Sersic profiles. The bulge-to-disk ratio and disk scale lengths are taken from de Lucia et al. (2006). Half-light radii for bulges are estimated using the empirical absolute-magnitude vs. half-light radius relation given by Gonzalez et al. (2009). Comparisons between the redshift and number-magnitude distributions of the simulated catalogs with those derived from deep imaging and spectroscopic surveys showed that the de Lucia et al. models under-predict the density of sources at faint magnitudes and high redshifts. To correct for these effects, sources are cloned in magnitude and redshift space until their densities reflect the average observed properties.

Quasar/AGN catalogs are generated using the Bonfigiorno et al. (2007) luminosity function for  $M_B < -15$ , over an area of  $100 \text{ deg}^2$ . Their observed SEDs are generated using a composite rest-frame spectrum derived from SDSS data by Vanden Berk et al. (2001). The host galaxy is selected to have the closest match to the preferred stellar mass and color at the AGN's redshift, following the results from Xue et al. (2010). Each galaxy hosts at most one AGN, and no explicit distinction is made between low-luminosity AGN and quasars that dramatically outshine their host galaxies. The light curve for each AGN is generated using a damped ran-

dom walk model and prescriptions given by MacLeod et al. (2010).

Asteroids are simulated using the Solar System models of Grav et al. (2007). They include: Near Earth Objects (NEOs), Main Belt Asteroids, the Trojans of Mars, Jupiter, Saturn, Uranus, and Neptune, Trans Neptunian Objects, and Centaurs. Spectral energy distributions are assigned using the C and S type asteroids of DeMeo et al. (2009). Positions for the 11 million asteroids in the simulation are stored within the base catalog (sampled once per night for the ten year duration of the LSST survey). We generate accurate ephemerides of all asteroids falling within a given LSST point using the *PyOrb* software package (Granvik et al. 2009). With typically 8000 sources per LSST field of view, this procedure significantly reduces the computational resources required to simulate asteroid ephemerides.

### 2.7.3. Image Simulations

The framework described above provides a parametrized view of the sky above the atmosphere. To generate images, photons are drawn from the spectral energy distribution of each source (scaled to the appropriate flux density based on the apparent magnitude of a source and accounting for the spatial distribution of light for extended sources). Each photon is ray-traced through the atmosphere, telescope and camera to generate a CCD image. The atmosphere is modeled using a Taylor frozen screen approximation (with the atmosphere described by six layers). The density fluctuations within these screens are described by a Kolmogorov spectrum with an outer scale (typically 10m to 200m). All screens move during an exposure with velocities derived from NOAA measurements of the wind velocities above the LSST site in Chile. Typical velocities are on the order of  $20 \text{ m s}^{-1}$ , and are found to have a seasonable dependence that is modeled when generating the screens. Each photon's trajectory is altered due to refraction as it passes through each screen.

After the atmospheric refraction, photons are reflected and refracted by the optical surfaces within the telescope and camera. The mirrors and lenses are simulated using geometric optics techniques in a fast ray-tracing algorithm and all optical surfaces include a spectrum of perturbations based on design tolerances. Each optic moves according to its six degrees of freedom within tolerances specified by the LSST system. Fast techniques for finding intercepts on the aspheric surface and altering the trajectory of a photon by reflection or wavelength-dependent refraction have been implemented to optimize the efficiency of the simulated images. Wavelength and angle-dependent transmission functions are incorporated within each of these techniques, including simulation of the telescope spider.

Ray tracing of the photons continues into the silicon of the detector. The conversion probability, refraction as a function of wavelength and temperature, and charge diffusion within the silicon are modeled for all photons. Photons are pixelated and the readout process simulated including blooming, charge saturation, charge transfer inefficiency, gain and offsets, hot pixels and columns, and QE variations. The sky background is added as a post-processing step, and includes Rayleigh scattering of the



FIG. 17.— A simulated image of a single LSST CCD (covering a  $13.3 \times 13.3$  arcmin<sup>2</sup> region of the sky). The image is a color composite (Lupton et al. 2004) from a set of 30 second *gri* visits.

moon's light, based on SEDs for the full moon and the dark sky. The background is vignetted according to the results of ray-trace simulations.

The simulator generates  $\sim 300,000$  photons per second on an average workstation. To produce simulated data corresponding to a night of regular LSST operations requires approximately 0.5-1 million CPU hours and, therefore, necessitates the use of large compute clusters. An example of a simulated image is shown in Fig. 17.

### 3. ANTICIPATED DATA PRODUCTS AND THEIR CHARACTERISTICS

The LSST observing strategy is designed to maximize the scientific throughput by minimizing slew and other downtime and by making appropriate choices of the filter bands given the real-time weather conditions. Using

simulated surveys produced with the Operations Simulator described in § 2.7.1, we illustrate predictions of LSST performance with two examples.

#### 3.1. The Baseline LSST Surveys

The fundamental basis of the LSST concept is to scan the sky deep, wide, and fast, and to obtain a dataset that simultaneously satisfies the majority of the science goals. We present here a specific realization, the so-called “universal cadence”, which yields the main deep-wide-fast survey and meets our core science goals. However, at this writing, there is a vigorous discussion of cadence plans in the LSST community, exploring variants and alternatives that enhances various specific science programs, while maintaining the science requirements described in

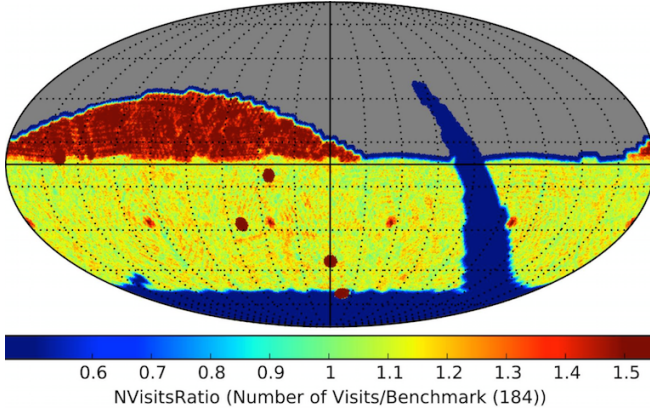


FIG. 18.— The distribution of the  $r$  band visits on the sky for a simulated realization of the baseline cadence. The sky is shown in the equal-area Mollweide projection in equatorial coordinates (the vernal equinoctial point is in the center, and the right ascension is increasing from right to left). The number of visits for a 10-year survey, normalized to the SRD design value of 184, is color-coded according to the legend. The two regions with smaller number of visits than the main survey (“mini-surveys”) are the Galactic plane (arc on the right) and the region around the South Celestial Pole (bottom). The so-called “northern Ecliptic region” (upper left) has received more visits than the main survey in this particular simulation (in order to increase completeness for moving objects by increasing the coverage of the Ecliptic plane). Deep drilling fields, with a much higher number of visits than the main survey, are also visible as small circles. The fields were dithered on sub-field scales and pixels with angular resolution of  $\sim 30$  arcmin were used to evaluate and display the coverage.

the SRD.

The main deep-wide-fast survey will use about 90% of the observing time. The remaining 10% of the observing time will be used to obtain improved coverage of parameter space such as very deep ( $r \sim 26$ ) observations, observations with very short revisit times ( $\sim 1$  minute), and observations of “special” regions such as the Ecliptic, Galactic plane, and the Large and Small Magellanic Clouds. We are also considering a third type of survey, micro-surveys, that would use about 1% of the time (which still represents 25 nights on a unique 8m-class telescope).

### 3.1.1. The Main Deep-Wide-Fast Survey

The observing strategy for the main survey will be optimized for the homogeneity of depth and number of visits. In times of good seeing and at low airmass, preference is given to  $r$ -band and  $i$ -band observations. As often as possible, each field will be observed twice, with visits separated by 15-60 minutes. This strategy will provide motion vectors to link detections of moving objects in the Solar System, and fine-time sampling for measuring short-period variability. The ranking criteria also ensure that the visits to each field are widely distributed in position angle on the sky and rotation angle of the camera in order to minimize systematic effects in galaxy shape determination.

The universal cadence provides most of LSST’s power for detecting Near Earth Objects (NEO) and naturally incorporates the southern half of the ecliptic within its 18,000 square degrees (the northern half lies above the desired airmass limits,  $X \lesssim 1.5$ ). NEO sample completeness for the smallest bodies ( $\sim 140$ m in diameter, per the Congressional NEO mandate) is greatly enhanced, however, by the addition of a crescent on the sky within 10

degrees of the northern ecliptic (see Fig. 18). Thus, we plan to extend the universal cadence to this region using the  $r$  and  $i$  filters only, along with more relaxed limits on airmass and seeing. Relaxed limits on airmass and seeing are also adopted for  $\sim 700$  deg $^2$  around the South Celestial Pole, allowing coverage of the Large and Small Magellanic Clouds.

Finally, the universal cadence proposal excludes observations in a region of 1,000 square degrees around the Galactic Center, where the high stellar density leads to a confusion limit at much brighter magnitudes than those attained in the rest of the survey. Within this region, the Galactic Center proposal provides 30 observations in each of the six filters, distributed roughly logarithmically in time (it may not be necessary to use the  $u$  and  $g$  filters for this heavily extinguished region).

The resulting sky coverage for the LSST baseline cadence, based on detailed operations simulations, is shown for the  $r$  band in Fig. 18. The anticipated total number of visits for a ten-year LSST survey is about 2.8 million ( $\sim 5.6$  million 15-second long exposures). The per-band allocation of these visits is shown in Table 1.

### 3.1.2. Mini-surveys

Although the uniform treatment of the sky provided by the universal cadence proposal can satisfy the majority of LSST scientific goals, roughly 10% of the time will be allocated to other strategies that significantly enhance the scientific return. These surveys aim to extend the parameter space accessible to the main survey by going deeper or by employing different time/filter sampling.

As an example of a mini-survey, consider a program that uses one hour of observing time per night to observe a relatively small region of sky to substantially greater depth in individual visits. Accounting for read-out time and filter changes, it could obtain about 50 consecutive 15-second exposures in each of four filters in an hour. If a field is visited every two days over four months, about 600 deg $^2$  can be observed with this cadence over 10 years. Taking weather into account, the selected fields would each have on average about 40 hour-long sequences of 200 exposures each. Each observation in a sequence would have an equivalent 5- $\sigma$  depth of  $r \sim 24.5$ , and each filter subsequence when coadded would be 2 magnitudes deeper than the main survey visits ( $r \sim 26.5$ ). When all 40 sequences and the main survey visits are coadded, they would extend the depth to  $r \sim 28$ .

This data set would be excellent for a wide variety of science programs. The individual sequences would be sensitive to 1% variability on hourly time scales, allowing discovery of planetary eclipses. If these fields were selected at Galactic latitudes of  $|b| \sim 30$  deg, they would include about 10 million stars with  $r < 21$  observed with signal-to-noise ratio above 100 in each visit. When subsequences from a given night were coadded, they would provide dense time sampling to a faint limit of  $r \sim 26.5$  (assuming observations in 4 bands, every 2 days over 120 days, and accounting for weather losses), and thus enable deep searches for SN, trans-Neptunian objects, and other faint transient, moving and variable sources. For example, the SN sample would be extended to redshifts of  $z \sim 1.2$ , with more densely sampled light curves than obtained from the universal cadence. Such sequences would also serve as excellent tests of our photometric calibra-

TABLE 2  
THE PARAMETERS FROM Eqs. 5 AND 6

	<i>u</i>	<i>g</i>	<i>r</i>	<i>i</i>	<i>z</i>	<i>y</i>
$m_{sky}^a$	22.9	22.3	21.2	20.5	19.6	18.6
$\theta^b$	0.77	0.73	0.70	0.67	0.65	0.63
$\gamma^c$	0.037	0.038	0.039	0.039	0.040	0.040
$k_m^d$	0.451	0.163	0.087	0.065	0.043	0.138
$C_m^e$	22.92	24.29	24.33	24.20	24.07	23.69
$m_5^f$	23.68	24.89	24.43	24.00	24.45	22.60
$\Delta C_m^{\infty,g}$	0.67	0.21	0.11	0.08	0.05	0.04
$\Delta C_m(2)^h$	0.24	0.09	0.05	0.04	0.03	0.02
$\Delta m_5^i$	0.21	0.15	0.14	0.13	0.13	0.15

<sup>a</sup> The expected median zenith sky brightness at Cerro Pachón, derived from the median dark sky brightness observed by SDSS (AB mag arcsec<sup>-2</sup>).

<sup>b</sup> The expected delivered median zenith seeing (arcsec). For larger airmass,  $X$ , seeing is proportional to  $X^{0.6}$ .

<sup>c</sup> The band-dependent parameter from Eq. 5.

<sup>d</sup> Adopted atmospheric extinction.

<sup>e</sup> The band-dependent parameter from Eq. 6.

<sup>f</sup> The typical  $5\sigma$  depth for point sources at zenith, assuming exposure time of  $2 \times 15$  sec, and observing conditions as listed. For larger airmass the  $5\sigma$  depth is brighter; see the bottom row.

<sup>g</sup> The loss of depth due to instrumental noise (assuming 9 e<sup>-</sup> per pixel and readout, and two readouts per visit).

<sup>h</sup> Additive correction to  $C_m$  when exposure time is doubled from its fiducial value to 60 sec.

<sup>i</sup> The loss of depth at airmass of  $X = 1.2$  due to seeing degradation and increased atmospheric extinction.

tion procedures.

The LSST has already selected four distant extragalactic survey fields<sup>87</sup> that the project guarantees to observe as Deep Drilling Fields with deeper coverage and more frequent temporal sampling than provided by the standard LSST observing pattern. These fields (Elias S1, XMM-LSS, Extended Chandra Deep Field-South, and COSMOS) are well-studied survey fields with substantial existing multiwavelength coverage and other positive attributes. These four fields are only the first chosen for deep-drilling observations; more such fields will be chosen later.

The baseline universal cadence is by no means the definitive plan for the entire survey. Rather, it represents a proof of concept that it is indeed possible to design a universal cadence which addresses a wide variety of science goals in a nearly optimal way. We are undertaking a vigorous and systematic research effort to explore the enormously large parameter space of possible surveys. The scientific commissioning period will be used to test the usefulness of various observing modes and to explore alternative strategies. Proposals from the community for specialized cadences (such as mini-surveys and micro-surveys) will also be considered.

### 3.2. Detailed Analysis of Simulated Surveys

As examples of analysis enabled by the Operations Simulator, we describe determination of the completeness of the LSST NEO sample, and estimation of errors expected for trigonometric parallax and proper motion measurements. In both examples, the conclusions crucially depend on assumed signal-to-noise ratios, described next.

<sup>87</sup> For details, see <http://www.lsst.org/News/enews/deep-drilling-201202.html>

#### 3.2.1. Expected Photometric Signal-to-Noise Ratio

The output of operations simulations is a data stream consisting of a position on the sky and the time of observation, together with observing conditions such as seeing and sky brightness. The expected photometric error (the inverse of the signal-to-noise ratio) for a single visit can be written as

$$\sigma_1^2 = \sigma_{sys}^2 + \sigma_{rand}^2, \quad (4)$$

where  $\sigma_{rand}$  is the random photometric error and  $\sigma_{sys}$  is the systematic photometric error (includes errors due to, e.g., imperfect modeling of the point spread function, but does not include errors in absolute photometric zeropoint). The calibration system and procedures are designed to maintain  $\sigma_{sys} < 0.005$  mag. Based on SDSS experience (Sesar et al. 2007), the random photometric error for point sources, as a function of magnitude, is well described<sup>88</sup> by

$$\sigma_{rand}^2 = (0.04 - \gamma) x + \gamma x^2 \text{ (mag}^2\text{)}, \quad (5)$$

with  $x \equiv 10^{0.4(m-m_5)}$ . Here  $m_5$  is the  $5\sigma$  depth (for point sources) in a given band, and  $\gamma$  depends on the sky brightness, readout noise, etc. Detailed determination of the system throughput yields the values of  $\gamma$  listed in Table 2. The  $5\sigma$  depth for point sources is determined from

$$m_5 = C_m + 0.50(m_{sky} - 21) + 2.5 \log_{10}(0.7/\theta) + 1.25 \log_{10}(t_{vis}/30) - k_m(X - 1) \quad (6)$$

where  $m_{sky}$  is the sky brightness (AB mag arcsec<sup>-2</sup>),  $\theta$  is the seeing (FWHM, in arcsec),  $t_{vis}$  is the exposure time (seconds),  $k$  is the atmospheric extinction coefficient, and  $X$  is airmass.

The constants  $C_m$  depend on the overall throughput of the instrument and are computed using currently the best available throughput estimates for optical elements and sensors. The resulting  $C_m$  values are listed in Table 2 and in all six bands they imply single visit depths (also listed in Table 2) in the range between minimum and design specification values from the Science Requirements Document listed in Table 1. The differences in performance between LSST and, for example, SDSS are easily understood<sup>89</sup>.

The structure of eq. 6 nicely illustrates decoupling between the system sensitivity which is fully absorbed into  $C_m$  and observing conditions (system deployment parameters) specified by  $m_{sky}$ ,  $\theta$ ,  $t_{vis}$ ,  $k_m$  and  $X$ . The computation of  $C_m$  listed in Table 2 assumed instrumental noise of 9 e<sup>-</sup> per pixel and per readout, which has by and large negligible effect on  $m_5$  in all bands except for the *u* band. This loss of depth due to instrumental noise,  $\Delta C_m^\infty$ , is listed in Table 2; it also corresponds to additive

<sup>88</sup> Eq. 5 can be derived from  $\sigma_{rand} = N/S$ , where  $N$  is noise and  $S$  is signal, and by assuming that  $N^2 = N_o^2 + \alpha S$ . The constants  $N_o$  and  $\alpha$  can be expressed in terms of a single unknown constant  $\gamma$  by using the condition that  $\sigma_{rand} = 0.2$  for  $m = m_5$ .

<sup>89</sup> SDSS data typically reach a  $5\sigma$  depth for point sources of  $r = 22.5$  with an effective aperture of  $D = 2.22$  m, an exposure time of  $t_{vis} = 54$  sec, the median *r* band sky brightness of  $r_{sky} = 20.9$  mag arcsec<sup>-2</sup>, the median seeing of  $\theta = 1.5$  arcsec, and the median airmass of  $X = 1.3$ . In comparison, the LSST loss of depth is 0.32 mag due to shorter exposures, while the gains are 1.17 mag due to larger aperture, 0.83 mag due to better seeing, 0.20 mag due to fainter sky, for the net gain of  $\sim 1.9$  mag.

correction to  $C_m$  when the exposure time  $t_{vis} \rightarrow \infty$ . To predict  $5\sigma$  depths for exposure time  $\tau$  times longer than the fiducial  $t_{vis} = 30$  sec., the following correction has to be added to  $C_m$  listed in Table 2:

$$\Delta C_m(\tau) = \Delta C_m^\infty - 1.25 \log_{10} \left[ 1 + \frac{10^{(0.8 \Delta C_m^\infty)} - 1}{\tau} \right]. \quad (7)$$

Of course,  $\Delta C_m(\tau = 1) = 0$ . Again, this effect is only substantial in the  $u$  band, as demonstrated by  $\Delta C_m(\tau = 2)$  listed in Table 2.

The loss of depth at the airmass of  $X = 1.2$  due to seeing degradation and increased atmospheric extinction is listed in the last row in Table 2. Note that the uncertainty of limiting depth predictions due to unpredictable solar activity (which influences the night sky brightness, Patat 2008) is about 0.1-0.2 mag.

### 3.2.2. The NEO Completeness Analysis

To assess the LSST completeness for PHAs, the PHA population is represented by a size-limited complete sample of 800 true PHAs whose orbital elements are taken from the Minor Planet Center. The simulated baseline survey is used to determine which PHAs are present in each exposure and at what signal-to-noise ratio they were observed. In addition to seeing, atmospheric transparency, and sky background effects (see eq. 6), the signal-to-noise computation takes into account losses due to non-optimal filters and object trailing. Using SDSS observations of asteroids (Ivezić et al. 2001), we adopt the following mean colors to transform limiting (AB) magnitudes in LSST bandpasses (listed in Table 2) to an ‘effective’ limiting magnitude in the standard  $V$  band:  $V - m = (-2.1, -0.5, 0.2, 0.4, 0.6, 0.6)$  for  $m = (u, g, r, i, z, y)$ . Due to very red  $V - u$  colors, and the relatively bright limiting magnitude in the  $y$  band, the smallest objects are preferentially detected in the  $griz$  bands. The correction for trailing is implemented by subtracting from the right-hand side of eq. 6

$$\Delta m_5^{\text{trailing}} = 1.25 \log_{10} \left( 1 + 0.028 \frac{v t_{vis}}{\theta} \right), \quad (8)$$

where the object’s velocity,  $v$ , is expressed in deg. day $^{-1}$ . For the nominal exposure time of 30 seconds and  $\theta = 0.7$  arcsec, the loss of limiting magnitude is 0.14 mag for  $v = 0.25$  deg. day $^{-1}$ , typical for objects in the main asteroid belt, and 0.43 mag for  $v = 1.0$  deg. day $^{-1}$ , typical of NEOs passing near Earth.

For a survey that has a completeness to NEOs above 60%, each additional one magnitude of depth for a given survey cadence increases the completeness by another 10%. An object’s orbit is considered to be determined if the object was detected on at least three nights during a single lunation, with a minimum of two visits per night. The same criterion has been used in NASA studies, and is confirmed as reliable by a detailed analysis of orbital linking and determination using the Moving Object Processing System (MOPS) code (Jedicke et al. 2005) developed by the Pan-STARRS project (and adopted by LSST in a collaborative effort with Pan-STARRS). The MOPS software system and its algorithms are significantly more advanced than anything previously fielded for this purpose to date. Realistic MOPS simulations show >99%

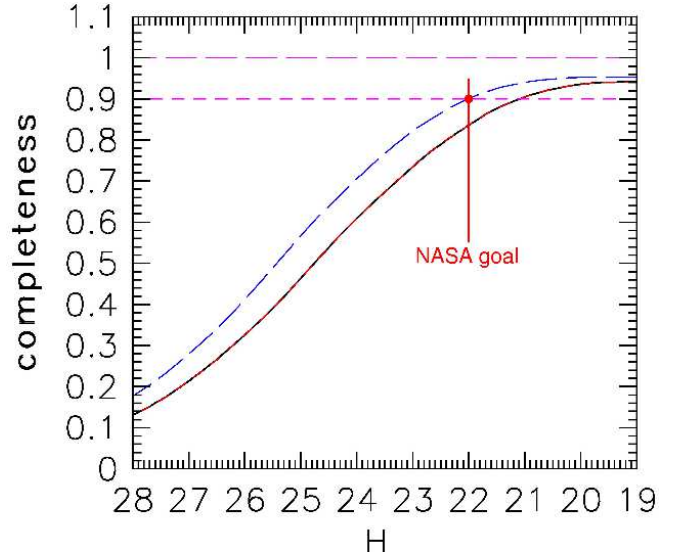


FIG. 19.— Completeness of the LSST survey for PHAs brighter than a given absolute magnitude (related to the size of the object and albedo;  $H=22$  mag is equivalent to a typical 140m asteroid and  $H=24$  mag is equivalent to a 50m asteroid). Two scenarios are shown: the lower curve is the 10-year long baseline survey with a 5% NEO optimization, and it reaches a completeness of 84%. The upper dashed curve results from spending 15% of the observing time in an NEO optimized mode, and running the survey for 12 years. It meets the 90% completeness level for 140m objects mandated by the Congress.

linking efficiency across all classes of Solar System objects. For the LSST baseline cadence, objects counted as having well-determined orbits are observed on 20 different nights on average over ten years. A more stringent requirement that an object must be detected on at least five nights per lunation decreases the completeness by typically 3%. The completeness is also a function of the assumed size distribution of NEOs, the flatter the distribution, the higher the completeness, and different assumptions contribute a systematic uncertainty of about 2%.

The LSST baseline cadence provides orbits for 82% of PHAs larger than 140 meters after 10 years of operations. This can be increased to 84% completeness (90% for sizes above 200 meters) with minor changes to the cadence, such as requiring that all observations North of  $\delta = +5^\circ$ ) are obtained in the  $r$  band. The completeness curve as a function of an object’s size is shown in Fig. 19 (lower curve). This cadence spends 5% of the total observing time on NEO-optimized observations north of  $\delta = +5^\circ$ .

Various adjustments to the baseline cadence can boost the completeness for 140m and larger PHAs to 90%. We find that such variations can have an unacceptably large impact on other science programs, if the 90% completeness is to be reached within the 10 year survey lifetime. However, with a minor adjustment of the baseline cadence, such that 15% of the time is spent north of  $\delta = +5^\circ$  to reach fainter limiting magnitudes, this completeness level can be reached with a 12 year survey, and with a negligible effect on other science goals. The completeness curve as a function of an object’s size for such a modified cadence is shown in Fig. 19 (upper curve).

Our analysis assumes that no NEOs are known prior to LSST. Currently known NEOs do not have a significant impact on this calculation.

### 3.2.3. The Expected Accuracy of Trigonometric Parallax and Proper Motion Measurements

Given the observing sequence for each sky position in the main survey, we generate a time sequence of mock astrometric measurements. The assumed astrometric accuracy is a function of signal-to-noise ratio. Random astrometric errors per visit are modeled as  $\theta/SNR$ , with  $\theta = 700$  mas and  $SNR$  determined using eq. 6. The estimated proper motion and parallax accuracy at the bright end ( $r < 20$ ) is driven by systematic errors due to the atmosphere. Systematic errors of 10 mas are added in quadrature, and are assumed to be uncorrelated between different observations of a given object. Systematic and random errors become similar at about  $r = 22$ , and there are about 100 stars per LSST sensor ( $0.05 \text{ deg}^2$ ) to this depth (and fainter than the LSST saturation limit at  $r \sim 16$ ) even at the Galactic poles.

Data from the Subaru telescope indicate that systematic errors of 10 mas on spatial scales of several arcminutes are realistic. Even a drift-scanning survey such as SDSS delivers uncorrelated systematic errors (dominated by seeing effects) at the level of 20-30 mas (measured from repeated scans; Pier et al. 2003); the expected image quality for LSST will be twice as good as for SDSS. Furthermore, there are close to 1000 galaxies per sensor with  $r < 22$ , which will provide exquisite control of systematic astrometric errors as a function of magnitude, color and other parameters, and thus enable absolute proper motion measurements.

The astrometric transformations for a given CCD and exposure, and proper motion and parallax for all the stars from a given CCD, are simultaneously solved for using an iterative algorithm. The astrometric transformations from pixel to sky coordinates are modeled using low-order polynomials and standard techniques developed at the U.S. Naval Observatory (Monet et al. 2003). The expected proper motion and parallax errors for a 10-year long baseline survey, as a function of apparent magnitude, are summarized in Table 3. Blue stars (e.g., F/G stars) fainter than  $r \sim 23$  will have about 50% larger proper motion and parallax errors than given in the table due to decreased numbers of  $z$  and  $y$  band detections. The impact on red stars is smaller due to a relatively small number of observations in the  $u$  and  $g$  bands, but extremely red objects, such as L and T dwarfs, will definitely have larger errors, depending on details of their spectral energy distributions. After the first three years of the survey, the proper motion errors will be about five

TABLE 3

THE EXPECTED PROPER MOTION, PARALLAX AND ACCURACY FOR A 10-YEAR LONG BASELINE SURVEY.

$r$ mag	$\sigma_{xy}^a$ mas	$\sigma_\pi^b$ mas	$\sigma_\mu^c$ mas/yr	$\sigma_1^d$ mag	$\sigma_C^e$ mag
21	11	0.6	0.2	0.01	0.005
22	15	0.8	0.3	0.02	0.005
23	31	1.3	0.5	0.04	0.006
24	74	2.9	1.0	0.10	0.009

<sup>a</sup> Typical astrometric accuracy (rms per coordinate per visit);

<sup>b</sup> Parallax accuracy for 10-year long survey;

<sup>c</sup> Proper motion accuracy for 10-year long survey;

<sup>d</sup> Photometric error for a single visit (two 15-second exposures);

<sup>e</sup> Photometric error for coadded observations (see Table 1).

times as large, and parallax errors will be about twice as large, as the values given in Table 3; the errors scale as  $t^{-3/2}$  and  $t^{-1/2}$ , respectively. This error behavior is a strong independent argument for a survey lifetime of at least 10 years (c.f. §2).

For comparison with Table 3, the SDSS-POSS proper motion measurements have an accuracy of  $\sim 5$  mas  $\text{yr}^{-1}$  per coordinate at  $r = 20$  (Munn et al. 2004). Gaia is expected to deliver parallax errors of 0.3 mas and proper motion errors of 0.2 mas  $\text{yr}^{-1}$  at its faint end at  $r \sim 20$  (Perryman et al. 2001). Hence, LSST will smoothly extend Gaia’s error vs. magnitude curve 4 magnitudes fainter.

### 3.3. Data Products

Data collected by the LSST telescope and camera will be automatically processed to *data products* – catalogs, alerts, and reduced images – by the LSST Data Management system (§ 2.6.3). These products are designed to be sufficient to enable a large majority of LSST science cases, without the need to work directly with the raw pixels. We give a high-level overview of the LSST data products here; further details may be found in the LSST Data Products Definition Document (Jurić et al. 2013).

Two major categories of data products will be produced and delivered by LSST DM:

- **Level 1 data products**, designed to support the discovery, characterization, and rapid follow-up of time-dependent phenomena (“transient science”). These will be generated continuously every observing night, by detecting and characterizing sources in images differenced against deep templates. They will include alerts to objects that were newly discovered, or have changed brightness or position at a statistically significant level. The alerts to such events will be published within 60 seconds of observation.

In addition to transient science, Level 1 data products will support discovery and follow-up of objects in the Solar System. Objects with motions sufficient to cause trailing in a single exposure will be identified and flagged as such when the alerts are broadcast. Those that are not trailed will be identified and linked based on their motion from observation to observation, over a period of a few days. Their orbits will be published within 24 hours of identification. The efficiency of linking (and thus the completeness of the resulting orbit catalog) will depend on the final observing cadence chosen for LSST, as well as the performance of the linking algorithm (§ 3.2.2).

- **Level 2 data products** are designed to enable systematics- and flux-limited science, and will be made available in annual Data Releases. These will include the (reduced and raw) single-epoch images, deep coadds of the observed sky, catalogs of objects detected in LSST data, catalogs of sources (the detections and measurements of objects on individual visits), and catalogs of “forced sources” (measurements of flux on individual visits

at locations where objects were detected by LSST or other surveys). LSST data releases will also include fully reprocessed Level 1 data products, as well as all metadata and software necessary for the end-user to reproduce any aspect of LSST data release processing.

A noteworthy aspect of LSST Level 2 processing is that it will largely rely on **multi-epoch model fitting**, or ***MultiFit***, to perform near-optimal characterization of object properties. That is, while the coadds will be used to perform object *detection*, the *measurement* of their properties will be performed by simultaneously fitting (PSF-convolved) models to single-epoch observations. An extended source model – a constrained linear combination of two Sérsic profiles – and a point source model with proper motion – will generally be fitted to each detected object<sup>90</sup>.

Secondly, for the extended source model fits, the LSST will characterize and store the shape of the associated likelihood surface (and the posterior), and not just the maximum likelihood values and covariances. The characterization will be accomplished by sampling, with up to  $\sim 200$  (independent) likelihood samples retained for each object. For storage cost reasons, these samples may be retained only for those bands of greatest interest for weak lensing studies.

While a large majority of science cases will be adequately served by Level 1 and 2 data products, a limited number of highly specialized investigations may require custom, user-driven, processing of LSST data. This processing will be most efficiently performed at the LSST Archive Center, given the size of the LSST data set and the associated storage and computational challenges. To enable such use cases, the LSST DM system will devote the equivalent of 10% of its processing and storage capabilities to creation, use, and federation of **Level 3** (user-created) data products. It will also allow the science teams to use the LSST database infrastructure to store and share their results.

To further enable user-driven Level 3 processing, the LSST software stack has been explicitly architected with reusability and extendability in mind, and will be made available to the LSST user community (§ 2.6.4). This will allow the LSST users to more rapidly develop custom Level 3 processing codes, leveraging 15+ years of investment and experience put into LSST codes. In addition to executing such customized codes at the LSST data centers, LSST users will be able to run it on their own computational resources as well.

We have described that approximately 10% of the observing time will be devoted to mini-surveys that do not follow the LSST baseline cadence (§ 3.1.2). The data products for these programs will be generated using the same processing system and exhibit the same general characteristics of Level 1 and 2 data products, but these

<sup>90</sup> For performance reasons, it is likely that only the point source model will be fitted in the most crowded regions of the Galactic plane.

data may be reduced on a somewhat different timescale.

### 3.4. Data Mining Challenges

The characterization (unsupervised machine learning) and classification (supervised machine learning) of massive, multivariate data catalogs such as those generated by the LSST are major research challenges for data-intensive astronomy (Tyson et al. 2008b; Ivezić et al. 2008b; Bloom et al. 2008; Borne 2008; Ivezić et al. 2014). To address these questions, the statistics and machine-learning research communities are collaborating with LSST scientists to develop new algorithms that will enable the full scientific potential of the LSST, including:

- Rapid characterizations and probabilistic classifications for the million sources detected in difference images each night.
- Identification of unusual classes of astronomical sources using outlier detection techniques that are robust to noise and image processing defects.
- Characterization of novel and unexpected behavior in the time domain from time series data.
- Measurements of the clustering of stars and galaxies (including higher order statistics) using fast algorithms for point processes.
- The application of dimensionality-reduction techniques to determine important physical correlations within large multi-variate catalogs.
- Model or hypothesis testing that can verify existing (or generate new) astronomical hypotheses with strong statistical confidence, using millions of training samples.

## 4. EXAMPLES OF LSST SCIENCE PROJECTS

The design and optimization of the LSST system leverages its unique capability to scan a large sky area to a faint flux limit in a short amount of time. The main product of the LSST system will be a multi-color *ugrizy* image of about half the sky to unprecedented depth ( $r \sim 27.5$ ). For a comparison, the best analogous contemporary dataset is that of SDSS, which provides *ugriz* images of about a quarter of the sky to  $r \sim 22.5$ , with twice as large seeing (see Figs. 20 and 21). A major advantage of LSST is the fact that this deep sky map will be produced by taking hundreds of shorter exposures (see Table 1). Each sky position within the main survey area will be observed about 1000 times, with time scales spanning seven orders of magnitude (from 30 sec to 10 years), and produce over *a trillion photometric measures* of celestial sources.

It is not possible to predict all the science that LSST data will enable. We now briefly discuss a few projects to give a flavor of anticipated studies, organized by the four science themes that drive the LSST design (although some projects span more than one theme). For an in-depth discussion of LSST science cases, we refer the reader to the LSST Science Book.

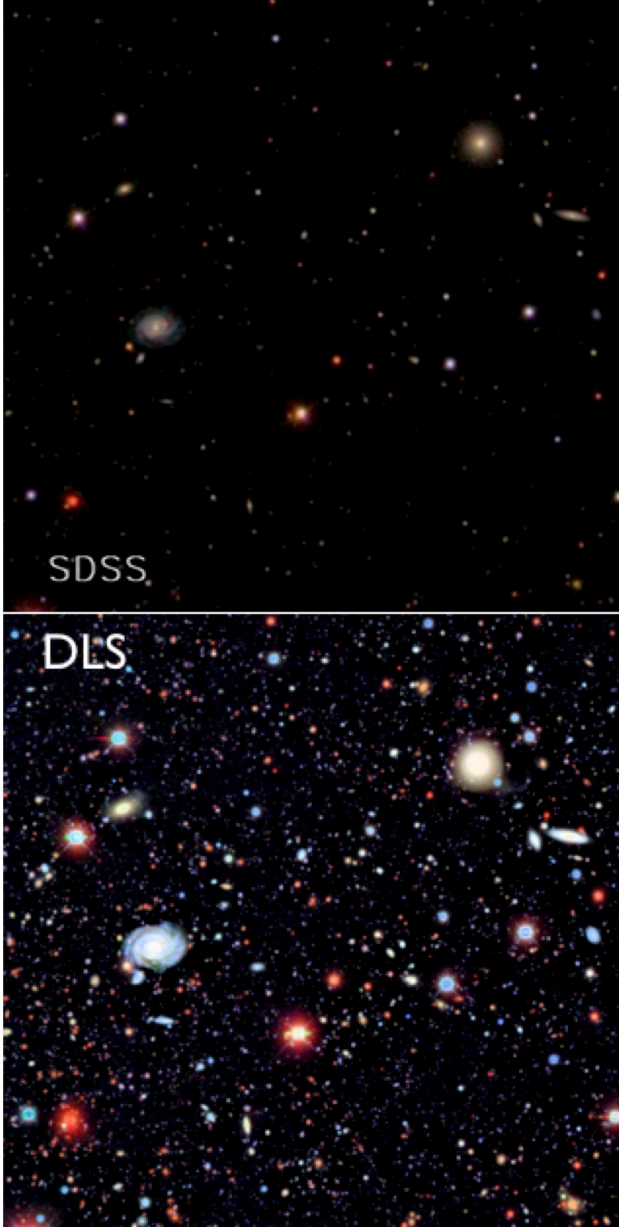


FIG. 20.— A comparison of  $\sim 7.5 \times 7.5$  arcmin $^2$  images of the same area of sky (centered on  $\alpha=9^h 20' 47''$  and  $\delta=30^\circ 8' 12''$ ) obtained by the SDSS (top,  $r < 22.5$ ) and the Deep Lens Survey (bottom,  $r < 24.5$ ). These are *gri* composites, colorized following Lupton et al. (2004). The depth gain for the bottom image is mostly due to the lower surface brightness limit, which is also responsible for the apparent increase of galaxy sizes. LSST will obtain  $\sim 100$  *gri* color images to the same depth ( $\sim 200$  for the *riz* composites) of each point over half the Celestial sphere (18,000 deg $^2$ , equivalent to 1.15 million  $\sim 7.5 \times 7.5$  arcmin $^2$  regions), and with better seeing. After their coaddition, the final image will be another  $\sim 3$  mag deeper (a faint limit of  $r = 27.5$  for point sources).

#### 4.1. Probing Dark Energy and Dark Matter

A unique aspect of LSST as a probe of dark energy and dark matter is the use of multiple cross-checking probes that reach unprecedented precision (see Fig. 22). Any given probe constrains degenerate combinations of cosmological parameters, and each probe is affected by different systematics, thus the combination of probes allows systematics to be calibrated out and for degeneracies to

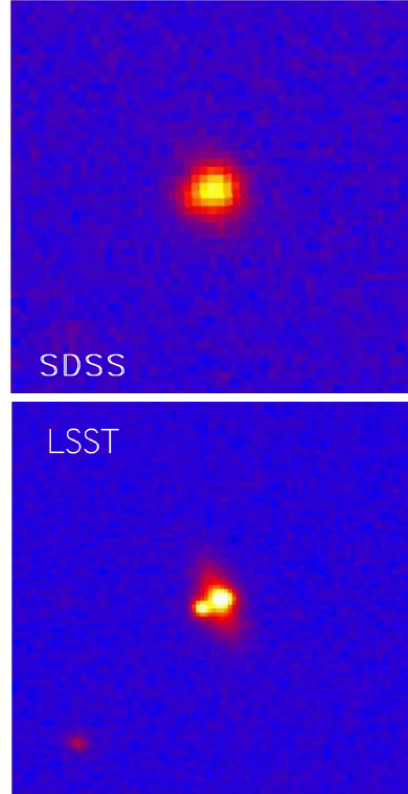


FIG. 21.— A comparison of angular resolution for  $20 \times 20$  arcsec $^2$  images obtained by the SDSS (top, median seeing of 1.5 arcsec) and expected from LSST (bottom, seeing of 0.7 arcsec). The images show a lensed SDSS quasar (SDSS J1332+0347, Morokuma et al. 2007); the bottom image was taken with Suprime-cam at Subaru. Adapted from Blandford et al. (2008).

be broken. Dark energy manifests itself in two ways. The first is the relationship between redshift and distance (the Hubble diagram), or equivalently the expansion rate of the Universe as a function of cosmic time. The second is the rate at which matter clusters with time. Structure formation involves a balance between gravitational attraction of matter over-densities and the rapid expansion of the background. Thus, quantifying the rate of growth of structures from early times until the present provides additional tests of the energy contents of the Universe and their interactions.

The joint analysis of LSST weak lensing and BAO is particularly powerful in constraining the dynamical behavior of dark energy, i.e., how it evolves with cosmic time or redshift (Hu & Jain 2004; Zhan 2006). By simultaneously measuring the growth of large-scale structure, and luminosity and angular distances as functions of redshift (via weak lensing, BAO, SN, and cluster counting), LSST data can reveal whether the recent cosmic acceleration is due to dark energy or modified gravity (Lue, Scoccimarro & Starkman 2004; Knox, Song & Tyson 2006; Ishak, Upadhye & Spergel 2006; Jain & Zhang 2008; Oguri & Takada 2011; Jain et al. 2013; Weinberg et al. 2013).

Over a broad range of accessible redshifts, the simple linear model for the dark energy equation of state ( $w = w_0 + w_a(1 - a)$ ) is a poor representation of more general dark energy theories. Barnard et al. (2008) have

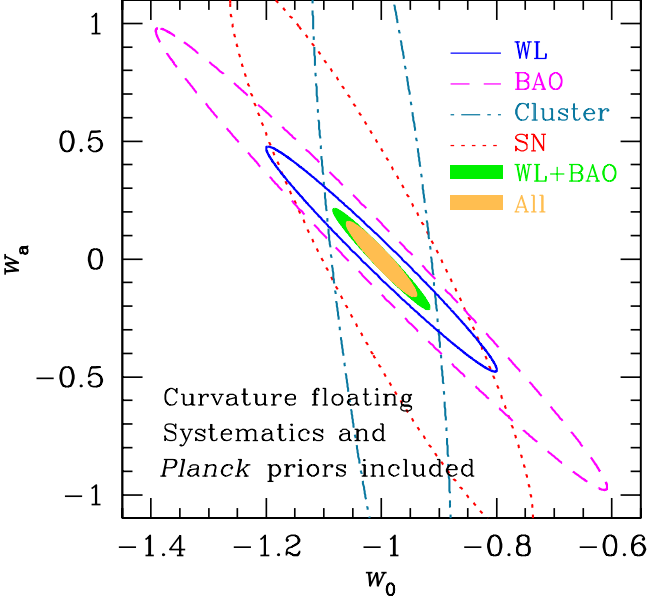


FIG. 22.— Constraints on the dark energy equation of state ( $w = w_0 + w_a(1 - a)$ ) from LSST cosmological probes. The various ellipses assume constraints from BAO (dashed line), cluster counting (dash-dotted line), supernovae (dotted line), WL (solid line), joint BAO and WL (green shaded area), and all probes combined (yellow shaded area). The BAO and WL results are based on galaxy-galaxy, galaxy-shear, and shear-shear power spectra only. Adding other probes such as strong lensing time delay and higher-order galaxy and shear statistics will further improve the constraints.

shown that in a high-dimensional dark energy model space, LSST data could lead to a hundred- to thousand-fold increase in precision over precursor experiments about to be undertaken, thereby confirming its status as a premier Stage IV experiment in the sense of Albrecht et al. (2006).

The power and accuracy of LSST dark energy and dark matter probes are a result of the enormous samples that LSST will have, including several billion galaxies and millions of Type Ia supernovae. At  $i < 25.3$  (SNR > 20 for point sources), the photometry of galaxies will be of high enough quality to give photometric redshifts with an accuracy ( $\sigma/(1+z)$ ) of 1-2% (only 10% of the sample will have redshift errors larger than 4%); the sample to this limit will include about four billion galaxies. At a slightly brighter cut, there will be about 40 galaxies arcmin $^{-2}$  with shapes measured well enough for weak lensing measurements. The median redshift for this sample will be  $z \sim 1.2$ , with the third quartile at  $z \sim 2$ . It will be possible to further improve photometric redshift calibration by cross-correlating the photometric sample with redshift surveys of galaxies and quasars in the same fields (Newman 2008; Matthews & Newman 2010; Menard et al. 2013).

The main LSST observables in the context of dark energy and matter will be

- Measurements of the two-point auto- and cross-correlation of shear across multiple redshift bins (Fig. 23). There will be over 50 of these auto and cross power spectra constructed from the shape catalog with excellent photometric redshifts (Jain & Taylor 2003).
- Higher-order shear and galaxy statistics that can

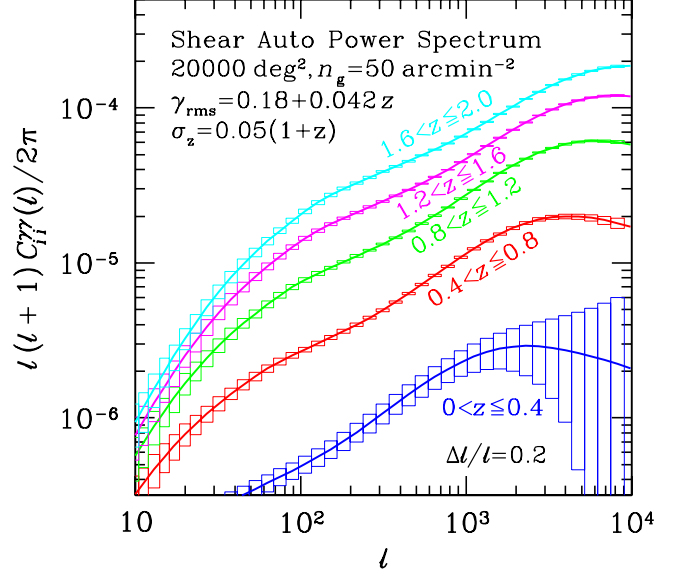


FIG. 23.— The lensing shear auto power spectra constructed from 5 redshift bins ( $l$  is the multipole moment of the distribution on the sky). Only the 5 auto-power spectra of each redshift bin among the available 15 spectra are displayed, and the solid curves show the predictions for the concordance  $\Lambda$ CDM model. The boxes show the expected 1- $\sigma$  measurement error (in bins of  $\Delta l/l = 0.2$ ) from the full LSST 10-year survey due to the sample (i.e., cosmic) variance which dominates at about  $l < 100$ , and intrinsic ellipticities which dominate at  $l > 1000$  (Zhan 2006).

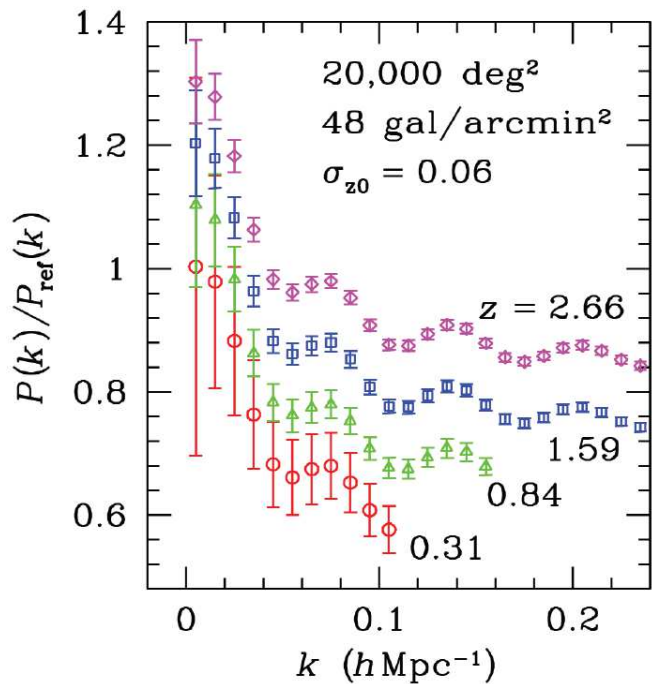


FIG. 24.— Simulations of the ratio of the measured galaxy power spectrum to a featureless reference power spectrum in various redshift bins (shifted vertically for clarity), for the full LSST survey using conservative photometric redshift errors. The several peaks visible in each curve are the signature of baryon acoustic oscillations (Eisenstein et al. 2005; Cole et al. 2005; Anderson et al. 2014). LSST will measure the angular diameter distance over this redshift range with an accuracy of  $\sim 1\%$  (Zhan & Knox 2006).

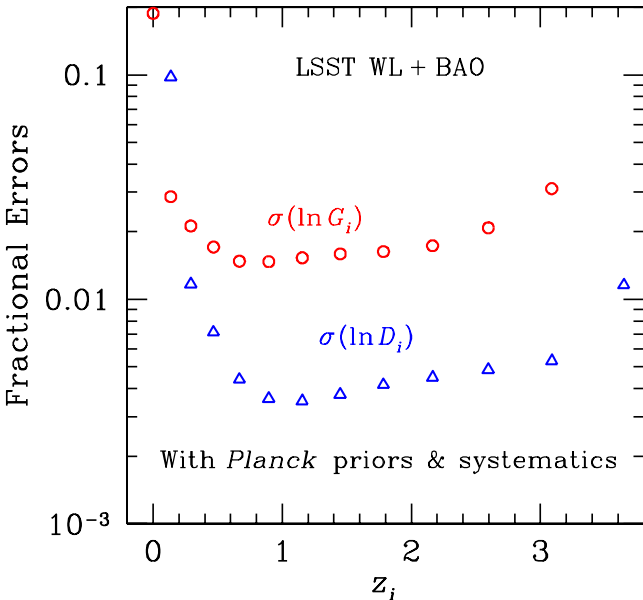


FIG. 25.— Marginalized  $1\sigma$  errors on the comoving distance (open triangles) and growth factor (open circles) parameters from the joint analysis of LSST BAO and WL (galaxy-galaxy, galaxy-shear, and shear-shear power spectra) with a conservative level of systematic uncertainties in the photometric redshift error distribution and additive and multiplicative errors in the shear and galaxy power spectra. The maximum multipole used for WL is 2000, and that for BAO is 3000 [with the additional requirement that  $\Delta_{\delta}^2(\ell/D_A; z) < 0.4$ ]. The growth parameters are evenly spaced in  $\log(1+z)$  between  $z = 0$  and 5, and the distance parameters start at  $z_1 = 0.14$ . The error of each distance (growth) parameter is marginalized over all the other parameters including growth (distance) parameters. The joint constraints on distance are relatively insensitive to the assumed systematics (Zhan, Knox & Tyson 2009).

improve dark energy constraints and provide self-calibration of various systematics (Takada & Jain 2004; Dolney, Jain & Takada 2006; Huterer et al. 2006). They are also probes of both primordial non-Gaussianities and those caused by non-linear structure.

- Similarly, weak lens magnification tomography (Morrison et al. 2012) offers a complementary probe of a mix of cosmic geometry and growth of dark matter structure.
- The galaxy-mass correlation function of billions of galaxies (as a function of their photometric redshift) probes the growth of dark matter large-scale structure and is a diagnostic of the underlying cosmology (Choi et al. 2012). Combining this with the galaxy-velocity power spectrum estimated from spectroscopic observations of millions of galaxies could probe General Relativity at high redshift (Reyes et al. 2007).
- Baryon Acoustic Oscillations in the galaxy angular correlation functions. The standard ruler of the sound horizon at decoupling which is imprinted on the mass distribution at all redshifts provides a direct way of measuring the angular diameter distance as a function of redshift (Fig. 24; Eisenstein, Hu & Tegmark 1998; Cooray et al. 2001; Blake & Glazebrook 2003; Hu & Haiman 2003; Linder 2003;

Seo & Eisenstein 2003). LSST photo-z BAO will achieve percent level precision on the angular diameter distance at  $\sim 10$  redshifts logarithmically spaced between  $z = 0.4$  to 3.6 with this CMB-calibrated standard ruler. When combined with CMB and weak lensing (WL) cosmic shear, this combination of probes yields tight constraints on the dynamical behavior of dark energy (Fig. 25). In particular, high-redshift BAO data can break the degeneracy between curvature and dark energy, and constrain  $\Omega_k$  to within 0.001.

- Supernovae. The two LSST observing programs are complementary: the main survey will obtain light curves in six bands and photometric redshifts of about 300,000 Type Ia supernovae per year (permitting a search for a “third parameter” which, if not understood, may introduce systematic error in luminosity evolution; Wood-Vasey et al. 2007), and the rapid sampling “mini-survey” of selected areas will yield well-sampled light curves of tens of thousands of supernovae to a limiting redshift beyond one (leading to an independent test of dark energy dynamics; Riess et al. 2007).
- Unique constraints on anisotropy of cosmological parameters over the sky using SN, WL and BAO, which will test fundamental cosmological assumptions of homogeneity and isotropy. For example, WL+BAO and SN can separately probe anisotropy of dark energy (Zhan, Knox & Tyson 2009).
- The shape of the power spectrum of dark matter fluctuations measured by the LSST weak lensing maps will constrain the sum of neutrino masses with an accuracy of 0.04 eV or better (Cooray 1999; Song & Knox 2004; Hannestad, Tu & Wong 2006). The current best limit, as derived from a combination of WMAP, the SDSS power spectrum, SN, and the Ly $\alpha$  forest, is 0.17 eV (Seljak et al. 2006).
- Hundreds of millions of galaxy-galaxy lenses will provide the needed statistics to probe dark matter halo profiles and substructure (Mandelbaum et al. 2006). The image fluxes in several thousand well-measured strongly lensed quasars will enable constraints of the dark matter mass function on small scales (Dalal & Kochanek 2002).
- The abundance of galaxy clusters as a function of mass and redshift is sensitive to cosmological parameters (SciBook, Ch. 13). LSST will produce a large catalog of clusters detected through their member galaxy population out to and beyond redshift unity. In addition, LSST will identify optical counterparts and provide deep optical imaging for clusters detected in other wavebands (e.g., Staniszewski et al. 2009).
- The distribution of strongest WL shear peaks with redshift is closely related to the galaxy cluster abundance, but has the potential to be a more robust and more directly calibratable statistic. This is a simultaneous probe of the universal mass function and the growth of structure, and provides a

useful constraint on dark energy (Wang et al. 2005). LSST will find over 200,000 such shear peaks on galaxy cluster scales.

- LSST will discover several hundred galaxy clusters that produce multiple-image lenses of background objects. Cluster mass reconstruction based on the multiple image positions can probe the cluster inner mass profile, and can provide a separate test of cosmology, especially in cases with strongly lensed background objects at different redshift (Porciani & Madau 2000; Oguri & Kawano 2003).
- Time delays of galaxy-scale lensed quasars will allow one to measure Hubble's constant (e.g. Suyu et al. 2010) in hundreds or thousands of systems; sub-percent level precision in  $H(z)$  should be achievable (Coe & Moustakas 2009), providing a further independent dark energy probe. Time delays for quasars multiply lensed by clusters as a function of redshift are an independent test of dark energy (Kundić et al. 1997). The natural timescale (many months to years) is well matched to the LSST survey (Oguri & Marshall 2010).

#### 4.2. Taking an Inventory of the Solar System

The small bodies of the Solar System, such as main-belt asteroids, the Trojan populations of the giant planets and the Kuiper Belt objects, offer a unique insight into its early stages because they provide samples of the original solid materials of the solar nebula. Understanding these populations, both physically and in their number and size distribution, is a key element in testing various theories of Solar System formation and evolution.

The baseline LSST cadence will result in orbital parameters for several million objects; these will be dominated by main-belt asteroids, with light curves and multi-color photometry for a substantial fraction of detected objects. This dataset will yield 10 to 100 times more objects than are currently available with orbits, colors, and variability information. LSST is capable of reaching the Congressional target completeness of 90% for PHAs larger than 140 m ( $\S$  3.2.2), and will detect over 30,000 TNOs brighter than  $r \sim 24.5$  using its baseline cadence. LSST will be capable of detecting objects like Sedna to beyond 100 AU, thus enabling *in situ* exploration far beyond the edge of the Kuiper belt at  $\sim 50$  AU. Because most of these objects will be observed several hundred times, accurate orbital elements, colors, and variability information will also be available.

The following are some examples of the LSST science opportunities in Solar System science:

- Studies of the distribution of orbital elements for over 5 million main-belt asteroids as a function of color-based taxonomy (see Fig. 26) and size; size distributions of asteroid families (Parker et al. 2008) and their correlations with age (Jedicke et al. 2004; Nesvorný et al. 2005); dynamical effects (Bottke et al. 2001); and studies of object shapes and spin states using light curve inversion techniques (Pravec & Harris 2000; Durech et al. 2009).
- Studies of transient activity in asteroids (active asteroids or main belt comets, Hsieh & Jewitt 2006),

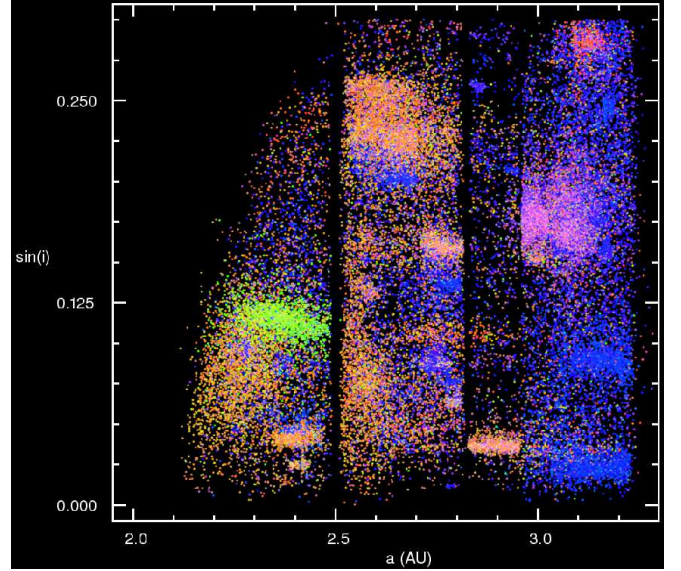


FIG. 26.— An example of color-based asteroid taxonomy. The figure shows the distribution of asteroids in the proper semi-major axis vs.  $\sin(i)$  plane for 45,000 asteroids with colors measured by SDSS (Parker et al. 2008). The color of each dot is representative of the object's color. Note the strong correlation between asteroid families (objects in distinct regions of the plane) and colors. There are at least five different taxonomic types distinguishable with SDSS measurements; LSST color measurements of asteroids will be more than twice as accurate and will increase the number of objects by roughly two orders of magnitude.

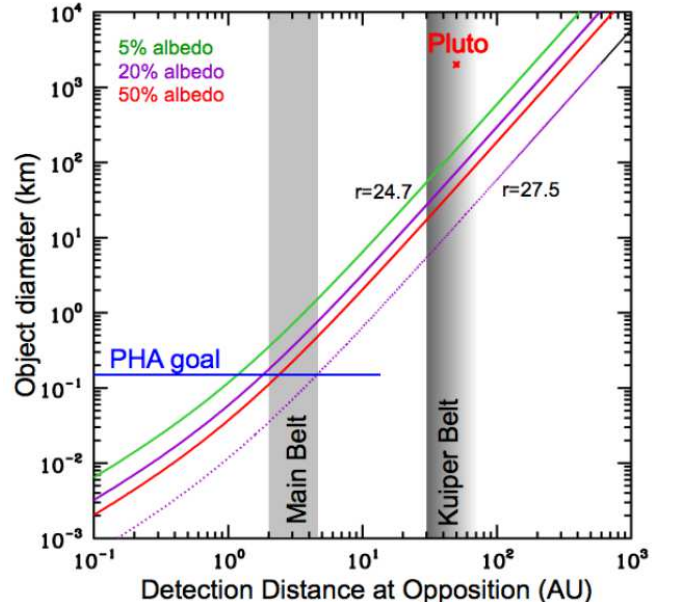


FIG. 27.— The LSST detection limits for distant Solar System objects as a function of distance. Moving objects with diameters as small as 100m in the main asteroid belt and 100km in the Kuiper Belt (TNOs) will be detected in individual visits, depending on the albedo. Specialized deeper observations (see  $\S$  3.1.2) will detect TNOs as small as 10 km. Adapted from Jones et al. (2007).

due to mass loss with associated extended morphology. Only a few such objects are currently known (Jewitt et al. 2011; Jewitt 2012); LSST will increase the sample of such objects to  $\sim 100$ .

- Studies of the distribution of orbital elements for about 100,000 NEOs as a function of color

and size (Rabinowitz 1993; Dandy, Fitzsimmons & Collander-Brown 2002); correlations with the analogous distributions for main-belt objects, and studies of object shapes and structure using light curves.

- Studies of the distribution of orbital elements for close to 300,000 Jovian Trojan asteroids as a function of color and size (Jewitt, Trujillo & Luu 2000; Yoshida & Nakamura 2005; Szabo et al. 2007); the search for dynamical families (Knežević & Milani 2005); studies of shapes and structure using light curves.
- Studies of the distribution of orbital elements for about 30,000 TNOs (see Fig. 27) as a function of color and size; the search for dynamical families (Marcus et al. 2011); studies of shapes and structure using light curves (Duncan & Levison 1995; Trujillo, Jewitt & Luu 2001; Gladman et al. 2001; Bernstein et al. 2004; Elliot et al. 2005; Jones et al. 2006; Doressoundiram et al. 2007).
- An unbiased and complete census of both Jupiter-family and Oort-cloud comets; six-band subarcsecond spatial profiles to a faint surface brightness limit; temporally resolved activity (Lowry et al. 1999; A'Hearn 2004).
- Searching for objects with perihelia out to several hundred AU. For example, an object like Sedna (Brown, Trujillo & Rabinowitz 2004) would be detectable at 130 AU. This will result in a much larger, well-understood sample of inner Oort Cloud objects like Sedna and 2012 VP113 (Trujillo & Sheppard 2014). Studying the distribution of their orbits (in particular including any clustering in the argument of perihelion) will constrain models of the birth environment of the Solar System and any potential nearby stellar passages (Kaib & Quinn 2008; Levison et al. 2010; Brasser et al. 2012).
- Mapping the propagation of interplanetary coronal mass ejections using induced activity in a large sample of comets at different heliocentric distances (SciBook Ch. 5).

#### 4.3. Exploring the Transient Optical Sky

Time domain science will greatly benefit from LSST's unique capability to simultaneously provide large area coverage, dense temporal coverage, accurate color information, good image quality, and rapid data reduction and classification. Since LSST extends time-volume space more than one hundred times over current surveys (e.g., Morokuma et al. 2008), the most interesting science may well be the discovery of new classes of objects. There are many projects that LSST data products will enable:

- Detection and measurement of gamma-ray burst afterglows and transients (e.g., Zhang & Mészáros 2004; Zhang et al. 2006; Kann et al. 2010) to high redshift ( $\sim 7.5$ ).
- Studies of optical bursters (those varying faster than  $1 \text{ mag hr}^{-1}$ ) to  $r \sim 25 \text{ mag}$ .

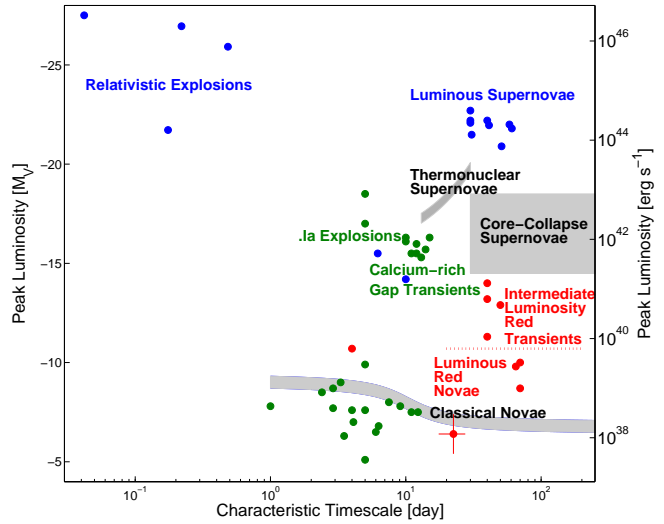


FIG. 28.— The phase space of cosmic explosive and eruptive transients as represented by their absolute  $V$  band peak brightness and the event timescale (adapted from Kulkarni et al. 2007). LSST will open up large regions of this phase space for systematic exploration by extending time-volume space over 100 times over existing surveys.

- Gravitational micro-lensing in the Local Group and beyond (de Jong, Kuijken & Héraudeau 2008).
- Studies of known and unusual SN populations and parametrization of their light curves (e.g., Hoeflich, Wheeler & Thielemann 1998; Wang et al. 2003; Howell et al. 2007; Kowalski et al. 2008; Hicken et al. 2009; Foley 2012).
- Studies of dwarf novae, including their use as probes of stellar populations and structure in the Local Group (Neill & Shara 2005; Shara 2006; Shen & Bildsten 2009).
- A deep search for new populations of novae and supernova progenitors (Smartt 2009; Thompson et al. 2009; Smith et al. 2011; see Fig. 28).
- Search for stellar tidal disruptions by nuclear supermassive black holes (Evans & Kochanek 1989; Gezari et al. 2008; Strubbe & Quataert 2009; Bloom et al. 2011; Gezari 2012), as well as binary supermassive black holes in the in-spiral phase (e.g., Cuadra et al. 2009). Measurements of rates as function of galaxy type, redshift, and level of nuclear activity to understand the apparent diversity of these events in terms of total power, effective temperature, and jet launching efficiency.
- Discovery and characterization of thousands of hot Jupiters in exoplanetary systems via the transit method (Wright et al. 2012). LSST will extend the extrasolar planet census to larger distances within the Galaxy, thus enabling detailed studies of planet frequency as a function of stellar metallicity and parent population (e.g., Hartman et al. 2009; Bayliss & Sackett 2011). The out-of-transit variability of exoplanet host stars will also provide characterization of the system via flaring behavior and stellar age via gyrochronology, the latter helping constrain theories of tidal evolution and migration in giant planets.

- A study of quasar variability using accurate, multi-color light curves for a few million quasars, leading to constraints on the accretion physics and nuclear environments (de Vries, Becker & White 2003; Vanden Berk et al. 2004, MacLeod et al. 2010). Relations between quasar variability properties and luminosity, redshift, rest-frame wavelength, time scale, color, radio-jet emission, black-hole mass, and Eddington-normalized luminosity will be defined with massive statistics, including the potential to detect rare but important events such as jet flares and obscuration events. Microlensing events will also be monitored in the  $\sim 4000$  gravitationally-lensed quasars discovered by LSST and used to measure the spatial structure of quasar accretion disks.
- The superb continuum light curves of AGN will enable economical “piggyback” reverberation-mapping efforts using spectroscopy of emission lines (Doron & Eliran 2012). These results will greatly broaden the luminosity-redshift plane of reverberation-mapped AGNs with black-hole mass estimates. For LSST data alone, the inter-band continuum lags will provide useful structural information.
- Optical identification for transients and variables detected in other electromagnetic wavebands, from gamma rays to radio. Examples include optical and gamma ray variability in blazars (Hovatta et al. 2014), radio transients associated with tidal disruption flares (Giannios & Metzger 2011), and radio counterparts to supernovae and GRBs (Gal-Yam et al. 2006). Deep optical observations with LSST may also help illuminate the nature of the still-mysterious Lorimer Bursts (Lorimer et al. 2007; Thornton et al. 2013).
- Optical identification of counterparts to non-electromagnetic sources, such as gravitational waves and neutrino detections (LIGO<sup>91</sup>, ICE-CUBE<sup>92</sup>). LSST’s unique ability to characterize the faint variable sky over large areas will be important not only for detection of associated sources but for eliminating potential false positives (Nissanke, Kasliwal & Georgieva 2013; Metzger & Berger 2012).

#### 4.4. Mapping the Milky Way

The LSST will map the Galaxy in unprecedented detail, and by doing so revolutionize the fields of Galactic Astronomy and Near-field Cosmology. The great detail with which the Milky Way can be studied complements the statistical power of extra-galactic observations. The overarching goal of near-field cosmology is to use spatial, kinematic, and chemical data sets of stars to reveal the structure and evolution history of the Milky Way and its environment. LSST will reveal this fossil record in great detail and provide a Rosetta Stone for extragalactic astronomy by setting the context within which we interpret these broader data sets. Moreover, different candidate

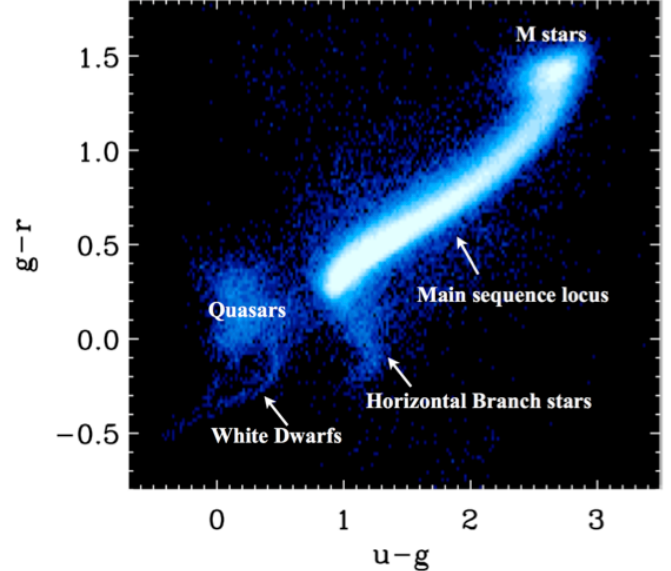


FIG. 29.— The  $g - r$  vs.  $u - g$  color-color diagram for about a million points sources from SDSS Stripe 82 area. Accurate multi-color photometry contains information that can be used for source classification and determination of detailed stellar properties such as effective temperature and metallicity. LSST will enable such measurements for billions of stars.

supersymmetric particle dark matter models predict different mass clustering on small scales, and thus different mass functions for subhalos of the Milky Way. Thus the LSST census of faint satellites and stellar streams in the halo will offer a unique means to constrain the particle nature of dark matter.

The LSST will produce a massive and exquisitely accurate photometric and astrometric data set for about 20 billion Milky Way stars. The coverage of the Galactic plane will yield data for numerous star-forming regions, and the  $y$  band data will penetrate through the interstellar dust layer. Photometric metallicity measurements (see Figs. 29 and 30) will be available for about 200 million main-sequence F/G stars which will sample the halo to distances of 100 kpc (Ivezić et al. 2008a; An et al. 2013). No other existing or planned survey will provide such a powerful dataset to study the outer halo: Gaia is flux limited at  $r = 20$ , and the Dark Energy Survey (Rossetto et al. 2011) and Pan-STARRS both lack observations in the  $u$  band, necessary for estimating metallicity. The LSST in its standard surveying mode will be able to detect RR Lyrae variables (pulsating stars and standard candles) and classical novae (exploding stars and standard candles) at a distance of 400 kpc and hence explore the extent and structure of our halo out to half the distance to the Andromeda galaxy. Thus, the LSST will enable studies of the distribution of main-sequence stars beyond the presumed edge of the Galaxy’s halo (see Fig. 31), of their metallicity distribution throughout most of the halo, and of their kinematics beyond the thick disk/halo boundary. LSST will also obtain direct distance measurements via trigonometric parallax below the hydrogen-burning limit for a representative thin-disk sample.

In addition to the study of hydrogen burning stars, LSST will uncover the largest sample of stellar remnants to date. Over 97% of all stars eventually exhaust their fuel and cool to become white dwarfs. Given the age

<sup>91</sup> <http://www.ligo.caltech.edu>

<sup>92</sup> <http://icecube.wisc.edu>

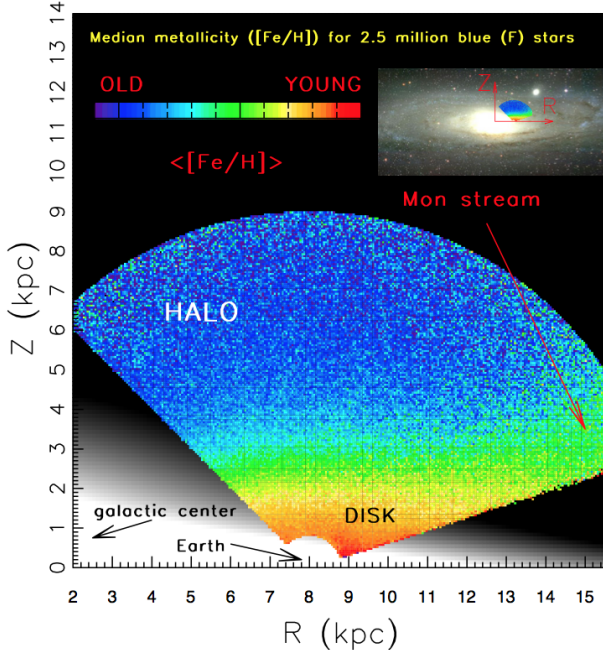


FIG. 30.— The median metallicity map for 2.5 million main-sequence F-type stars within 10 kpc from the Sun (adapted from Ivezić et al. 2008a). The metallicity is estimated using  $u - g$  and  $g - r$  colors measured by SDSS. The position and size of the mapped region, relative to the rest of the Milky Way, is illustrated in the top right corner, where the same map is scaled and overlaid on an image of the Andromeda galaxy. The gradient of the median metallicity is essentially parallel to the  $Z$  axis, except in the Monoceros stream region, as marked. LSST will extend this map out to 100 kpc, using a sample of over 100 million main-sequence F stars.

of the Galactic halo, a significant fraction of the mass in this component may reside in these remnant stars (e.g., Alcock et al. 2000; Tisserand et al. 2007) and therefore their discovery directly constrains the Galactic mass budget. These large populations of disk and halo white dwarfs will provide unprecedented constraints on the luminosity function of these stars, which will directly yield independent ages for the Galactic disk and halo (e.g., through the initial-final mass relation, Kalirai et al. 2008).

The sky coverage of LSST naturally targets both field stars and star clusters. To date, no systematic survey of the stellar populations of Southern hemisphere clusters has been performed (e.g., such as the CFHT Open Star Cluster Survey, or the WIYN Open Star Cluster Survey in the North; Kalirai et al. 2001; Mathieu 2000). Multi-band imaging of these co-eval, co-spatial, and iso-metallic systems will provide vital insights into fundamental stellar evolution. For example, the depth of LSST will enable construction of luminosity and mass functions for nearby open clusters down to the hydrogen burning limit and beyond. Variations in the initial mass function will be studied as a function of environment (e.g., age and metallicity). The wide-field coverage will also allow us to track how the stellar populations in each cluster vary as a function of radius, from the core to beyond the tidal radius. Fainter remnant white dwarfs will be uncovered in both open and globular clusters (the nearest of which are all in the South), thereby providing a crucial link to the properties of the now evolved stars in each system.

In summary, the LSST data will revolutionize studies of the Milky Way and the entire Local Group. We list

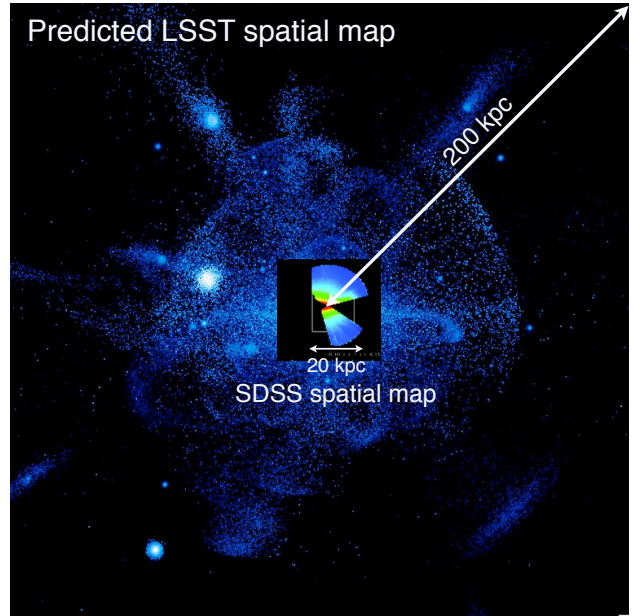


FIG. 31.— A predicted spatial distribution of stars out to 150 kpc from the center of the Milky Way, from Bullock and Johnston (2005). LSST will resolve main sequence turnoff stars out to 300 kpc, ten times more volume than shown here, enabling a high-fidelity spatial map over the entire observed virial volume. Overlaid on this prediction is the observed SDSS stellar number density map based on main sequence stars with  $0.10 < r - i < 0.15$  (Jurić et al. 2008). This map extends up to  $\sim 20$  kpc from the Sun, with the white box showing a scale of 20 kpc across and the left side aligned with the Galactic center. The revolutionary Galaxy map provided by SDSS is only complete to  $\sim 40$  kpc, or only  $\sim 1\%$  of the virial volume. However, the outermost reaches of the stellar halo are predicted to bear the most unique signatures of our Galaxy's formation (Johnston et al. 2008; Cooper et al. 2010). LSST will be the only survey capable of fully testing such predictions.

a few specific Galactic science programs that LSST will enable:

- High-resolution studies of the distribution of stars in the outer halo in the six-dimensional space spanned by position, metallicity and proper motions (e.g., Girard et al. 2006; Bell et al. 2008; Jurić et al. 2008; Ivezić et al. 2008a; Bond et al. 2010).
- The most complete search possible for halo streams, Galaxy satellites and intra-Local Group stars (e.g., Belokurov et al. 2007a; Walsh, Willman, & Jerjen 2009; Bochanski et al. 2014).
- Deep and highly accurate color-magnitude diagrams for over half of the known globular clusters, including tangential velocities from proper motion measurements (An et al. 2008; Casetti-Dinescu et al. 2007).
- Mapping the metallicity, kinematics and spatial profile of the Sgr dwarf tidal stream (e.g., Ibata et al. 2001; Majewski et al. 2003; Law, Johnston & Majewski 2005; Belokurov et al. 2014) and the Magellanic stream (Zaritsky et al. 2004).
- The measurement of the internal motions of Milky Way dwarf galaxies, thereby constraining their density profiles and possibly the nature of dark matter (e.g., Walker & Peñarrubia 2011).

- Detailed constraints on the formation and evolution of the populations within the Galactic Bulge, as traced by the spatial distribution, motion, and chemistry of  $\sim 10^{7-8}$  of its stars (e.g., Hill et al. 2011; Ness et al. 2014).
- Studies of the clumpiness of the gravitational potential in the Galaxy using fragile wide-angle binaries selected with the aid of trigonometric and photometric parallaxes, and common proper motion (e.g., Yoo, Chanamé & Gould 2004; Longhiano & Binggeli 2010).
- Detailed studies of variable star populations; 2% or better accurate multicolor light curves will be available for a sample of at least 50 million variable stars (Sesar et al. 2007), enabling studies of cataclysmic variables, eclipsing binary systems, and rare types of variables.
- Discovery of rare and faint high proper motion objects: probing the faint end of the stellar mass function (Lepine 2008; Finch et al. 2010), and searching for free-floating planet candidates (Lucas & Roche 2000; Luhman 2014).
- Direct measurement of the faint end of the stellar luminosity function using trigonometric parallaxes (Reid et al. 2002) and a complete census of the solar neighborhood to a distance of 100 pc based on trigonometric parallax measurements for objects as faint as  $M_r = 17$  ( $\sim 1.5$  brown dwarfs). For example, LSST will deliver 10% or better distances for a sample of about 2,500 stars with  $18 < M_r < 19$ .
- The separation of halo M sub-dwarfs from disk M dwarfs, using the  $z - y$  color which is sensitive to their rich molecular band structure (West et al. 2011; Bochanski et al. 2013).
- Studies of white dwarfs using samples of several million objects, including the determination of the halo white dwarf luminosity function (SciBook Ch. 6).
- Measurements of physical properties of stars using large samples of eclipsing binary stars (Stassun et al. 2013).
- High-resolution three-dimensional studies of interstellar dust using 5-color SEDs of main sequence stars (Planck Collaboration 2011; Berry et al. 2012; Green et al. 2014).
- A census of AGB stars in the Galaxy by searching for resolved envelopes and optical identifications of IR counterparts (e.g., from the WISE survey), and by using long-term variability and color selection (Ivezić 2007c).
- A complete census of faint populations in nearby star forming regions using color and variability selection (e.g., Briceno et al. 2005).

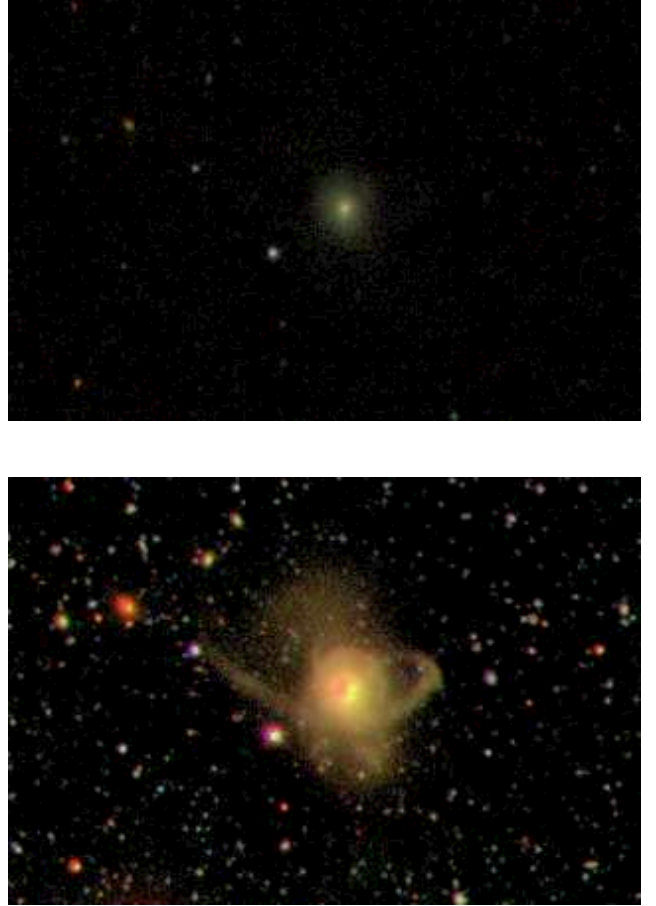


FIG. 32.— A comparison of an SDSS image ( $2 \times 4 \text{ arcmin}^2$  *gri* composite) showing a typical galaxy at a redshift of  $\sim 0.1$  (top) with a similar *BVR* composite image of the same field obtained by the MUSYC survey (bottom; Gawiser et al. 2006). The MUSYC image is about 4 mag deeper than the SDSS image (and about 1 mag less deep than the anticipated LSST 10-year coadded data). Note the rich surface brightness structure seen in the MUSYC image that is undetectable in the SDSS image.

#### 4.5. Additional Science Projects

The experience with any large survey (e.g., SDSS, 2MASS, GALEX, to name but a few) is that much of their most interesting science is often unrelated to the main science drivers, and is often unanticipated at the time the survey is designed. LSST will enable far more diverse science than encompassed by the four themes that drive the system design. We list a few anticipated major programs.

- Detailed studies of galaxy formation and evolution using their distribution in luminosity-color-morphology space as a function of redshift. For example, LSST will enable studies of the rest-frame UV emission, similar to those based on GALEX data for local galaxies, to a redshift of  $\sim 2$  for an unprecedentedly large number of galaxies. These studies project onto many axes:
  - the evolution of the galaxy luminosity function with redshift, as a function of morphology and color;
  - the evolution of the galaxy color distribution over a wide range of rest-frame wavelengths,

and as a function of luminosity and morphology;

- bulge-disk decomposition, as a function of luminosity and color, over a large redshift range;
  - detailed distribution of satellite galaxies in luminosity-color-morphology space as a function of luminosity, color, and morphology of the primary galaxy;
  - correlations of luminosity, color and morphology with local environment, and as a function of redshift (see Figs. 32 and 33);
  - the properties of galaxy groups as a function of cosmic time.
- AGN census to very faint luminosity and large redshift limit (Ivezić et al. 2013), yielding 10-40 million objects (see Fig. 34). By reaching substantially further down the AGN luminosity function over a very large solid angle, LSST data will test evolutionary cosmic downsizing scenarios, and lead to a much clearer understanding of black-hole growth during the first Gyr. For example, LSST should discover  $\sim 1000$  AGNs at  $z \sim 6 - 7.5$ , representing a dramatic increase over present samples (Brandt et al. 2007; see also SciBook Ch. 10).
  - LSST data will allow good constraints on AGN lifetimes, or at least the timescales over which they make distinct accretion-state transitions, due to large sample size and survey lifetime (e.g., Martini & Schneider 2003).
  - The first wide field survey of ultra low surface brightness galaxies, with photometric redshift information. The currently available samples are highly incomplete, especially in the Southern Hemisphere (see Fig. 7 in Belokurov et al. 2007a).
  - Search for strong gravitational lenses to a faint surface brightness limit (e.g., Bartelmann et al. 1998; Tyson, Kochanski & Dell’Antonio 1998; Belokurov et al. 2007b), which can be used to explore the dark matter profiles of galaxies (e.g., Treu et al. 2006).

#### 4.5.1. Synergy with other projects

LSST will not operate in isolation and will greatly benefit from other precursor and coeval data at a variety of wavelengths, depths, and timescales. For example, in the optical, most of the Celestial Sphere will be covered to a limit several magnitudes fainter than LSST saturation ( $r \sim 16$ ), first by the combination of SDSS, PS1, the Dark Energy Survey (Flaughler 2006) and SkyMapper (Keller et al. 2007), and then by the Gaia survey. The SkyMapper survey will obtain imaging data in the southern sky to similar depths as SDSS, the PS1 surveys provided multi-epoch data deeper than SDSS in the northern sky, and the Dark Energy Survey will scan  $\sim 5000$  deg $^2$  to similar depth as Pan-STARRS in the southern sky. Despite the lack of the  $u$  band data and a depth about a magnitude shallower, the Pan-STARRS surveys will represent a valuable complement to LSST in providing North sky coverage to a limit fainter than that of

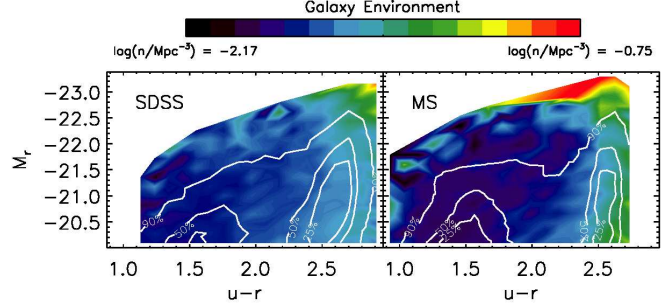


FIG. 33.— A comparison of the distribution of galaxies in luminosity-color-density space measured by SDSS (left) and a model based on the Millennium simulation (right). The linearly-spaced contours outline the distribution of a volume-limited sample of galaxies in the plotted diagram, and the color-coded background shows the median environmental density (computed using the ten nearest neighbors) for galaxies with the corresponding luminosity and color. Such multi-variate distributions encode rich information about formation and evolution of galaxies. Galaxies detected by SDSS are representative of the low-redshift Universe (the median redshift is  $\sim 0.1$ ). The LSST will enable such studies as a function of redshift, to  $z \sim 2$ . Adapted from Cowan & Ivezić (2008).

SDSS and SkyMapper. LSST and Gaia will be highly complementary datasets for studying the Milky Way in the multi-dimensional space of three-dimensional positions, proper motions and metallicity (Ivezić, Beers & Jurić 2012). The Gaia survey will provide calibration checks at the bright end for proper motions and trigonometric parallax measurements by LSST, and LSST will extend the Gaia survey by four magnitudes. The LSST data stream will invigorate subsequent investigations by numerous other telescopes that will provide additional temporal, spectral and spatial resolution coverage.

WFIRST and Euclid will carry out wide-field imaging surveys in the near-infrared, giving highly complementary photometry to LSST. The resulting galaxy SEDs should give rise to even better photometric redshifts, as well as tighter constraints on stellar masses and star formation histories crucial for galaxy evolution studies. The weak lensing analyses from space and from the ground will also be highly complementary, and will provide crucial cross-checks of one another.

LSST will also enable multi-wavelength studies of faint optical sources using gamma-ray, X-ray, IR and radio data. For example, the SDSS detected only 1/3 of all 20cm FIRST sources (Becker et al. 1995) because it was too shallow by  $\sim 4$  mag for a complete optical identification. Similarly, deep optical data are required for identification of X-ray sources (Brandt & Hasinger 2005).

LSST will provide a crucial complementary capability to space experiments operating in other wavebands, such as the ongoing NuSTAR Mission (Harrison et al. 2013) and the *Fermi* Gamma-ray Space Telescope (e.g., Atwood et al. 2010). The Laser Interferometer Gravitational Wave Observatory (LIGO) may detect ultracompact binaries and black hole mergers through the gravitational wave outburst that should be emitted during the final stages of such events. LSST has the potential to measure the electromagnetic signal that accompanies the gravitational wave emission, thereby providing an accurate position on the sky for the system, which is crucial for subsequent observations. LSST will also add new value to the archives for billion-dollar class space missions such as Chandra, XMM-Newton, Spitzer, Herschel, etc.,

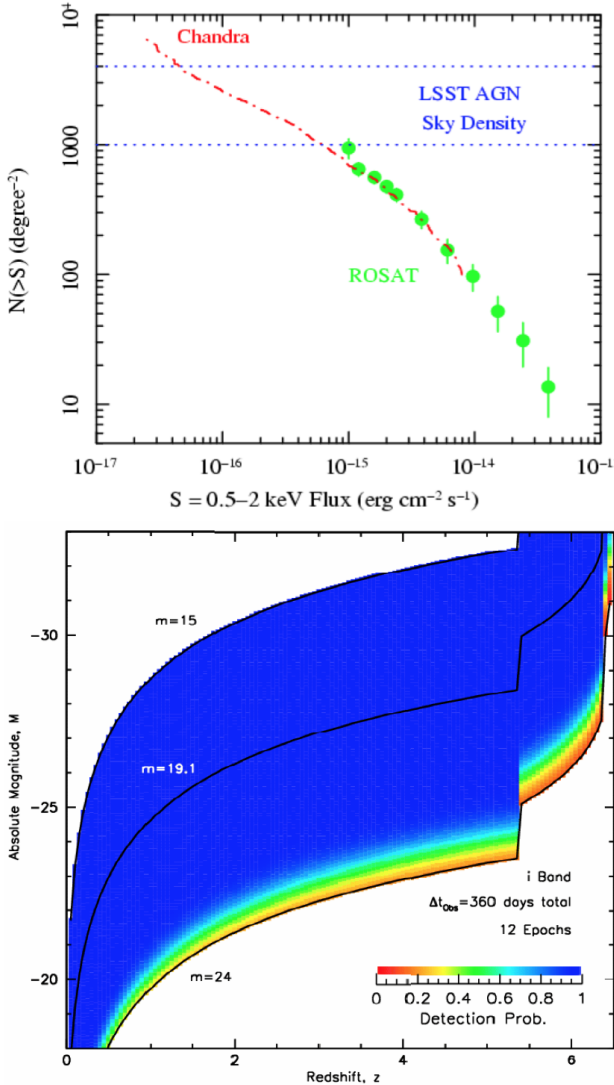


FIG. 34.— The LSST will deliver AGN sky densities of  $1000\text{--}4000 \text{ deg}^{-2}$ , which is competitive with the deepest pencil-beam surveys to date, such as the Chandra Deep Fields (top panel). The total LSST AGN yield, selected using colors and variability, should be well over 10 million objects. The bottom panel shows the expected distribution of these objects in the absolute magnitude vs. redshift plane, color-coded by the probability for an object to be detected as variable after 1 year of observations. Note that quasars will be detected to their formal luminosity cutoff ( $M < -23$ ) even at redshifts of  $\sim 5$ . Adapted from Brandt et al. (2007).

because deep optical multi-color data will enable massive photometric studies of sources from these missions; any areas of the sky – whether by design or by serendipity – in which past, present, or future multiwavelength surveys overlap with LSST sky coverage, will be further promoted by LSST investigations to “optical plus multiwavelength Selected Areas”. Last but not least, the huge samples of various astronomical source populations will yield extremely rare objects for investigations by powerful facilities such as JWST (Gardner et al. 2006) and the next generation of 20-40 meter telescopes.

In summary, the diversity of science enabled by LSST will be unparalleled, extending from the physics of gravity and the early Universe to the properties of “killer” asteroids. While there are other projects that aim to address some of the same science goals, no other project

matches this diversity and LSST’s potential impact on society in general.

## 5. COMMUNITY INVOLVEMENT

LSST has been conceived as a public facility: the database that it will produce, and the associated object catalogs that are generated from that database, will be made available to the U.S. and Chilean scientific communities, to international partners and to the public at large, with no proprietary period. We are working with international partners to make LSST data products available worldwide. The LSST data management system will provide user-friendly tools to access this database and to support user-initiated queries, run on LSST computers, either at the archive facility or at the data access centers. We expect that many, perhaps even the majority, of LSST discoveries will come from research astronomers with no formal affiliation to the project, from students, and from interested amateurs, intrigued by the accessibility to the Universe that this facility uniquely provides. For example, because of its interest in the large public data access of the LSST program, Google has joined the LSST team.

The SDSS provides a good example for how the scientific community can be effective in working with large, publicly available astronomical data sets. The SDSS has published a series of large incremental data releases via a sophisticated database, roughly once per year, together with a paper describing the content of each data release, and extensive on-line documentation giving instructions on downloading the catalogs and image data (see <http://www.sdss.org>). The overwhelming majority of the almost 6000 refereed papers based on SDSS data to date have been written by scientists from outside the project, and include many of the most high-profile results that have come from the facility.

Nevertheless, it is clear that many of the highest priority LSST science investigations will require organized teams of professionals working together to optimize science analyses and to assess the importance of systematic uncertainties on the derived results. To meet this need, eleven science collaborations have been established by the project in core science areas. For example, the LSST Dark Energy Science Collaboration includes members with interests in the study of dark energy and related topics in fundamental physics with LSST data. As of the time of this contribution, there are over 700 participants in these collaborations, mostly from LSST member institutions. One may contact the chairs of each science collaboration to learn the application process to join; all those at US and Chilean institutions, as well as named individuals from institutions in other countries which have signed Memoranda of Agreement to contribute to LSST operations costs are eligible. It is anticipated that the LSST science community will perform its analyses using LSST computational facilities, and the system has been sized accordingly.

As we design our observing strategies, we are actively seeking and implementing input by the LSST science community. The LSST science collaborations in particular have helped develop the LSST science case and continue to provide advice on how to optimize their science with choices in cadence, software, and data systems. The Science Collaborations are expected to play a role in the

system optimization during the commissioning period. We will continue this review when the survey starts, and will maintain our design of flexible cadence structure.

The Science Advisory Committee (SAC), chaired by Michael Strauss, provides a formal, and two-way, connection to the external science community served by LSST. This committee takes responsibility for policy questions facing the project and also deals with technical topics of interest to both the science community and the LSST Project. The SAC minutes and notes are available publically. Membership of this committee is as follows: N. Brandt (Penn State), H. Ferguson (STScI), C. Hirata (Ohio State), L. Hunter (UC Santa Cruz), J. Kalirai (STScI), B. Jain (UPenn), M. Kasliwal (Carnegie), D. Kirkby (UC Irvine), R. Malhotra (U Arizona), R. Mandelbaum (Carnegie Mellon), D. Minniti (U Catolica, Chile), R. Muñoz (U. Chile), M. Strauss (Princeton), L. Walkowicz (Adler), B. Willman (Haverford), and M. Wood-Vasey (U Pittsburgh).

## 6. EDUCATIONAL AND SOCIETAL IMPACTS

The impact – and enduring societal significance – of the LSST will exceed its direct contributions to advances in physics and astronomy. LSST is uniquely positioned to have high impact with the interested public and K-12 educational programs. Engaging the public in LSST activities has, therefore, been part of the project design from the beginning. With its open data policy, survey mode of operations and data products that offer vast potential for discovery, LSST facilitates the active engagement of a broad community with pathways to lifelong learning. LSST will contribute to the national goals of enhancing science literacy and increasing the global competitiveness of the US science and technology workforce. We intend to develop in our audience the awareness that they are part of a dynamic universe that changes on many time scales.

We will use three primary techniques to accomplish these goals: visualization, utilization of real data, and active engagement in the research process. These techniques will be executed via three primary components: a dynamic, immersive public web presence featuring LSST discoveries; a physical presence in classrooms and science centers; and an emphasis on citizen science, that is, participation in the research process by non-specialists. LSST’s “movie of the Universe” will offer a new window on the sky for curious minds of all ages. It is not unreasonable to anticipate tens of millions of public users browsing the LSST sky, exploring discoveries as they are broadcast and monitoring objects of interest. For users just browsing, interfaces such as Sky in Google Earth or Microsoft’s World Wide Telescope will serve images. For those wanting a deeper experience, LSST will provide a value-added interface for web-based immersive delivery of dynamic multi-media content related to LSST discoveries.

LSST data can become a key part of projects emphasizing student-centered research in middle school, high school, and undergraduate settings. Web-based instructional materials, on-line professional development, and software tools will facilitate both formal and lifelong learning opportunities. Citizen science is an integral component of the overall LSST EPO program, allowing us to actively engage a large and broad community

in the excitement of exploration. LSST EPO expects to operate at least one “Citizen Science” project at all times and provide properly constructed data products, tools, and interfaces to facilitate efforts outside LSST. A few dozen “power users” at major science centers, which in turn will reach 10-20 million participants annually, will incorporate LSST skymaps, discoveries, and scientists into displays and live sky shows. We will provide a specialized data access interface to expedite access at digital planetariums; kiosks bridging museum experiences to classroom and lifelong learning will be developed. This involvement and active participation will allow LSST to fulfill its public responsibility and extend its scientific potential - a truly transformative idea for the 21<sup>st</sup> century telescope system.

## 7. SUMMARY AND CONCLUSIONS

Until recently, most astronomical investigations have focused on small samples of cosmic sources or individual objects. Over the past decade, however, advances in technology have made it possible to move beyond the traditional observational paradigm and to undertake large-scale sky surveys, such as SDSS, 2MASS, GALEX and many others. This observational progress, based on a synergy of advances in telescope construction, detectors, and above all, information technology, has had a dramatic impact on nearly all fields of astronomy, many areas of fundamental physics, and society in general. The LSST builds on the experience of these surveys and addresses the broad goals stated in several nationally endorsed reports by the U.S. National Academy of Sciences. The 2010 report “New Worlds, New Horizons in Astronomy and Astrophysics” by the Committee for a Decadal Survey of Astronomy and Astrophysics ranked LSST as its top priority for large ground-based programs.

The realization of the LSST involves extraordinary engineering and technological challenges: the fabrication of large, high-precision optics; construction of a huge, highly-integrated array of sensitive, wide-band imaging sensors; and the operation of a data management facility handling tens of terabytes of data each day. The design and development effort, which has been underway since 2006 and will continue through the onset of construction, includes structural, thermal, and optical analyses of all key hardware subsystems, vendor interactions to determine manufacturability, explicit prototyping of high-risk elements, prototyping and development of data management systems, and extensive systems engineering studies. Over 200 technical personnel at a range of institutions are currently engaged in this program.

In September 2013, LSST passed the NSF Final Design Review for construction, and in May 2014 the National Science Board approved the project. The fabrication of the primary/tertiary mirror has been completed. In 2014 LSST transitioned from the design and development phase to construction, and the Associated Universities for Research in Astronomy (AURA) has formal responsibility for the LSST project. The U.S. Department of Energy is supporting the cost of constructing the camera. LSST has high visibility in the high-energy physics community, both at universities and government laboratories. The project is scheduled to begin regular survey operations by 2022 (it will take about five years from the start of the federal construction phase to full system

integration and the beginning of the commissioning period). The construction cost of LSST is being borne by the US National Science Foundation, the Department of Energy, generous contributions from several private foundations and institutions, and the member institutions of the LSST Corporation. The LSST budget includes a significant EPO program.

The LSST survey will open a movie-like window on objects that change brightness, or move, on timescales ranging from 10 seconds to 10 years. The survey will have a raw data rate of about 15 TB per night (about the same as one complete Sloan Digital Sky Survey per night), and will collect over 100 PB of data over its lifetime, resulting in an incredibly rich and extensive public archive that will be a treasure trove for breakthroughs in many areas of astronomy and physics. About 20 billion galaxies and a similar number of stars will be detected – for the first time in history, the number of cataloged celestial objects will exceed the number of living people! About a thousand observations of each position across half of the Celestial Sphere will represent the greatest movie of all time: assuming HDTV resolution (2.1 Mpix/frame) with 30 frames per second, and 270 color images per position (e.g., the *ugr* and *izy* color-composites, c.f. Table 1), it would take about eleven uninterrupted months to view this color movie (equivalent to about 4,000 feature films).

LSST has been conceived as a public facility: the database that it will produce, and the associated object catalogs that are generated from that database, will be made available to the U.S. and Chilean scientific communities and to the public at large with no proprietary period. We are working with prospective foreign partners to make all of the LSST data more broadly available worldwide. As of 2014, scientists in 67 institutions from 28 countries have expressed interest in contributing significantly to the LSST operating costs in exchange for data access. The software which creates the LSST database will be open source. LSST will be a significant milestone in the globalization of the information revolution. The vast relational database of 32 trillion observations of 40 billion objects will be mined for the unexpected and used for precision experiments in astrophysics. LSST will be in some sense an internet telescope: the ultimate network peripheral device to explore the Universe, and a shared resource for all humanity.

#### ACKNOWLEDGMENTS

In 2003, the LSST Corporation was formed as a non-profit 501(c)3 Arizona corporation with headquarters in Tucson, AZ. Membership has since expanded to more than forty institutional members including Adler Planetarium, Argonne National Laboratory, Brookhaven Na-

tional Laboratory, California Institute of Technology, Carnegie Mellon University, Chile, Columbia University, Cornell University, Drexel University, Fermi National Accelerator Laboratory, George Mason University, Google Inc., Harvard-Smithsonian Center for Astrophysics, Institut de Physique Nucléaire et de Physique des Particules, Johns Hopkins University, Kavli Institute for Particle Astrophysics and Cosmology – Stanford University, Las Cumbres Observatory Global Telescope Network, Inc., Lawrence Livermore National Laboratory, Los Alamos National Laboratory, National Optical Astronomy Observatory, National Radio Astronomy Observatory, Northwestern University, Oxford University, Princeton University, Purdue University, Research Corporation for Science Advancement, Rutgers University, SLAC National Accelerator Laboratory, Space Telescope Science Institute, Texas A&M University, The Pennsylvania State University, The University of Arizona, University of California at Davis, University of California at Irvine, University College London, University of Illinois at Urbana-Champaign, University of Michigan, University of Pennsylvania, University of Pittsburgh, University of Washington, and Vanderbilt and Fisk Universities.

LSST is a public-private partnership. Design and development activity is supported by in part the National Science Foundation under Scientific Program Order No. 9 (AST-0551161), Scientific Program Order No. 1 (AST-0244680) through Cooperative Agreement AST-0132798, and grant AST-0441069. Portions of this work are supported by the Department of Energy under contract DE-AC02-76SF00515 with the Stanford Linear Accelerator Center, contract DE-AC02-98CH10886 with Brookhaven National Laboratory, contract DE-AC52-07NA27344 with Lawrence Livermore National Laboratory, and grant DE-FG02-07ER41505. A portion of this work was conducted at the Jet Propulsion Laboratory, California Institute of Technology, under a contract with NASA. Gifts by the Charles Simonyi Fund for Arts and Sciences, and Bill Gates, and grants by W. M. Keck Foundation and the TABASGO Foundation are gratefully acknowledged. Additional funding has been provided by private gifts, grants to universities, and in-kind support at Department of Energy laboratories and other LSSTC Institutional Members.

NOAO is operated by the Association of Universities for Research in Astronomy, Inc. (AURA) under cooperative agreement with the National Science Foundation.

This work was supported in part by National Science Foundation Grant No. PHYS-1066293 and the hospitality of the Aspen Center for Physics.

We thank Chris Borden, Tim Knauer and Branimir Sesar for valuable comments.

#### APPENDIX

#### Version History

Version 1.0 (May 15, 2008): the first posting.

Version 2.0 (June 7, 2011): acknowledged the Decadal Survey 2010 report; updated construction schedule; updated expected performance in Table 2; added sections on LSST simulations and data mining; updated several figures; updated references; expanded author list.

Version 3.0 (August 26, 2014): acknowledged the start of federal construction; updated system description and science examples, updated several figures; refreshed references; expanded author list.

## REFERENCES

- Abazajian, K.N., Adelman-McCarthy, J.K., Agüeros, M.A. et al. 2009, *Astrophysical Journal Supplements*, 182, 543
- A'Hearn, M.F. 2004, in *Comets II*, M.C. Festou, H.U. Keller, and H.A. Weaver (eds.), University of Arizona Press, Tucson, p.17-22
- Aihara, H., Allende Prieto, C., An, D., et al. 2011, *Astrophysical Journal Supplement*, 195, 26
- Albrecht, A., Bernstein, G., Cahn, R. 2006, Report of the Dark Energy Task Force, arXiv:0609591
- Alcock, C., Allsman, R.A., Alves, D.R., et al. 2000, *Astrophysical Journal*, 542, 281
- Amores, E.B. & Lépine, J.R.D. 2005, *Astronomical Journal*, 130, 659
- An, D., Johnson, J. A., Clem, J. L., et al. 2008, *Astrophysical Journal Supplement*, 179, 326
- An, D., Beers, T. C., Johnson, J. A., et al. 2013, *Astrophysical Journal*, 763, 65
- Anderson, G.P., Berk, A., Acharya, P.K., et al. 1999, in "Optics in Atmospheric Propagation and Adaptive Systems III", A. Kohnle & J.D. Gonglewski, eds., Proceedings of the SPIE, 3866, 2
- Anderson, S.F., Haggard, D., Homer, L., et al. 2005, *Astronomical Journal*, 130, 2230
- Anderson, L., Aubourg, É., Bailey, S. et al. 2014, *Monthly Notices of the Royal Astronomical Society*, 441, 24
- Angel, R., Lesser, M. & Sarlot, R. 2000, in "Imaging the Universe in Three Dimensions: Astrophysics with Advanced Multi-wavelength Imaging Devices", W. Bruegel and J. Bland-Hawthorn, eds., ASP Conference Series, 195, 81
- Atwood, W.B., Abdo, A.A., Ackerman, M., et al., 2009, *Astrophysical Journal*, 697, 1071
- Barnard, M., Abrahamse, A., Albrecht, A., Bozek, B. & Yashar, M., 2008, *Physical Review D*, 78, 043528
- Bartelmann, M. & Schneider, P. 2001, *Physics Reports*, 340, 291
- Bartelmann, M., Huss, A., Colberg, J.M., Jenkins, A. & Pearce, F.R. 1998, *Astronomy & Astrophysics*, 330, 1
- Batista, V., Beaulieu, J.P., Gould, A., et al. 2014, *Astrophysical Journal*, 780, 54
- Bayliss, D.D.R. & Sackett, P.D. 2011, *Astrophysical Journal*, 743, 103
- Beaulieu, J.P., Bennett, D.P., Fouqué, P., et al. 2006, *Nature*, 439, 437
- Becker, A.C., Wittman, D.M., Boeshaar, P.C., et al. 2004, *Astrophysical Journal*, 611, 418
- Becker, R.H., White, R.L., & Helfand, D.J. 1995, *Astrophysical Journal*, 450, 559
- Bell, E.F., Zucker, D.B., Belokurov, V. et al. 2008, *Astrophysical Journal*, 680, 295
- Belokurov, V., Zucker, D.B., Evans, N.W., et al. 2007a, *Astrophysical Journal*, 654, 897
- Belokurov, V., Evans, N.W., Moiseev, A., et al. 2007b, *Astrophysical Journal*, 671, L9
- Belokurov, V., Koposov, S. E., Evans, N.W., et al. 2014, *MNRAS*, 437, 116
- Bergeron, P., Wesemael, F. & Beauchamp, A. 1995, *Publications of the Astronomical Society of the Pacific*, 107, 1047
- Bernstein, G.M., Trilling, D.E., Allen, R.L., et al. 2004, *Astronomical Journal*, 128, 1364
- Berry, M., Ivezić, Ž., Sesar, B., et al. 2012, *Astrophysical Journal*, 757, 166
- Blake, C. & Glazebrook, K. 2003, *Astrophysical Journal*, 594, 665
- Blandford, R.D., Marshall, P., Oguri, M., et al. 2008, *American Astronomical Society, AAS Meeting #211, #137.07*
- Bloom, J.S., Starr, D.L., Butler, N.R. et al. 2008, *Astronomische Nachrichten*, 329, 284
- Bloom, J.S., Giannios, D., Metzger, B.D., et al. 2011, *Science*, 333, 203
- Bochanski, J.J., West, A.A., Hawley, S.L. & Covey, K.R. 2007, *Astronomical Journal*, 133, 531
- Bochanski, J.J., Savcheva, A., West, A.A. & Hawley, S.L. 2013, *Astronomical Journal*, 145, 40
- Bochanski, J.J., Willman, B., West, A.A., Strader, J. & Chomiuk, L. 2014, *Astronomical Journal*, 147, 76
- Bond, N.A., Ivezić, Ž., Sesar, B., et al. 2010, *Astrophysical Journal*, 716, 1
- Bongiorno, A., Zamorani, G., Gavignaud, I., et al. 2007, *Astronomy & Astrophysics*, 472, 443
- Borne, K. 2008, *Astronomische Nachrichten*, 329, 255
- Bottke, W.F., Vokrouhlický, D., Brož, M., Nesvorný, D. & Morbidelli, A. 2001, *Science*, 294, 1693
- Brandt, N., Anderson, S.F., Ballantyne, D.R., et al. 2007, *American Astronomical Society, AAS Meeting #211, #137.09*
- Brandt, N. & Hasinger, G. 2005, *ARA&A*, 43, 827
- Brasser, R., Duncan, M. J., Levison, H. F., Schwamb, M. E. & Brown, M. E. 2012, *Icarus*, 217, 1
- Briceno, C., Calvet, N., Hernandez, J., et al. 2005, *Astronomical Journal*, 129, 907
- Brown, M.E., Trujillo, C. & Rabinowitz, D. 2004, *Astrophysical Journal*, 617, 645
- Bruzual, G. & Charlot, S. 2003, *MNRAS*, 344, 1000
- Budavári, T., Connolly, A.J., Szalay, A.S., et al. 2003, *Astrophysical Journal*, 595, 59
- Bullock, J.S. & Johnston, K.V. 2005, *Astrophysical Journal*, 635, 931
- Burke, D., Axelrod, T., Bartlett, J., et al. 2007, *American Astronomical Society, AAS Meeting #211, #137.23*
- Burrows, D., Sudarsky, D. & Hubeny, I. 2006, *Astrophysical Journal*, 640, 1063
- Carollo, D., Beers, T.C., Lee, Y.S., et al. 2007, *Nature*, 450, 1020
- Casetti-Dinescu, D.I., Girard, T.M., Herrera, D., et al. 2007, *Astronomical Journal*, 134, 195
- Charbonneau, D., Brown, T.M., Latham, D.W. & Mayor, M. 2000, *Astrophysical Journal*, 529, L45
- Choi, A., Tyson, J.A., Morrison, C.B., et al. 2012, *Astrophysical Journal*, 759, 101
- Choi, J.Y., Han, C., Udalski, A., et al. 2013, *Astrophysical Journal*, 768, 129
- Chou, M.Y., Majewski, S. R., Cunha, K., et al. 2007, *Astrophysical Journal*, 670, 346
- Coe, D. & Moustakas, L.A. 2009, *Astrophysical Journal*, 706, 45
- Cole, S., Percival, W.J., Peacock, J.A., et al. 2005, *Monthly Notices of the Royal Astronomical Society*, 362, 505
- Connolly, A.J., Peterson, J., Jernigan, J.G., et al. 2010, *Proc. SPIE* 7738, 773810
- Cooper, A.P., Cole, S., Frenk, C.S., et al. 2010, *MNRAS*, 406, 744
- Cooray, A.R. 1999, *Astronomy & Astrophysics*, 348, 31
- Cooray, A.R., Hu, W., Huterer, D. & Joffre, M. 2001, *Astrophysical Journal*, 557, L7
- Cowan, N. & Ivezić, Ž. 2008, *Astrophysical Journal*, 674, L13
- Cuadra, J., Armitage, P.J., Alexander, R.D., Begelman, M.C. 2009, *MNRAS*, 393, 1423
- Cushing, M.C., Rayner, J.T. & Vacca, W.D. 2005, *Astrophysical Journal*, 623, 1115
- Dalal, N. & Kochanek, C.S. 2002, *Astrophysical Journal*, 575, 25
- Dandy, C.L., Fitzsimmons, A. & Collander-Brown, S.J. 2002, *Icarus*, 163, 363
- De Lucia, G., Springel, V., White, S.D.M., Croton, D. & Kauffmann, G. 2006, *MNRAS*, 366, 499
- de Brujne, J.H.J. 2012, *Astrophysics and Space Science*, 341, 31
- de Jong, J.T.A., Kuijken, K.H. & Héraudeau, P. 2008, *Astronomy & Astrophysics*, 478, 755
- DeMeo, F.E., Binzel, R.P., Slivan, S.M. & Bus, S.J. 2009, *Icarus*, 202, 160
- de Vries, W.H., Becker, R.H., & White, R.L. 2003, *Astronomical Journal*, 126, 1217
- Djorgovski, S.G., Mahabal, A.A., Drake, A.J., et al. 2012, *Proceedings of the IAU*, 285, 141
- Dolney, D., Jain, B. & Takada, M. 2006, *MNRAS*, 366, 884
- Doressoundiram, A., Peixinho, N., Mouillet, A., et al. 2007, *Astronomical Journal*, 134, 2186
- Doron, C. & Eliran, D. 2012, *Astrophysical Journal*, 747, 62
- Drake, A.J., Beshore, E., Catelan, M., et al. 2010, arXiv:1009.3048
- Drake, A.J., Djorgovski, S.G., Mahabal, A., et al. 2009, *Astrophysical Journal*, 696, 870
- Duncan, M.J. & Levison, H.F. & Budd, S.M. 1995, *Astronomical Journal*, 110, 3073
- Durech, J., Kaasalainen, M., Warner, B.D., et al. 2009, *Astronomy & Astrophysics*, 493, 291
- Eisenstein, D.J., Zehavi, I., Hogg, D.W., et al. 2005, *Astrophysical Journal*, 633, 560
- Eisenstein, D.J., Hu, W. & Tegmark, M. 1998, *Astrophysical Journal*, 504, L57
- Elliott, J.L., Kern, S.D., Clancy, K.B., et al. 2005, *Astronomical Journal*, 129, 1117

- Evans, C.R. & Kochanek, C.S. 1989, *Astrophysical Journal*, 346, L13
- Finch, C. T., Zacharias, N. & Henry, T. J. 2010, *Astronomical Journal*, 140, 844
- Flaugher, B. 2006, Proc. of SPIE, Vol. 6269, 62692C
- Foley, R.J. 2012, *Astrophysical Journal*, 748, 127
- Fukugita, M., Ichikawa, T., Gunn, J.E., et al. 1996, *Astronomical Journal*, 111, 1748
- Gal-Yam, A., Ofek, E.O., Poznanski, D., et al. 2006, *Astrophysical Journal*, 639, 331
- Gardner, J.P., Mather, J.C., Clampin, M., et al. 2006, *Space Science Reviews*, 123, 485
- Garnavich, P.M., Smith, R.C., Miknaitis, G., et al. 2005, *American Astronomical Society, AAS Meeting #205*, #108.18
- Gawiser, E., van Dokkum, P.G., Herrera, D., et al. 2006, *Astrophysical Journal Supplement*, 162, 1
- Gezari, S. 2012, *European Physical Journal Web of Conferences*, 39, 3001
- Gezari, S., Basa, S., Martin, D.C., et al. 2008, *Astrophysical Journal*, 676, 944
- Gezari, S., Chornock, R., Rest, A., et al. 2012, *Nature*, 485, 217
- Giannios, D. & Metzger, B.D. 2011, *MNRAS*, 416, 2102
- Girard, T.M., Korcharin, V.I., Casetti-Dinescu, D.I., et al. 2006, *Astronomical Journal*, 132, 1768
- Gladman, B., Kavelaars, J.J., Petit, J.-M., et al. 2001, *Astronomical Journal*, 122, 1051
- González, J.E., Lacey, C.G., Baugh, C.M., Frenk, C.S. & Benson, A.J. 2009, *MNRAS*, 397, 1254
- Graham, M.J., Djorgovski, S.G., Drake, A.J., et al. 2014, *MNRAS*, 439, 703
- Granvik, M., Virtanen, J., Oszkiewicz, D. & Muinonen, K. 2009, *Meteoritics & Planetary Science*, 44, 1853
- Grav, T., Jedicke, R., Denneau, L., Holman, M.J. & Spahr, T. 2007, *BAAS*, 211, 4721
- Green, G. M., Schlaflly, E. F., Finkbeiner, D. P., et al. 2014, *Astrophysical Journal*, 783, 114
- Gunn, J.E., Carr, M., Rockosi, C., et al. 1998, *Astronomical Journal*, 116, 3040
- Gunn, J.E., Siegmund, W.A., Mannery, E.J., et al. 2006, *Astronomical Journal*, 131, 2332
- Hannestad, S., Tu, H. & Wong, Y.Y. 2006, *Journal of Cosmology and Astroparticle Physics*, 6, 25
- Harrison, F.A., Craig, W.W., Cristensen, F.E. et al. 2013, *Astrophysical Journal*, 770, 103
- Hartman, J.D., Gaudi, B.S., Holman, M.J., et al. 2009, *Astrophysical Journal*, 695, 336
- Helmi, A., Ivezić, Ž., Prada, F., et al. 2003, *Astrophysical Journal*, 586, 195
- Hicken, M., Wood-Vasey, W.M., Blondin, S., et al. 2009, *Astrophysical Journal*, 700, 1097
- Hill, V., Lecurer, A., Gómez, A., et al. 2011, *Astronomy & Astrophysics*, 534, 80
- Hoeflich, P., Wheeler, J.C. & Thielemann, F.K. 1998, *Astrophysical Journal*, 495, 617
- Hovatta, T., Pavlidou, V., King, O.G., et al. 2014, *MNRAS*, 439, 690
- Howell, D.A., Sullivan, M., Conley, A. & Carlberg, R. 2007, *Astrophysical Journal*, 667, 37
- Hsieh, H.H., & Jewitt, D. 2006, *Science*, 312, 561
- Hu, W. & Tegmark, M. 1999, *Astrophysical Journal*, 514, L65
- Hu, W. & Haiman, Z. 2003, *Physical Review D*, 68, 063004
- Hu, W. & Jain, B. 2004, *Physical Review D*, 70, 3009
- Huterer, D., Takada, M., Bernstein, G. & Jain, B. 2006, *MNRAS*, 366, 101
- Ibata, R., Irwin, M., Lewis, G.F. & Stolte, A. 2001, *Astrophysical Journal*, 547, L133
- Ishak, M., Upadhye, A. & Spergel, D.N. 2006, *Physical Review D*, 74, 043513
- Ivezić, Ž., Connolly, A.J., Vanderplas, J.T., and Gray, A. 2014, *Statistics, Data Mining, and Machine Learning in Astronomy*, Princeton University Press
- Ivezić, Ž., Tabachnik, S., Rafikov, R., et al. 2001, *Astronomical Journal*, 122, 2749
- Ivezić, Ž., Lupton, R.H., Schlegel, D., et al. 2003, *astro-ph/0309075*
- Ivezić, Ž., Tyson, J.A., Jurić, M. et al. 2007a, *Proceedings of IAU Symposium 236*. Edited by G.B. Valsecchi and D. Vokrouhlický. Cambridge: Cambridge University Press, 353 (also *astro-ph/0701506*)
- Ivezić, Ž., Smith, J. A., Miknaitis, G., et al. 2007b, *Astronomical Journal*, 134, 973
- Ivezić, Ž. 2007c, *ASP Conference Series*, Vol. 378, 485 (also *astro-ph/0701507*)
- Ivezić, Ž., Sesar, B., Jurić, M., et al. 2008a, *Astrophysical Journal*, 684, 287
- Ivezić, Ž., Axelrod, T., Becker, A. C., et al. 2008b, in *American Institute of Physics Conference Series*, ed. C. A. L. Bailer-Jones, Vol. 1082, 359 (also *arXiv:0810.5155*)
- Ivezić, Ž., Beers, T.C. & Jurić, M. 2012, *ARA&A*, 50, 251
- Ivezić, Ž., Brandt, W.N., Fan, X., et al. 2013, *arXiv:1312.3963*
- Jain, B. & Taylor, A. 2003, *Physical Review Letters*, 91, 1302
- Jain, B. & Zhang, P. 2008, *Physical Review D*, 78, 063503
- Jain, B., Vikram, V. & Sakstein, J. 2013, *Astrophysical Journal*, 779, 39
- Jedicke, R., Nesvorný, D., Whiteley, R., Ivezić, Ž., & Jurić, M. 2004, *Nature*, 429, 275
- Jedicke, R., Denneau, L., Grav, T., et al. 2005, *American Astronomical Society, AAS Meeting #207*, #121.02
- Jee, M.J. & Tyson, J.A. 2011, *PASP*, 123, 596
- Jewitt, D.C., Trujillo, C.A. & Luu, J.X. 2000, *Astronomical Journal*, 120, 1140
- Jewitt, D.C., Stuart, J.S., & Li, J. 2011, *Astronomical Journal*, 142, 28
- Jewitt, D.C. 2012, *Astronomical Journal*, 143, 66
- Johnston, K. V., Bullock, J. S., Sharma, S., et al. 2008, *Astrophysical Journal*, 689, 936
- Jones, R.L., Gladman, B., Petit, J.-M., et al. 2006, *Icarus*, 185, 508
- Jones, R.L., Chesley, S., Connolly, A.J., et al. 2007, *American Astronomical Society, AAS Meeting #211*, #137.14
- Jurić, M., Ivezić, Ž., Brooks, A., et al. 2008, *Astrophysical Journal*, 673, 864
- Jurić, M., et al. 2013, “LSST Data Products Definition Document” <http://ls.st/f15>, LSST Document Handle LSE-163
- Kaib, N. A. & Quinn, T. 2008, *Icarus*, 197, 221
- Kaiser, N., Aussel, H., Burke, B.E., et al. 2002, in “Survey and Other Telescope Technologies and Discoveries”, Tyson, J.A. & Wolff, S., eds. *Proceedings of the SPIE*, 4836, 154
- Kalirai, J.S., Hansen, B.M.S., Kelson, D.D., et al. 2008, *Astrophysical Journal*, 676, 594
- Kalirai, J.S., Richer, H.B., Fahlman, G.G., et al. 2001, *Astronomical Journal*, 122, 257
- Kann, D.A., Klose, S., Zhang, B., et al. 2010, *Astrophysical Journal*, 720, 1513
- Kaspi, S., Brandt, W.N., Maoz, D., et al. 2007, *Astrophysical Journal*, 659, 997
- Keller, S.C., Schmidt, B.P., Bessell, M.S., et al. 2007, *Publications of the Astronomical Society of Australia*, 24, 1
- Knežević, Z. & Milani, A. 2005, *Highlights of Astronomy*, Ed. O. Engvold. San Francisco, CA, p. 758
- Knox, L., Song, Y., Tyson, J.A. 2006, *Physical Review D*, 74, 3512
- Komatsu, E., Dunkley, J., Nolta, M.R., et al. 2009, *Astrophysical Journal*, 180, 330
- Kowalski, A., Hawley, S.L., Holtzman, J.A., Wisniewski, J.P. & Hilton, E.J. 2010, *Astrophysical Journal*, 714, L98
- Kowalski, M., Rubin, D., Aldering, G., et al. 2008, *Astrophysical Journal*, 686, 749
- Kulkarni, S., Ofek, E.O., Rau, A., et al. 2007, *Nature*, 447, 458
- Kundić, T., Turner, E.L., Colley, W.N., et al. 1997, *Astrophysical Journal*, 482, 75
- Kurucz, R.L. 1979, *Astrophysical Journal Supp.*, 40, 1
- Kurucz, R.L. 1993, “CD-ROM No.13”, Cambridge, Mass., Smithsonian Astrophysical Observatory
- Lauirejs, R., Amiaux, J., Ardiuni, S. et al. 2011, *arXiv:1110.3193*
- Law, D.R., Johnston, K.V. & Majewski, S.R. 2005, *Astrophysical Journal*, 619, 807
- Law, N.M., Kulkarni, S.R., Dekany, R.G., et al. 2009, *PASP*, 121, 1395
- Lenz, D.D., Newberg, J., Rosner, R., et al. 1998, *Astrophysical Journal Supp.*, 119, 121
- Lepine, S. 2008, *Astronomical Journal*, 135, 2177
- Levi, M., Bebek, C., Beers, T., et al. 2013, *arXiv:1308.0847*
- Levison, H. F., Duncan, M. J., Brasser, R. & Kaufmann, D. E. 2010, *Science*, 329, 187
- Linder, E.V. 2003, *Physical Review D*, 68, 083504
- Lintott, C., Schawinski, K., Bamford, S. 2011, *MNRAS*, 410, 166
- Longhitano, M. & Binggeli, B. 2010, *Astronomy & Astrophysics*, 509, 46

- Lorimer, D.R., Bailes, M., McLaughlin, M.A., Narkevic, D.J. & Crawford, F. 2007, *Science*, 318, 777
- Lowry, S.C., Fitzsimmons, A., Cartwright, I.M. & Williams, I.P. 1999, *Astronomy & Astrophysics*, 349, 649
- LSST Dark Energy Science Collaboration 2012, arXiv:1211.0310
- LSST Science Book, Version 2.0, <http://www.lsst.org/lsst/SciBook>, arXiv:0912.0201
- Lucas, P.W. & Roche, P.F. 2000, *MNRAS*, 314, 858
- Lue, A., Scoccimarro, R. & Starkman, G. 2004, *Physical Review D*, 69, 4005
- Luhman, K.L. 2014, *Astrophysical Journal*, 786, 18
- Lupton, R., Blanton, M.R., Fekete, G., Hogg, D.W., O'Mullane, W., Szalay, A., and Wherry, N. 2004, *Publications of the Astronomical Society of the Pacific*, 116, 133
- MacLeod, C.L., Ivezić, Ž., Kochanek, C.S., et al. 2010, *Astrophysical Journal*, 721, 1014
- Mahabal, A.A., Djorgovski, S.G., Drake, A.J., et al. 2011, *Bulletin of the Astronomical Society of India*, 39, 387
- Majewski, S.R., Skrutskie, M.F., Weinberg, M.D. & Ostheimer, J.C. 2003, *Astrophysical Journal*, 599, 1082
- Mamajek, E.E. 2012, arXiv:1210.1616
- Mandelbaum, R., Seljak, U., Kauffmann, G., Hirata, C.M. & Brinkmann, J. 2006, *MNRAS*, 368, 715
- Marcus, R.A., Ragozzine, D., Murray-Clay, R.A. & Holman, M.J. 2011, *Astrophysical Journal*, 733, 40
- Martin, D.C., Fanson, J., Schiminovich, D., et al. 2006, *Astrophysical Journal*, 619, L1
- Martini, P. & Schneider, D.P. 2003, *Astrophysical Journal*, 597, 109
- Mathieu, R. 2000, *Proceedings from ASP Conference*, 198, R. Pallavicini, G. Micela, and S. Sciortino, eds. 517
- Matthews, D.J. & Newman, J.A. 2010, *Astrophysical Journal*, 721, 456
- Ménard, B., Scranton, R., Schmidt, S., et al. 2013, arXiv:1303.4722
- Metzger, B.D. & Berger, E. 2012, *Astrophysical Journal*, 746, 48
- Monet, D.G., Levine, S.E., Canzian, B., et al. 2003, *Astronomical Journal*, 125, 984
- Morokuma, T., Inada, N., Oguri, M., et al. 2007, *Astronomical Journal*, 133, 214
- Morokuma, T., Mamoru D., Naoki Y., et al. 2008, *Astrophysical Journal*, 676, 163
- Morrison, C.B., Scranton, R., Ménard, B., et al. 2012, *MNRAS*, 426, 2489
- Munn, J.A., Monet, D.G., Levine, S.E., et al. 2004, *Astronomical Journal*, 127, 3034
- Neill, J.D. & Shara, M.M. 2005, *Astronomical Journal*, 129, 1873
- Nemiroff, R.J. 2003, *Astronomical Journal*, 125, 2740
- Ness, M., Debattista, V. P., Bensby, T., et al. 2014, *Astrophysical Journal*, 787, L19
- Nesvorný, D., Jedicke, R., Whiteley, R. & Ivezić, Ž. 2005, *Icarus* 173, 132
- Newman, J. 2008, *Astrophysical Journal*, 684, 88
- Nissanke, S., Kasliwal, M. & Georgieva, A. 2013, *Astrophysical Journal*, 767, 124
- Oguri, M. & Kawano, Y. 2003, *MNRAS*, 338, L25
- Oguri, M., & Marshall, P.J. 2010, *MNRAS*, 405, 2579
- Oguri, M. & Takada, M. 2011, *Physical Review D*, 83, 023008
- Padmanabhan, N., Schlegel, D., Finkbeiner, D., et al. 2008, *Astrophysical Journal*, 674, 1217
- Parker, A., Ivezić, Ž., Jurić, M., et al. 2008, *Icarus*, 198, 138
- Patat, F. 2008, *A&A*, 481, 575
- Percival, W.J., Reid, B.A., Eisenstein, D.J., et al. 2010, *MNRAS*, 401, 2148
- Perlmutter, S., Aldering, G., Goldhaber, G., et al. 1999, *Astrophysical Journal*, 517, 565
- Perryman, M.A.C., de Boer, K.S., Gilmore, G., et al. 2001; *Astronomy & Astrophysics*, 369, 339
- Pettersen, B.R. & Hawley, S.L. 1989, *Astronomy & Astrophysics*, 217, 187
- Pier, J.R., Munn, J.A., Hindsley, R.B., et al. 2003, *Astronomical Journal*, 125, 1559
- Pinto, P.A., Smith, R.C., Garnavich, P.M., et al. 2005, *American Astronomical Society, AAS Meeting #205, #108.20*
- Planck Collaboration 2011, *Astronomy & Astrophysics*, 536, 23
- Porciani, C. & Madau, P. 2000, *Astrophysical Journal*, 532, 679
- Pravec, P. & Harris, A.W. 2000, *Icarus*, 148, 12
- Rabinowitz, D.L. 1993, *Astrophysical Journal*, 407, 412
- Reid, I. N., Gizis, J. E. & Hawley, S. L. 2002, *Astronomical Journal*, 124, 2721
- Reyes, R., Mandelbaum, R., Seljak, U., et al. 2010, *Nature*, 464, 256
- Richards, G.T., Fan, X., Newberg, H.J., et al. 2002, *Astronomical Journal*, 123, 2945
- Riess, A.G., Filippenko, A.V., Challis, P., et al. 1998, *Astronomical Journal*, 116, 1009
- Riess, A.G., Strolger, L-G., Casertano, S., et al. 2007, *Astrophysical Journal*, 659, 98
- Ross, N.P., Myers, A.D., Sheldon, E.S. et al. 2012, *Astrophysical Journal (Supplements)*, 199, 3
- Rossetto, B. M., Santiago, B. X., Girardi, L., et al. 2011, *Astronomical Journal*, 141, 185
- Rowe, J.F., Bryson, S.T., Marcy, G.W., et al. 2014, *Astrophysical Journal*, 784, 45
- Schlafly, E.F., Finkbeiner, D.P., Jurić, M. et al. 2012, *Astrophysical Journal*, 756, 158
- Schlegel, D.J., Finkbeiner, D.P. & Davis, M. 1998, *Astrophysical Journal*, 500, 525
- Scranton, R., Connolly, A., Krughoff, S., et al. 2007, *astro-ph/0709.0752*
- Schwamb, M. E., Brown, M. E., Rabinowitz, D. L. & Ragozzine, D. 2010, *Astrophysical Journal*, 720, 1691
- Seljak, U., Makarov, A., McDonald, P., et al. 2005, *Physical Review D*, 71, 3515
- Seo, H-J. & Eisenstein, D.J. 2003, *Astrophysical Journal*, 598, 720
- Sesar, B., Ivezić, Ž., Lupton, R.H., et al. 2007, *Astronomical Journal*, 134, 2236
- Sesar, B., Ivezić, Ž., Grammer, S.H., et al. 2010, *Astrophysical Journal*, 708, 717
- Shara, M.M. 2006, *Astronomical Journal*, 131, 2980
- Sharma, S., Johnston, K. V., Majewski, S. R., Bullock, J. & Muñoz, R. R. 2011, *Astrophysical Journal*, 728, 106
- Shen, K.J. & Bildsten, L. 2009, *Astrophysical Journal*, 692, 324
- Shields, G.A. & Bonning, E.W. 2008, *Astrophysical Journal*, 682, 758
- Skrutskie, M.F., Cutri, R.M., Stiening, R., et al. 2006, *Astronomical Journal*, 131, 1163.
- Smartt, S.J. 2009, *ARA&A*, 47, 63
- Smith, N., Li, W., Silverman, J.M., Ganeshalingam, M. & Filippenko, A.V. 2011, *MNRAS*, 415, 773
- Song, Y-S. & Knox, L. 2004, *Physical Review D*, 70, 63510
- Spergel, D., Gehrels, N., Breckinridge, J. et al. 2013, arXiv:1305.5422
- Staniszewski, Z., Ade, P.A.R., Aird, K.A., et al. 2009, *Astrophysical Journal*, 701, 32
- Stassun, K., Paegert, M., De Lee, N. M. & Cargile, P. 2013, *American Astronomical Society, AAS Meeting #221, #116.01*
- Strubbe, L.E. & Quataert, E. 2009, *MNRAS*, 400, 2070
- Stubbs, C.W. & Tonry, J., 2006, *Astrophysical Journal*, 646, 1436
- Stubbs, C.W., High, F.W., George, M.R., et al. 2007, *PASP*, 119, 1163
- Suyu, S.H., Marshall, P.J., Auger, M.W., et al. 2010, *Astrophysical Journal*, 711, 201
- Szabó, Gy.M., Ivezić, Ž., Jurić, M., & Lupton, R. 2007, *MNRAS*, 377, 1393
- Takada, M., Ellis, R.S., Chiba, M. et al. 2014, *PASJ*, 66, 1
- Takada, M. & Jain, B. 2004, *MNRAS*, 348, 897
- Thompson, T.A., Prieto, J.L., Stanek, K.Z., et al. 2009, *Astrophysical Journal*, 705, 1364
- Thornton, D., Stappers, B., Bailes, M., et al. 2013, *Science*, 341, 53
- Tisserand, P., Le Guillou, L., Afonso, C. et al. 2007, *Astronomy & Astrophysics*, 469, 387
- Tokovinin, A. 2002, *PASP*, 114, 1156
- Treu, T., Koopmans, L.V., Bolton, A.S., Burles, S., and Moustakas, L.A. 2006, *Astrophysical Journal*, 640, 662
- Trujillo, C.A., Jewitt, D.C. & Luu, J.X. 2001, *Astronomical Journal*, 122, 457
- Trujillo, C.A. & Sheppard, S. S. 2014, *Nature*, 507, 471
- Tyson, J.A., Kochanski, G.P. & Dell'Antonio, I.P. 1998, *Astrophysical Journal*, 498, L107
- Tyson, J.A., Roat, C., Bosch, J. & Wittman, D. 2008a, *Astronomical Data Analysis Software and Systems XVII*, ASP Conference Series, J. Lewis, R. Argyle, P. Bunclarck, D. Evans, and E. Gonzales-Solares, eds.

- Tyson, J. A., and LSST collaboration, 2008b, see [http://universe.ucdavis.edu/docs/LSST\\_petascale\\_challenge.pdf](http://universe.ucdavis.edu/docs/LSST_petascale_challenge.pdf)
- Vanden Berk, D.E., Richards, G.T., Bauer, A., et al. 2001, *Astronomical Journal*, 122, 549
- Vanden Berk, D.E., Wilhite, B.C., Kron, R.G., et al. 2004, *Astrophysical Journal*, 601, 692
- Walker, M. G. & Peñarrubia, J. 2011, *Astrophysical Journal*, 742, 20
- Walsh, S.M., Willman, B. & Jerjen, H. 2009, *Astronomical Journal*, 137, 450
- Wang, L., Goldhaber, G., Aldering, G. & Perlmutter, S. 2003, *Astrophysical Journal*, 590, 944
- Wang, S., Haiman, Z., May, M. & Kehayias, J. 2005, *astro-ph/0512513*
- Weinberg, D. H., Bullock, J. S., Governato, F., Kuzio de Naray, R. & Peter, A. H. G., 2013, arXiv:1306.0913
- Weinberg, D.H., Mortonson, M.J., Eisenstein, D.J., Hirata, C., Riess, A.G., & Rozo, E. 2013, *Physics Reports*, 530, 87
- West, A. A., Bochanski, J. J., Bowler, B. P., et al. 2011, *Astronomical Society of the Pacific Conference Series*, 448, 531
- Wood-Vasey, W.M., Miknaitis, G., Stubbs, C.W., et al. 2007, *Astrophysical Journal*, 666, 694
- Wright, J.T., Marcy, G.W., Howard, A.W., et al. 2012, *Astrophysical Journal*, 753, 160
- Xue, Y.Q., Brandt, W.N., Luo, B., et al. 2010, *Astrophysical Journal*, 720, 368
- Yoo, J., Chanamé, J. & Gould, A. 2004, *Astrophysical Journal*, 601, 311
- York, D.G., Adelman, J., Anderson, S., et al. 2000, *Astronomical Journal*, 120, 1579
- Yoshida, F. & Nakamura, T. 2005, *Astronomical Journal*, 130, 2900
- Zaritsky, D., Harris, J., Thompson, I. B., & Grebel, E. K., 2004, *Astronomical Journal*, 128, 1606
- Zhan, H. 2006, *Journal of Cosmology & Astroparticle Physics*, 8, 8
- Zhan, H. & Knox, L. 2006, *Astrophysical Journal*, 644, 663
- Zhan, H. & Knox, L. & Tyson, J.A. 2009, *Astrophysical Journal*, 690, 923
- Zhang, B. & Mészáros, P. 2004, *International Journal of Modern Physics A*, 19, 2385
- Zhang, B., Fan, Y.Z., Dyks, J., et al. 2006, *Astrophysical Journal*, 642, 354